11-9-2017

Synthesis, Characterization, and Application of Molybdenum Oxide Nanomaterials

Michael S. McCrory
University of South Florida, mmccrory@mail.usf.edu

Synthesis, Characterization, and Application of Molybdenum Oxide Nanomaterials

by

Michael S. McCrory

A dissertation submitted in partial fulfillment
of the requirements for the degree of
Doctor of Philosophy
Department of Mechanical Engineering
College of Engineering
University of South Florida

Co-Major Professor: Ashok Kumar, Ph.D.
Co-Major Professor: Manoj K. Ram, Ph.D.
Daniel Hess, Ph.D.
Sylvia Thomas, Ph.D.
Sagar Pandit, Ph.D.

Date of Approval:
November 2, 2017

Keywords: Battery, Decontamination, Photocatalyst,
Adsorbent, Methylene Blue

DEDICATION

I'd like to dedicate this work to grandma, Janet, and my parents, Gail and James. Thank you for everything; the love, support, encouragement, etc.

I'd also like to dedicate this work to my soon-to-be wife, Courtney. Words just cannot describe my feelings here, so I'll simply say thank you for everything and I love you.

ACKNOWLEDGMENTS

I would like to thank Dr. Ashok Kumar for his support throughout my time at USF. I would also like to thank Dr. Manoj Ram for all of his support and guidance; he worked countless hours with me (and other students), and without him I surely would not be graduating. I'd like to thank all of the committee members, Dr. Daniel Hess, Dr. Sylvia Thomas, and Dr. Sagar Pandit for taking time out of their busy schedules to be on my defense committee. I owe a special thanks to Dr. Hess for all of his support over the past 4+ years. It was an absolute pleasure and honor to work for him. I'd also like to thank my defense chair, Dr. Arash Takshi, for not only taking time to be here, but leading me through the final presentation I will make as a student at USF. I'd like to thank Dr. Rajiv Dubey, department chair, and Dr. Rasim Guldiken, graduate advisor, for their continued advice and support throughout my time here at USF, including allowing me to TA for all of these years. I'd like to thank Dr. Jose Zayas-Castro, and the rest of the College of Engineering, for their support over the years. I'd also like to thank Robert Tutfs, Jay Bieber, Richard Everly and Yusuf Emirov for all of their support and guidance in learning the characterization equipment in NREC.

Finally I'd like to thank all of my lab mates (current and former). We always had some great discussions, both educational and personal. You guys were great, and I wish you all the best in your future endeavors.

TABLE OF CONTENTS

LIST OF TABLES

LIST OF FIGURES

ABSTRACT

Nanostructured molybdenum trioxide (MoO_3) was synthesized and used as a precursor in a comparative study, along with commercial MoO_3, to synthesize molybdenum dioxide (MoO_2) nanoparticles. Scanning electron microscope (SEM) images revealed the particles to be approximately 30-50 nm in diameter. X-ray diffraction (XRD) confirmed MoO_3 was fully reduced to MoO_2 in all cases. Time dependent experiments showed that within two hours no traces of MoO_3 are present. All of the experiments showed the materials were excellent absorbent materials, as well as photocatalysts. Both MoO_2 materials performed almost exactly the same, with both samples being able to remove 100% of the methylene blue (MB) in one minute with light, and in two minutes without light.

The morphology of MoO_2 was controlled in a comparative study by varying the concentration of cetyltrimethylammonium bromide (CTAB) present during the hydrothermal reaction. As the concentration of CTAB increased, the morphology of the material changed from nanoparticles, to nanospheres, to microspheres, to hollow microspheres, and finally a highly agglomerated version of microspheres and particles combined, as confirmed by SEM images. A formation mechanism for the formation of the various sized spheres was proposed with a combination of aggregation and Ostwald ripening. XRD confirmed that all of the MoO_3 was reduced to MoO_2, along with no residual peaks from the CTAB that was present during the reaction. Upon trying to mix some of the materials into the MB solutions, it became obvious that some of the materials were hydrophobic. The decontamination results once again showed that the

synthesized MoO_2 materials were not only photocatalysts, but adsorbents as well. Samples synthesized with 0.1-5 mM CTAB were able to remove 100% of the MB in 10 minutes or less. Samples synthesized with 10 mM CTAB were able to remove 54.4% and 35% of the MB in 10 minutes, with and without light, respectively. Samples synthesized with 15 mM CTAB were able to remove 29.4% and 26.3% of the MB in 10 minutes, with and without light, respectively. The apparent decrease in decontamination performance was proposed to be caused by surface morphology induced hydrophobicity. A mechanism to describe why the hydrophobic particles were still able to decontaminate the water was proposed to be caused by coming into direct contact with the magnetic stirrer as the water level dropped due to sample collection.

MoO_2 nanoparticles were successfully synthesized onto a copper substrate, in a single step, via a hydrothermal synthesis technique. It is believed to be the first report of such a synthesis method. XRD confirmed all of the MoO_3 had been reduced to MoO_2, and also confirmed that no other compounds had formed between the molybdenum and copper. SEM images of the MoO_2 coated copper substrate showed uniform nanoparticles ranging from 30-50 nm. The MoO_2 coated copper substrate was able to decontaminate 57.5% of the MB from water in 10 minutes without exposure to light, while it was able to decontaminate 71.7% of the MB from water in 10 minutes with exposure to light.

CHAPTER 1: INTRODUCTION

1.1 Problem Description and Motivation

Molybdenum oxides have been proven to be a very promising material for a variety of applications, mainly in the world of Li-ion batteries, but there have also been a few reports using it to decontaminate water. There have been numerous reports of using molybdenum trioxide (MoO_3) as a photocatalyst, and the results have been incredibly promising; however, very little research has been done to investigate the use of molybdenum dioxide (MoO_2) for the same application.

Research has shown that the morphology of a material can greatly affect its properties, and that surfactants are one of the most common ways to control morphology during the synthesis process. Yet there are very few publications currently describing the morphology controlled synthesis of MoO_2.

Currently, most decontamination experiments are based off of a slurry, where the active material is mixed in with the polluted sample to perform the decontamination. While this method is very effective at assuring the active material comes into contract with the pollutant, but then basically becomes a pollutant of its own, that must be removed from the water through filtration, centrifugation, etc. Ideally, the active material could be coated on a substrate that was then submerged in the contaminated water. After the water had been decontaminated, the substrate could be removed, and the water would be clean without any further processing necessary.

The objectives of this dissertation are as follows:

- To investigate the decontamination of methylene blue (MB) in water using MoO_3 and MoO_2 nanoparticles.
- To determine the effect of various amounts of surfactant on the morphology of synthesized MoO_2 materials, and to measure the effect of the change in morphology on the decontamination of MB in water.
- To synthesize MoO_2 directly onto a copper substrate to decontaminate water.

1.2 Organization of the Dissertation

The structure of this dissertation can be summarized as follows.

Chapter 1 describes the problem and the motivation behind the study of decontaminating water using molybdenum dioxide, followed by the organization of this dissertation.

Chapter 2 is a literature review that covers various synthesis methods and applications for MoO_2. The main focus of this chapter is on the ability of MoO_2 to decontaminate water, however some very promising Li-ion battery results are also briefly discussed.

Chapter 3 describes the synthesis and characterization of MoO_2 nanoparticles using a MoO_3 precursor. Decontamination experiments were conducted, and for the first time it was shown that MoO_2 nanoparticles could decontaminate MB from the water, both with and without exposure to visible light.

Chapter 4 describes the morphology controlled synthesis of MoO_2 nanostructures by utilizing the assistance of a surfactant. Various morphologies were synthesized and characterized, and the data is arranged in a convenient table. Decontamination experiments were conducted for the various morphologies, and again the samples were able to decontaminate MB from the water with and without exposure to visible light.

Chapter 5 describes a novel method for the synthesis of MoO_2 nanoparticles directly onto a copper substrate. Decontamination experiments were conducted to determine the ability of the MoO_2 coated copper substrate to decontaminate MB from the water with and without exposure to visible light.

Chapter 6 concludes the dissertation with a summary of the major findings from all of the chapters, along with a discussion of the future recommended research regarding the use of MoO_2 to decontaminate water.

CHAPTER 2: LITERATURE REVIEW

2.1 Introduction

Molybdenum dioxide (MoO_2) has been researched for a variety of applications; mainly for Li-ion batteries [1-21], but also for removing Cr (VI) from wastewater[22], photocatalysts [23, 24], supercapacitors [24-26], pseudocapacitors [27], as well as a catalyst for oxidation of hydrocarbons [28]. There are a large variety of synthesis methods for MoO_2, including hydrothermal [7, 14, 16, 20, 24, 29-36], solution-phase [18, 37-39], solvothermal [21, 40, 41], spray pyrolysis [3], nanocasting [6, 19], electrodeposition [27], rheological phase reaction [8], sol-gel [12], chemical vapor deposition (CVD) [42], magnetron sputtering [15], immersion [43], and thermal decomposition [25]. Not only can MoO_2 be synthesized in a variety of ways, but it also has variety of morphologies, ranging from nanoparticles [5, 8, 10, 12, 14, 38], nanospheres [30], nanobars [30], nanoflakes [30], microspheres [3, 7, 22, 23, 44], nanowires [45], and nanorods [6], and more.

2.2 Use of MoO_2 in the Decontamination of Water

Huge amounts of organics waste are produced every day from various chemical and oil industries, textile industries, farming applications, and even at wastewater treatment facilities [46-50]. There are more than 100,000 commercially available dyes, with over 7×10^5 tons of dye-stuff produced annually [50]. If and when this organic waste makes it in to contact with people, it can cause serious damage to the respiratory, digestive, urinary, nervous and cardiovascular systems [51-57].Water containing some of these pollutants can be decontaminated in a variety of ways,

including reverse osmosis [58, 59], centrifuge [60, 61], ultraviolet (UV)-based filtration [62, 63], adsorption [64, 65], precipitation [60, 66], ozone [67, 68], micro and ultra filtration [69-71], biological treatment [72-74], and oxidation (through the use of photocatalysts) [23, 24, 51, 74-95].

Photocatalysts appear to be one of the most popular methods to decontaminate water due to the fact that the photocatalytic reaction can be powered by the visible and/or UV light coming from the sun. TiO_2 was the first photocatalyst discovered, back in 1969 by Fujishima and Honda [75]. The basic principal of a photocatalytic reaction is shown in Figure 2.1; where photons of light having a greater energy than the bandgap of the photocatalyst are adsorbed, transferring an electron from the valence band to the conduction band, generating an electron (e_{CB}^-) hole (h_{VB}^+) pair. These electron hole pairs can do one of two things, either recombine and generate heat, or react with available oxidants and reductants to produce OH and O_2 radicals, respectively, which finally break the dye down into carbon dioxide and water [96-102].

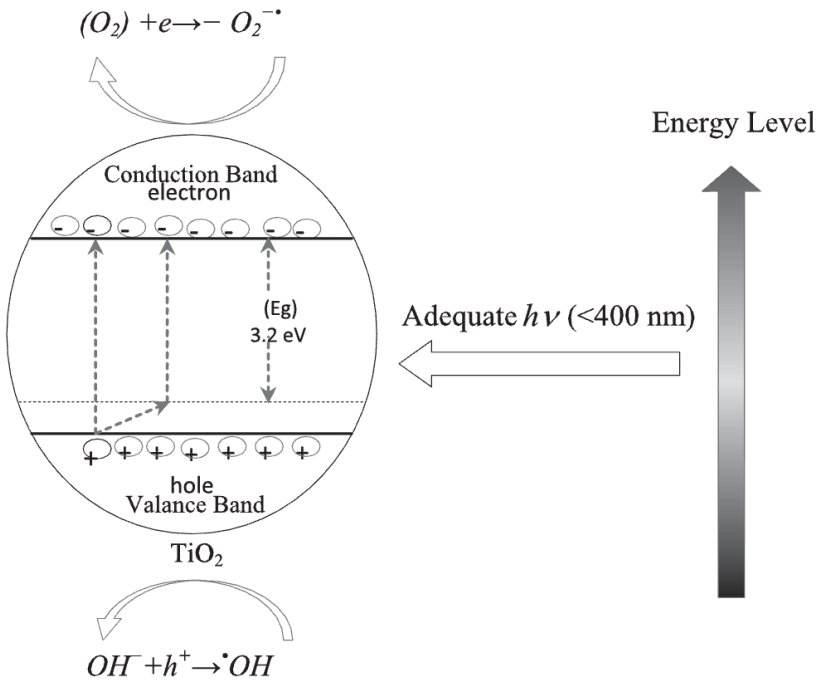

Figure 2.1 Energy band gap diagram of a TiO_2 spherical particle. Reprinted Journal of Environmental Management, Vol 98, M.R.D. Khaki, M.S. Shafeeyan, A.A.A. Raman, and W. Daud, Application of doped photocatalysts for organic pollutant degradation - A review, 78-94, 2017, with permission from Elsevier [98].

Reports on the photocatalytic properties of MoO_3 have also been reported, but there are only two reports for photocatalytic properties of MoO_2. Table 2.1 shows a summary of the available data for the photocatalytic properties of the various molybdenum oxide materials, along with a comparison to TiO_2. It should be noted that during all of these photocatalytic experiments, the particles were mixed into the contaminated solution, and allowed to mix for at least 30 minutes in the dark to reach an adsorption/desorption equilibrium of the dye on the surface of the particles.

Table 2.1 Various molybdenum oxide materials and their photocatalytic properties.

Sample	Sample Weight	Pollutant (volume)	Pollutant Concentration	Source of irradiation	Decontamination	Time	Ref.
TiO_2	250 mg	Methylene Blue (250 mL)	20 mg L^{-1}	No light exposure	<10%	5 h (300 min)	[97]
TiO_2	250 mg	Methylene Blue (250 mL)	20 mg L^{-1}	UV light	96%	5 h (300 min)	[97]
α-MoO_3	50 mg	Methylene Blue (100 mL)	10 mg L^{-1}	UV and visible light	87%	180 min	[103]
h-MoO_3	50 mg	Methylene Blue (100 mL)	10 mg L^{-1}	UV and visible light	97%	180 min	[103]
MoO_2	500 mg	Methylene Blue (50 mL)	10 mg L^{-1}	UV light	30%	140 min	[24]
MoO_2	500 mg	Rhodamine B (50 mL)	10 mg L^{-1}	UV light	70%	140 min	[24]
α-MoO_3	100 mg	Methylene Blue (100 mL)	1000 mg L^{-1}	Sunlight	99.7% (40% in dark)	150 min	[82]
MoO_3	50 mg	Methylene Blue (100 mL)	10 mg L^{-1}	Visible light	>90%	40 min	[95]
MoO_2	25 mg	Rhodamine B (50 mL)	10 mg L^{-1}	UV and visible light	15.8%	90 min	[23]
Graphene-α-MoO_3	10 mg	Methylene Blue (50 mL)	0.01 mM	UV light	97%	180 min	[86]
Graphene-α-MoO_3	10 mg	Methylene Blue (50 mL)	0.01 mM	Visible light	96%	240 min	[86]

While MoO_2 has seen a lot of research in other fields, it is clear that very little research has been done in relation to the decontamination of water using MoO_2. One of the few reports of decontamination using MoO_2 is briefly summarized below.

MoO_2 nanoparticles were synthesized via a hydrothermal synthesis technique using ammonium heptamolybdate, water, and ethylene glycol. The mixture was sealed in a teflon lined stainless steel pressure vessel and heated at 180 °C for 36 hours. The samples were dried in a vacuum oven at 60 °C overnight, and annealed in an argon tube furnace at 500 °C for 6 hours. The resulting MoO_2 nanoparticles are shown in Figure 2.2 [24].

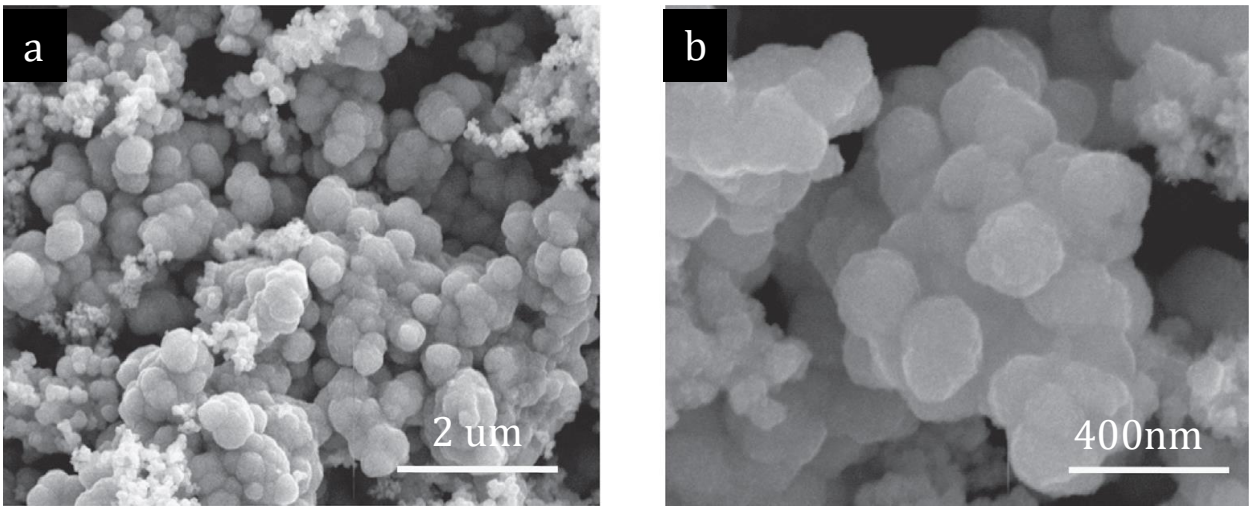

Figure 2.2 SEM images of the MoO_2 samples at a) low and b) higher magnifications. Reprinted from Ceramics International, Vol. 42, E. Zhou, C. Wang, Q. Zhao, Z. Li, M. Shao, X. Deng, X. Liu, X. Xu, Facile synthesis of MoO_2 nanoparticles as high performance supercapacitor electrodes and photocatalysts, pp. 2198-2203, Copyright 2012, with permission from Elsevier [24].

To measure the photocatalytic properties of the MoO_2 nanoparticles, 500 mg of sample was continuously stirred in to 50 mL of an aqueous organic dye solution with a concentration of 10 mg L^{-1}. The samples were allowed to mix in the dark to allow them to reach their adsorption/desorption equilibrium, before they were exposed to ultraviolet (UV) light from a 500 W mercury lamp. The degradation of the dye solutions was analyzed using a UV-visible spectrophotometer, measuring the peak intensity of the maximum absorption wavelength. The

results of the experiment are shown in Figure 2.3. The best results were 30% decontamination of MB, and 70% decontamination of RhB in 140 minutes.

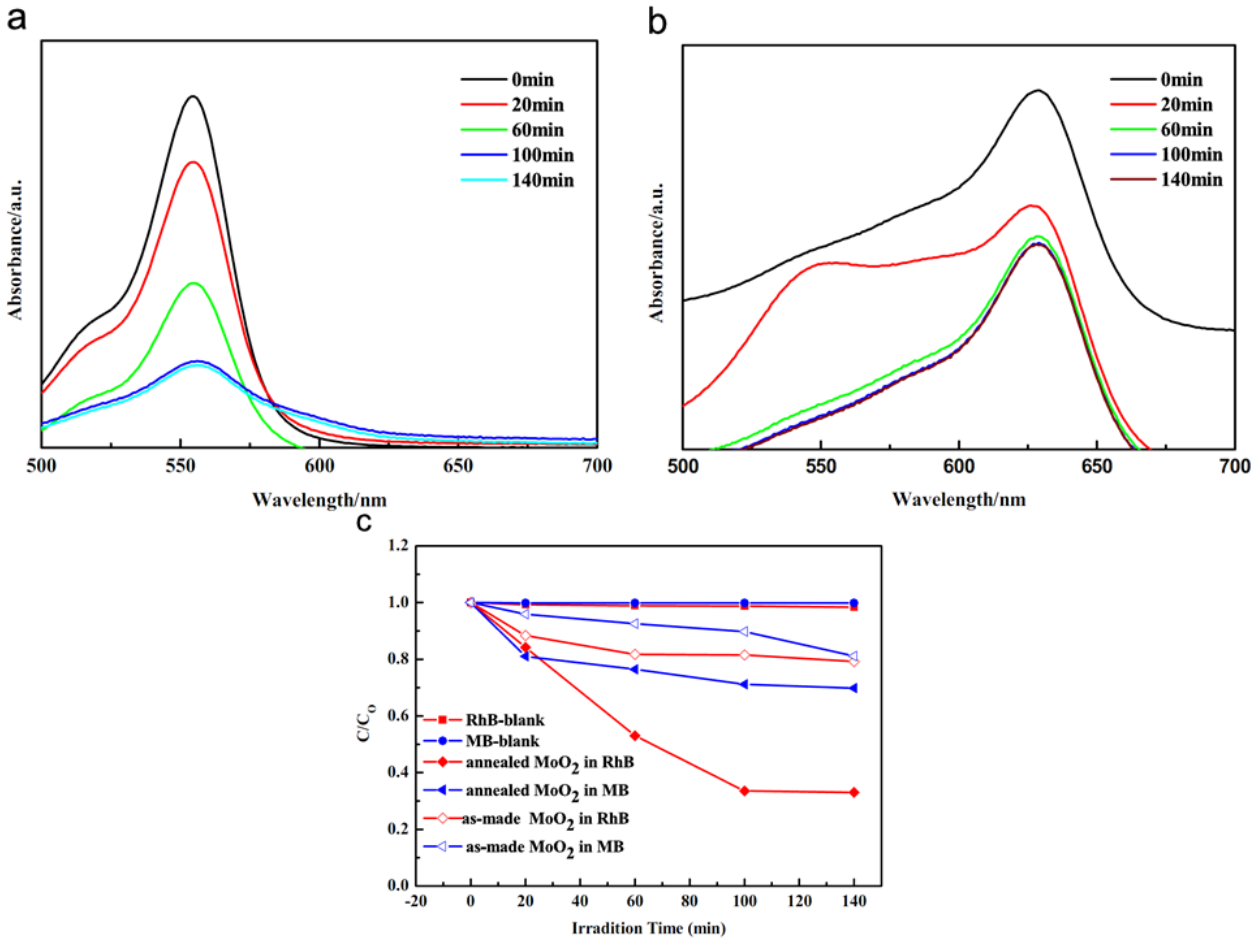

Figure 2.3 Absorption spectra of RhB (a) and MB (b) aqueous solution, the C/C_0 vs. time curves of RhB and MB (c). Reprinted from Ceramics International, Vol. 42, E. Zhou, C. Wang, Q. Zhao, Z. Li, M. Shao, X. Deng, X. Liu, X. Xu, Facile synthesis of MoO_2 nanoparticles as high performance supercapacitor electrodes and photocatalysts, pp. 2198-2203, Copyright 2012, with permission from Elsevier [24].

2.3 Use of MoO_2 in Li-Ion Batteries

Batteries have been around for a long time, but significant research into new battery chemistries has lagged behind the progress of the new devices constantly being developed. Figure 2.4 shows a plot of volumetric energy density versus gravimetric energy density for various battery chemistries [104], and it is clear that lithium ion batteries (LIBs) are the most promising, and are a perfect fit for the new devices because of its high density energy storage [104].

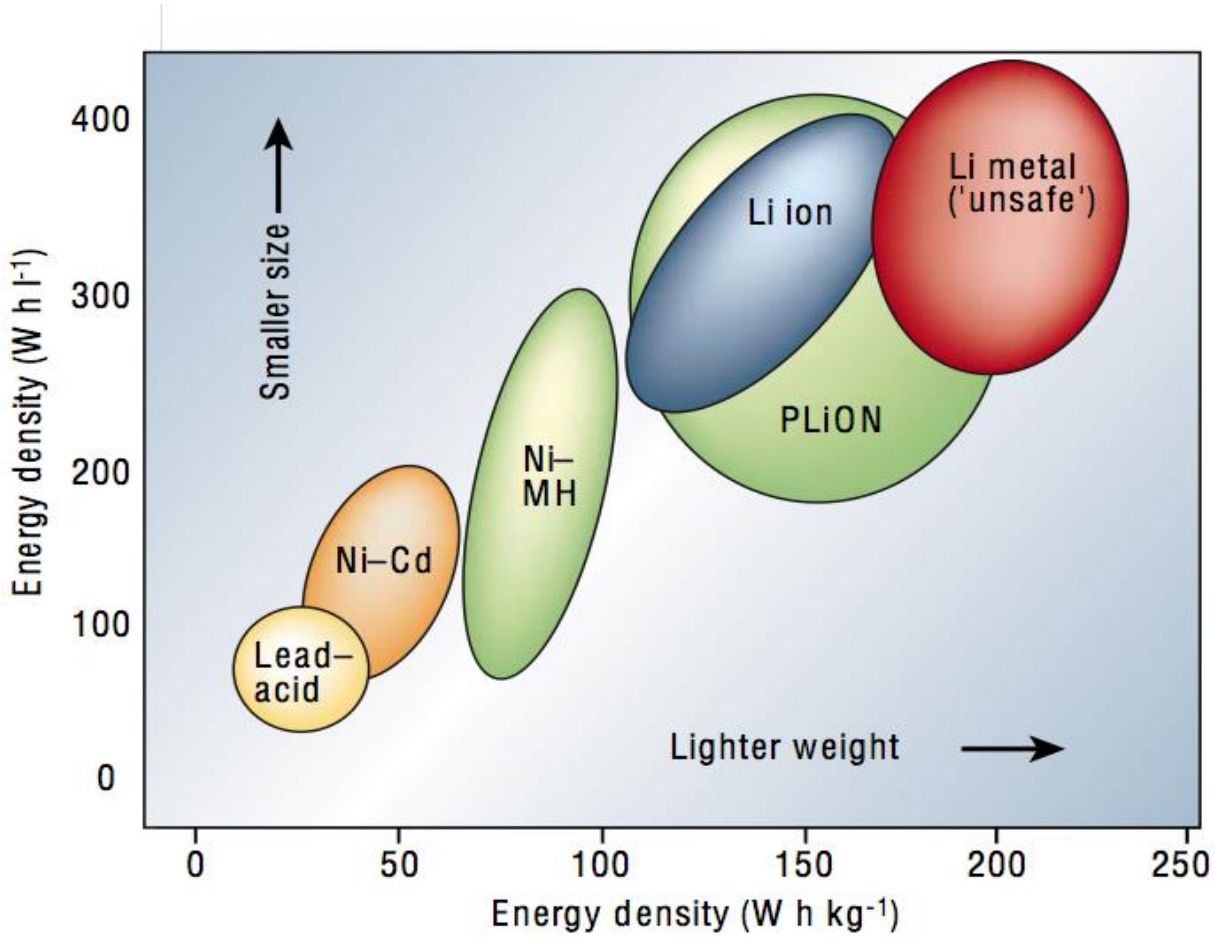

Figure 2.4 Comparison of the different battery technologies in terms of volumetric and gravimetric energy density. Reprinted by permission from Macmillan Publishers Ltd: [Nature], Ref. [104], copyright (2001).

A LIB consists of three main parts: the cathode, the anode and an electrolyte; which when combined form an electrochemical cell. These cells can then be connected in series and/or in parallel with other cells to produce the desired voltage and capacity, respectively [104]. The most common LIB configuration contains a graphite anode such as mesocarbon microbeads (MCMB), a lithium metal oxide cathode such as lithium cobalt oxide ($LiCoO_2$), and an electrolyte solution of lithium salt, such as lithium hexafluorophosphate ($LiPF_6$), in an organic solvent, such as ethylene carbonate (EC) or dimethyl carbonate (DMC) [105, 106]. A schematic of the basic layout is shown in Figure 2.5.

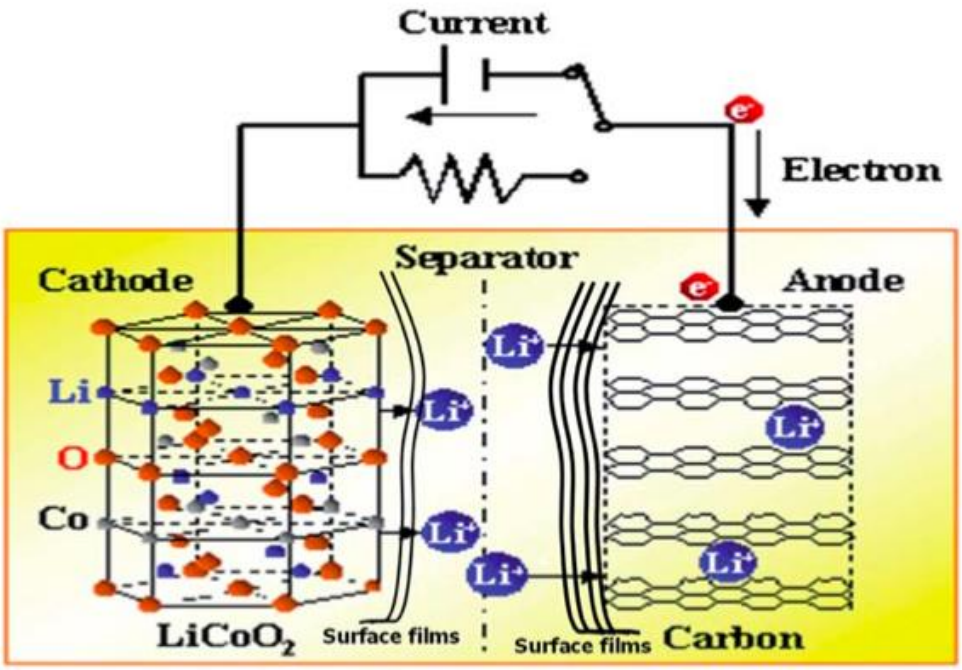

Figure 2.5 Schematic of the principle of LIB. Reproduced from Ref. [107] with permission of The Royal Society of Chemistry.

One of the biggest challenges facing current Li-ion battery technology is the low theoretical capacity of the graphite anode material. When in use as an anode material, graphite provides a usable capacity that is less than its already low theoretical capacity of 372 mA h g^{-1}. MoO_2 appears to be a great candidate to replace the typical graphite anode, due to its larger theoretical capacity of 828 mA h g^{-1}, low electrical resistivity of 8.8 x 10^{-5} Ω cm, and high density of 6.5 g cm^{-3} [11, 20, 32, 108-110]. One of the major drawback to MoO_2 is the intrinsic volume expansion that occurs during lithiation/delithiation, causing the electrode to be pulverized and lose storage capacity. This issue can be solved in several ways, including changing the particle morphology, or the addition of graphene to help buffer the massive volume changes that can occur [1-7, 22, 23, 26-28, 37, 44, 45, 111-113]. Some of the most promising results are briefly discussed below.

A self-assembled hierarchical MoO_2/graphene nanocomposite was synthesized using a solution-phase process and subsequent reduction [39]. First, graphene oxide (GO) was prepared using a modified Hummers method, and then a GO suspension was mixed with phosphomolybdic

acid, DI water, and hydrazine hydrate. The resulting black powder was dried in a vacuum and placed into a tube furnace to form a MoO_2/graphene nanocomposite, as shown in Figure 2.6 [39]. Rod like "maize cobs" can be seen in Figure 2.6a and 2.6b, which are approximately 1-3 μm in diameter and 5-10 μm in length. Upon closer inspection at high magnifications, it is clear that the graphene has wrapped around the 30-80 nm MoO_2 particles, as shown in Figure 2.6c and 2.6d.

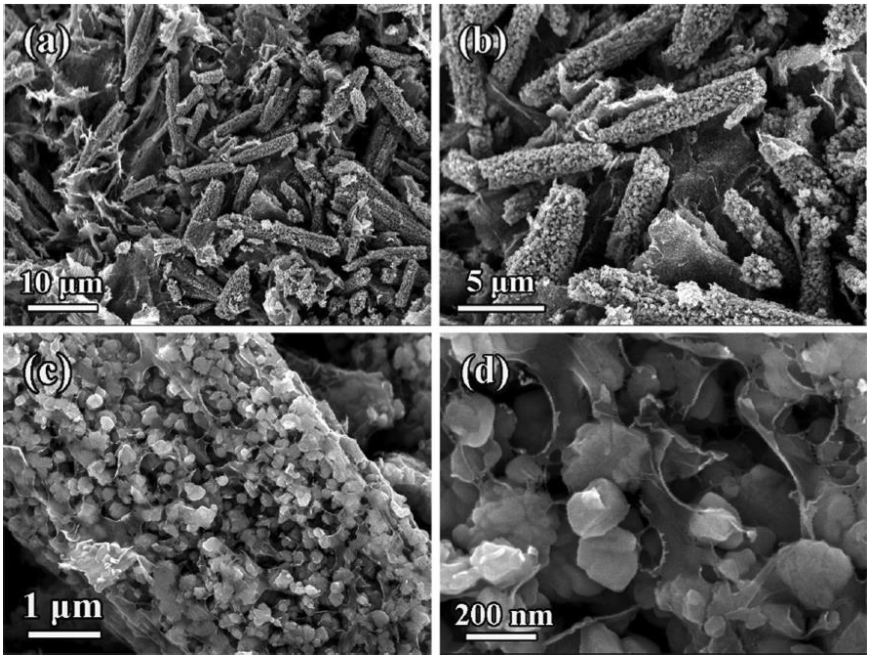

Figure 2.6 SEM images of the self-assembled hierarchical MoO_2/graphene nanocomposite. Reprinted with permission from Y. Sun, X. Hu, W. Luo, and Y. Huang, "Self-Assembled Hierarchical MoO_2/Graphene Nanoarchitectures and Their Application as a High-Performance Anode Material for Lithium-Ion Batteries," ACS Nano, vol. 5, no. 9, pp. 7100–7107. Copyright 2011 American Chemical Society [39].

Figure 2.7 shows the cyclic voltammetry for the self-assembled hierarchical MoO_2/graphene nanocomposite from 0.01 – 3 V at a scan rate of 0.1 mV s^{-1}. There are two main peaks at 1.49 V and 1.2 V in the cathodic scan that are evidence of lithium insertion causing a phase transformation from orthorhombic to monoclinic [21, 82–83]. The peak around 0.7 V in the first cycle is evidence of the formation of a solid electrolyte interphase (SEI) film [39]. Evidence of the monoclinic to orthorhombic phase transformation has been observed due to the presence of the sharp peaks at 1.50 V and 1.73 V, while the peaks in subsequent cycles at 1.54/1.73 V and

1.24/1.50 V are evidence of the lithium insertion and extraction of partially lithiated Li_xMoO_2 [19, 114].

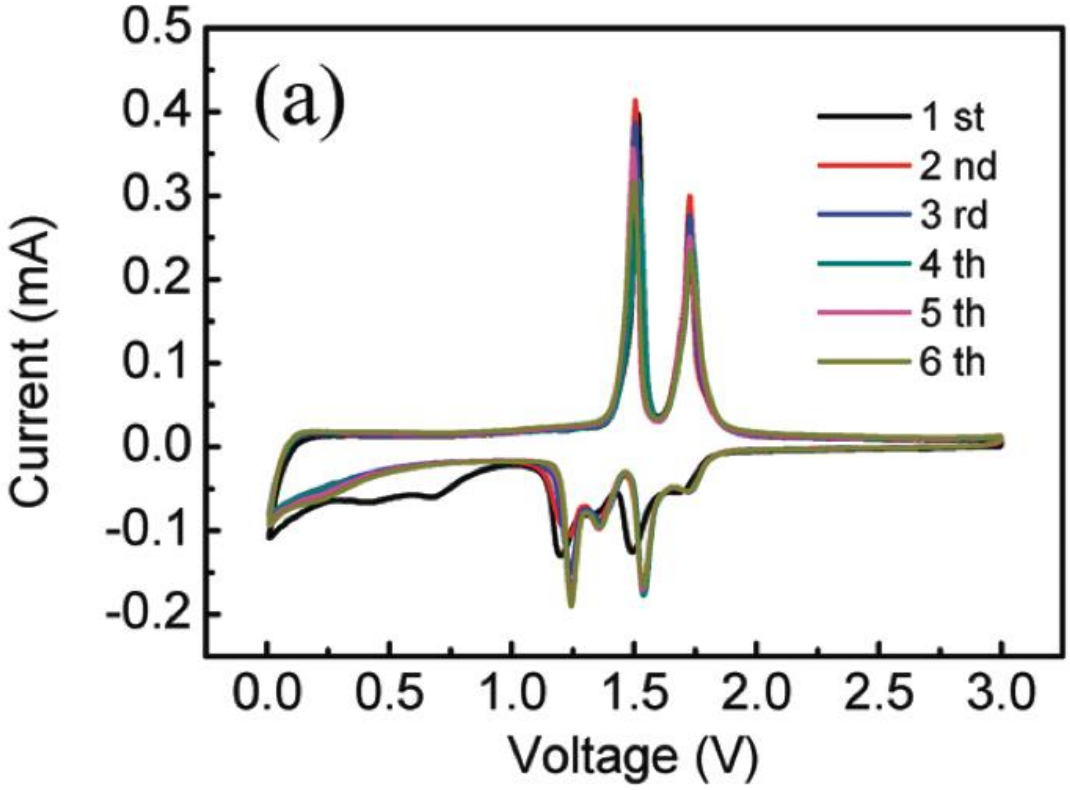

Figure 2.7 Cyclic voltammogram of the self-assembled hierarchical MoO_2/graphene nanocomposite. Reprinted with permission from Y. Sun, X. Hu, W. Luo, and Y. Huang, "Self-Assembled Hierarchical MoO_2/Graphene Nanoarchitectures and Their Application as a High-Performance Anode Material for Lithium-Ion Batteries," ACS Nano, vol. 5, no. 9, pp. 7100–7107. Copyright 2011 American Chemical Society [39].

Figure 2.8 shows the cycling performance of the self-assembled hierarchical MoO_2/graphene in the range of 0.01 - 3 V, at current densities of 1000, 1500, and 2000 mA g^{-1}. At a current density of 1000 mA g^{-1}, the initial discharge and charge capacities were measured to be 468.2 and 342.0 mA h g^{-1}, respectively [39]. After 70 cycles at 1000 mA g^{-1}, the capacity of the electrode actually increased to 597.9 mA h g^{-1}, which is a capacity retention of approximately 127% and may be attributed to the high active surface area as well as the buffering effects of graphene during volume expansion which prevents pulverization of the electrode [39, 84, 115-119].

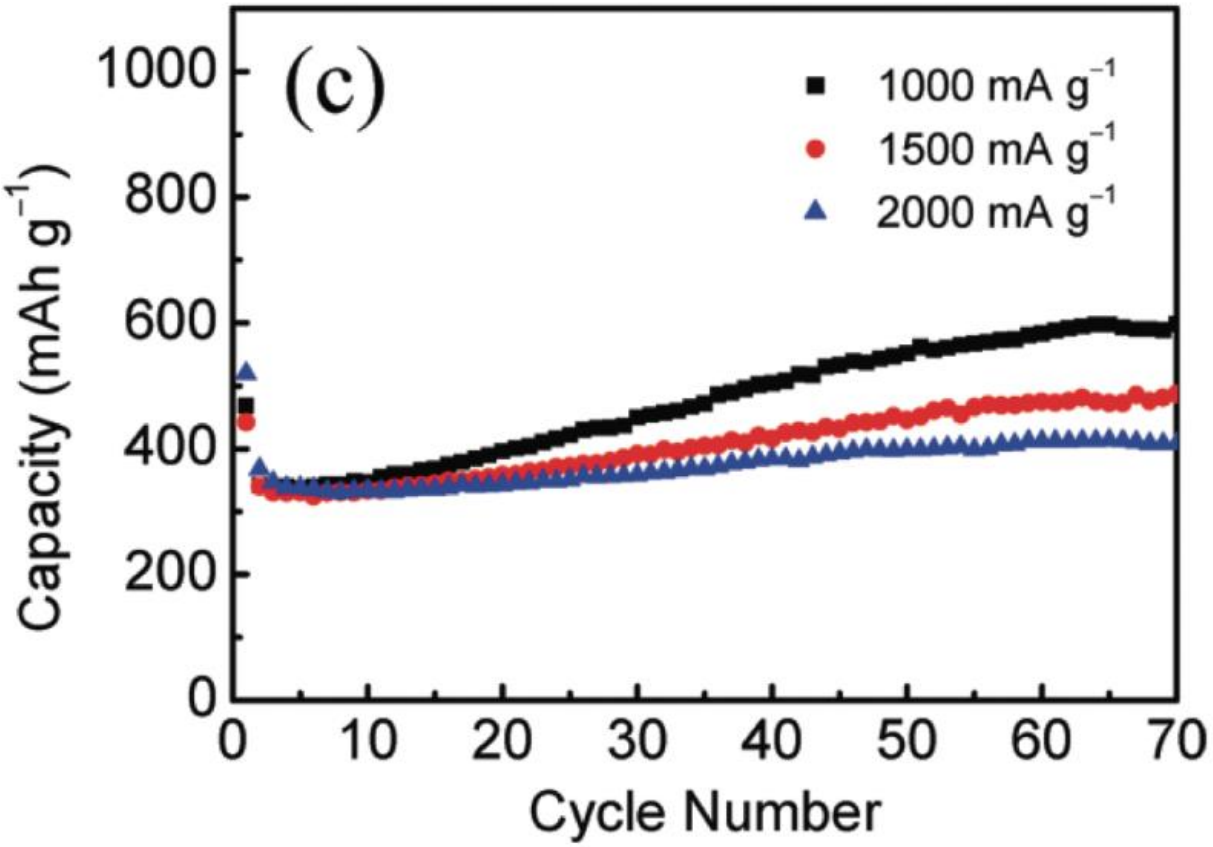

Figure 2.8 Cycling performance of the self-assembled hierarchical MoO_2/graphene in the range of 0.01 - 3 V, at current densities of 1000, 1500, and 2000 mA g-1. Reprinted with permission from Y. Sun, X. Hu, W. Luo, and Y. Huang, "Self-Assembled Hierarchical MoO_2/Graphene Nanoarchitectures and Their Application as a High-Performance Anode Material for Lithium-Ion Batteries," ACS Nano, vol. 5, no. 9, pp. 7100–7107. Copyright 2011 American Chemical Society [39].

A MoO_2-graphene composite was synthesized via a two-step hydrothermal-calcination method [20]. Briefly, GO was synthesized by a modified Hummers method. After reducing the pH to 1 using HCl, ammonium molybdate and ascorbic acid were added to the solution. The resulting mixture was heated in a teflon-lined stainless steel autoclave, then washed with distilled water and dried. The MoO_2-graphene precursor was then placed into an Argon atmosphere tube furnace to form a MoO_2-graphene nanocomposite, shown in Figure 2.9 [20]. It is clear from the figure that the MoO_2 particles have an average diameter of approximately 20 nm and that the graphene had wrapped around the particles.

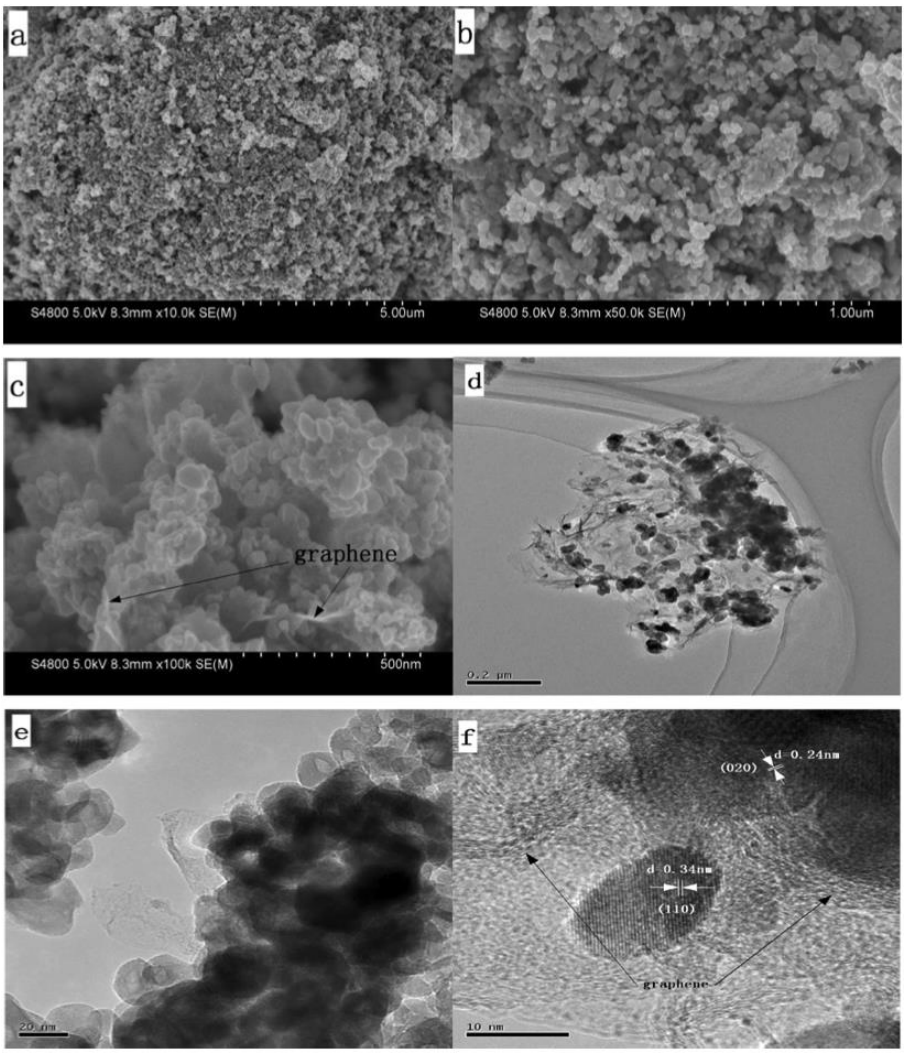

Figure 2.9 (a-c) are SEM images, and (d-f) are TEM images of the MoO_2-graphene nanocomposite. Reprinted from Electrochimica Acta, Vol. 79, Q. Tang, Z. Shan, L. Wang, and X. Qin, "MoO_2–graphene nanocomposite as anode material for lithium-ion batteries," pp. 148–153, Copyright 2012, with permission from Elsevier [20].

Figure 2.10 shows the cyclic voltammetry for the MoO_2-graphene nanocomposite from 0.01 – 2.5 V at a scan rate of 0.2 mV s^{-1}. There are three main peaks at 1.52 V, 1.15 V and 0.65 V in the cathodic scan. The peaks at 1.52 V and 1.15 V are evidence of lithium insertion causing a phase transformation from orthorhombic to monoclinic [20]. The peak around 0.65 V in the first cycle is evidence of the formation of a solid electrolyte interphase (SEI) film [20, 110, 120, 121]. The two sharp peaks in the first anodic scan at 1.50 V and 1.76 V are also evidence of the monoclinic to orthorhombic phase transformation [82–83][20], while the peaks in subsequent

cycles at 1.52/1.76 V and 1.23/1.50 V are evidence of the lithium insertion and extraction of partially lithiated Li_xMoO_2 [20].

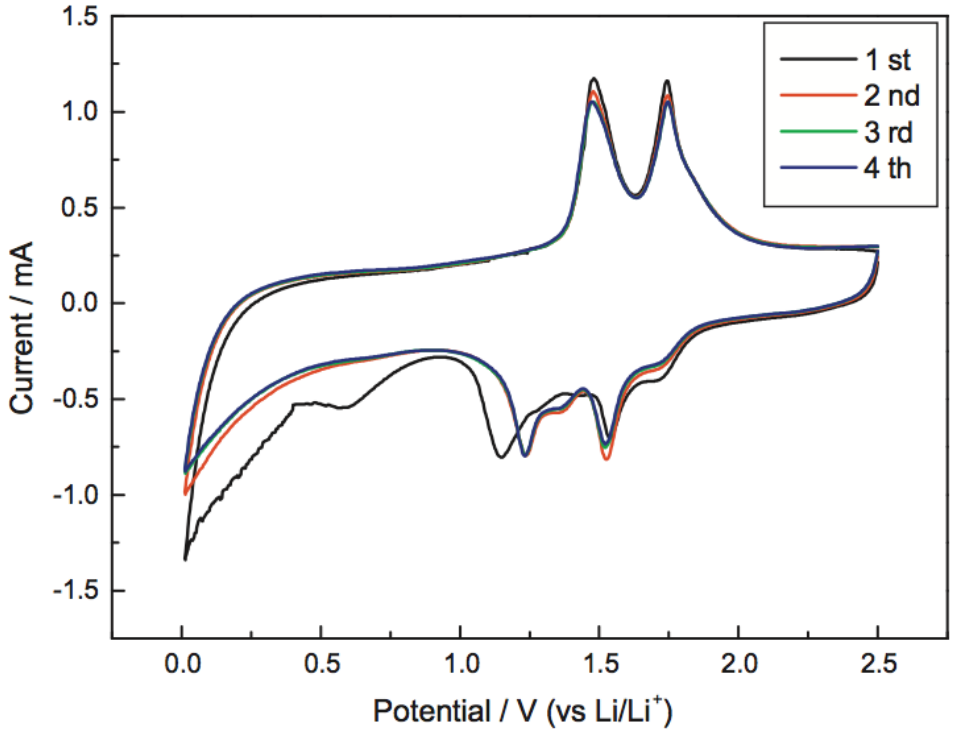

Figure 2.10 Cyclic voltammogram of the MoO_2-graphene nanocomposite. Reprinted from Electrochimica Acta, Vol. 79, Q. Tang, Z. Shan, L. Wang, and X. Qin, "MoO_2–graphene nanocomposite as anode material for lithium-ion batteries," pp. 148–153, Copyright 2012, with permission from Elsevier [20].

Figure 2.11 shows the cycling performance of the MoO_2/graphene nanocomposite in the range of 0.01 – 2.5 V, at current densities of 100 and 500 mA g^{-1}. At a current density of 100 mA g^{-1}, the initial discharge and charge capacities were measured to be 674.4 and 429.9 mA h g^{-1}, respectively [20]. After 50 cycles at 100 mA g^{-1}, the capacity of the electrode actually increases to 1013.7 mA h g^{-1}, and at 60 cycles the capacity is still 1009.9 mA h g^{-1}, which is higher than the theoretical capacity of bulk MoO_2 (828 mA h g^{-1}) [20, 110]. The MoO_2-graphene electrode had a capacity retention of approximately 150%, which may be attributed to the extra Li captured due to the reversible reaction of the –OH and –COOH surface groups of the graphene and the Li [20]. The performance of the nanocomposite is great, however without the graphene the

MoO_2 only had an approximate capacity of 300 mA h g^{-1}, compared to over 1000 mA h g^{-1} when combined with graphene.

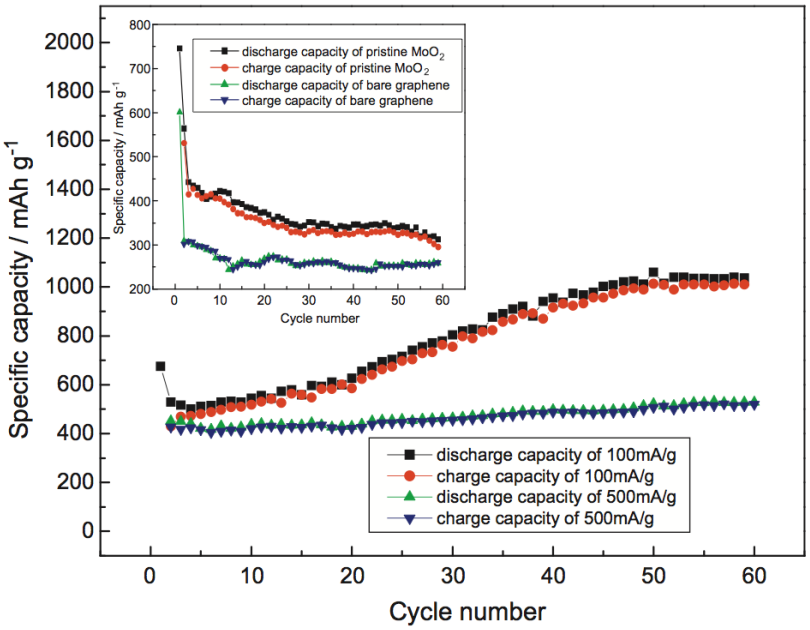

Figure 2.11 Cycling performance of the MoO_2-graphene nanocomposite from 0.01-2.5 V at 100 and 500 mA g^{-1}, with an insert of the cycling performance of both pure Graphene and pure MoO_2 at 100 mA g^{-1}. Reprinted from Electrochimica Acta, Vol. 79, Q. Tang, Z. Shan, L. Wang, and X. Qin, "MoO_2–graphene nanocomposite as anode material for lithium-ion batteries," pp. 148–153, Copyright 2012, with permission from Elsevier [20].

A MoO_2/graphene nanocomposite was synthesized using a low temperature solution-phase reduction process [37]. Briefly, GO was prepared using a modified Hummers method and was then mixed with ammonium heptamolybdate ($(NH_4)_6Mo_7O_{24}*4H_2O$), water, citric acid and poly(ethylene glycol) (PEG). . The resulting mixture was heated in a Teflon-lined stainless steel autoclave, resulting in a black MoO_2/graphene, which was then washed and dried in an inert atmosphere. Figures 2.12a and 2.12b are low and high magnification SEM images of the GO, respectively, showing the layered structure that is typical of graphene. Figure 2.12c is an SEM image of pure MoO_2 showing particles that interconnected with non-uniformed sized grains. Low and high magnification SEM images of the MoO_2/graphene nanocomposite are shown in Figure 2.12d and 2.12e, respectively, where the graphene appears to have fully penetrated the MoO_2.

Figure 2.12f is an elemental map of C, O, and Mo, as well as an EDS spectrum of the MoO_2/graphene nanocomposite. It is clear from the elemental maps that the graphene is uniformly distributed amongst the MoO_2 particles. The EDS spectrum shows only the presence of Mo, C, and O, indicating a complete reaction with no leftover contaminants.

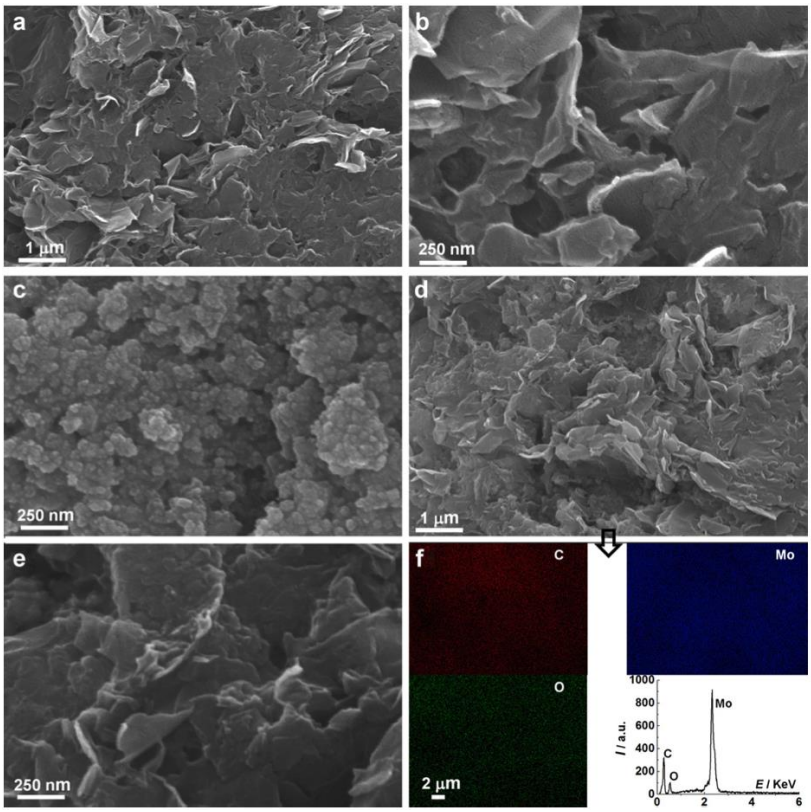

Figure 2.12 (a) and (b) are low and high magnification SEM images or pure graphene, (c) is an SEM image of pure MoO_2, (d) and (e) are low and high magnification SEM images of the MoO_2/graphene nanocomposite, and (f) is an elemental map of Mo, C, and O with an EDS of the MoO_2/graphene nanocomposite. Reprinted from Journal of Power Sources, Vol. 216, Bhaskar, A., M. Deepa, T.N. Rao, and U.V. Varadaraju, Enhanced nanoscale conduction capability of a MoO_2/Graphene composite for high performance anodes in lithium ion batteries, pp. 169-178., Copyright 2012, with permission from Elsevier [37].

Figure 2.13 shows the cyclic voltammetry for the MoO_2/graphene nanocomposite from 0.01 – 3 V at a scan rate of 0.1 mV s^{-1}. There are three main peaks at 1.56 V, 1.28 V and 0.7 V in the first cathodic scan. The peaks at 1.52 V and 1.15 V are evidence of lithium insertion causing a phase transformation from orthorhombic to monoclinic [37, 114]. The peak around 0.7 V in the first cycle is evidence of the formation of a solid electrolyte interphase film. The peaks in

subsequent cycles at 1.52/1.73 V and 1.26/1.51 V are evidence of the lithium insertion and extraction of partially lithiated Li_xMoO_2 [37].

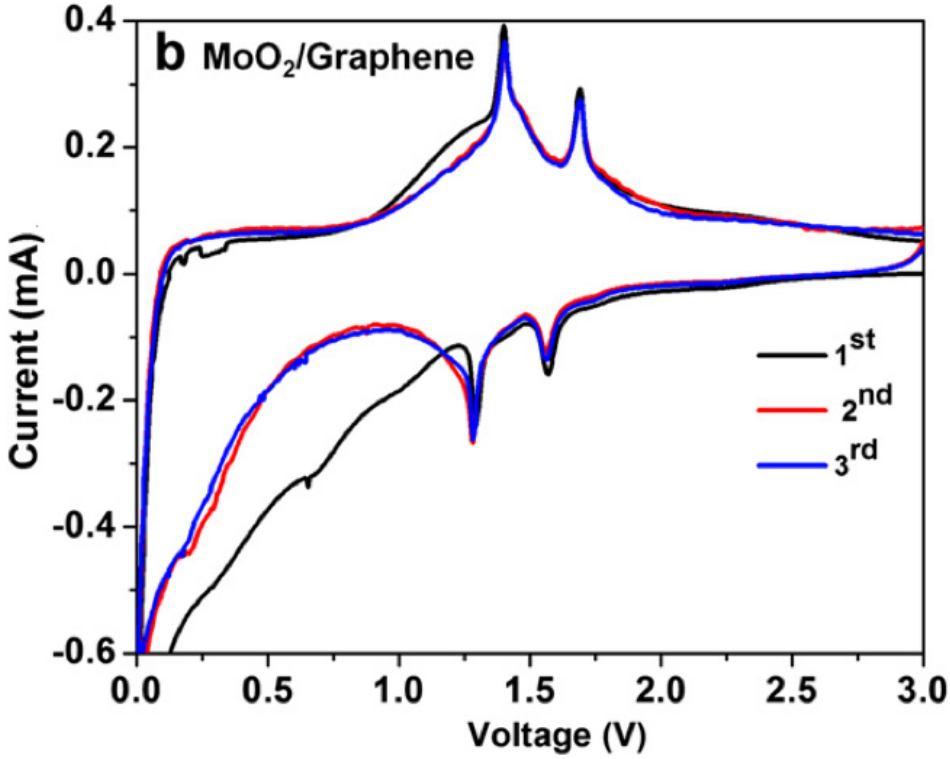

Figure 2.13 Cyclic voltammogram of the MoO_2/graphene nanocomposite. Reprinted from Journal of Power Sources, Vol. 216, Bhaskar, A., M. Deepa, T.N. Rao, and U.V. Varadaraju, Enhanced nanoscale conduction capability of a MoO_2/Graphene composite for high performance anodes in lithium ion batteries, pp. 169-178., Copyright 2012, with permission from Elsevier [37].

Figure 2.14 shows the cycling performance of the MoO_2/graphene nanocomposite in the range of 0.01 – 3.0 V, at a current density of 540 mA g^{-1}. The initial discharge and charge capacities were measured to be 1450 and 703.7 mA h g^{-1}, respectively. After 83 cycles at 540 mA g^{-1}, the capacity of the electrode actually increases to 769.3 mA h g^{-1}. After 1000 charge-discharge cycles the MoO_2/graphene, the capacity is still 530 mA h g^{-1} [37]. The MoO_2/graphene nanocomposite exhibited a capacity retention of approximately 75%, even after 100 cycles. The enhanced retention of the material is most likely due to the graphene layers preventing agglomeration of the MoO_2 nanoparticles, therefore reducing the amount of volume expansion during lithiation as well as increasing the charge transfer and transport [37].

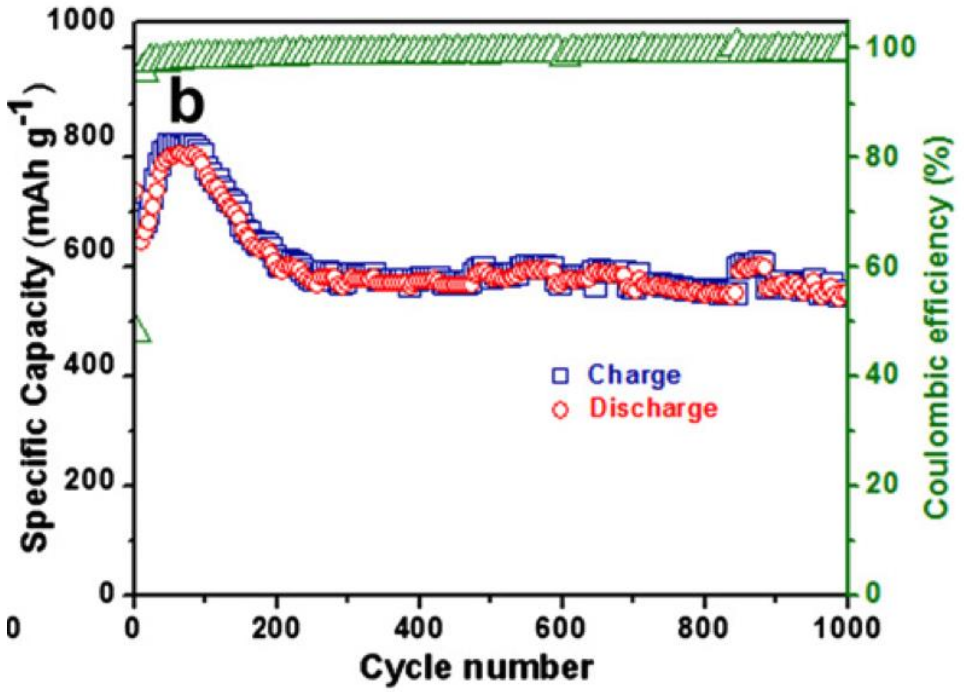

Figure 2.14 Cycling performance of the MoO_2/graphene nanocomposite. Reprinted from Journal of Power Sources, Vol. 216, Bhaskar, A., M. Deepa, T.N. Rao, and U.V. Varadaraju, Enhanced nanoscale conduction capability of a MoO_2/Graphene composite for high performance anodes in lithium ion batteries, pp. 169-178., Copyright 2012, with permission from Elsevier [37].

2.4 Conclusion

Out of all of the available methods to synthesize MoO_2, the hydrothermal synthesis method seems to be most popular, simply judging by the number of papers published using that method. The hydrothermal method is probably most popular due to its simplicity and ability to produce the desired material in a single step. A lot of the other methods require large vacuum chambers, expensive chemicals, or require constant human supervision. With the hydrothermal synthesis technique, all of the necessary precursors are simply added to the pressure vessel, sealed and then placed in the oven for the desired amount of time. This allows for more work to be done while the material is being synthesized.

It is clear that MoO_3 is an excellent photocatalysts, in most cases removing >90% of the pollutant within 3 hours. While MoO_3 certainly appears to be very promising materials for the decontamination of organic pollutants from water, not enough research has been done with MoO_2

to be able to determine its decontamination abilities. However, MoO_2 has been proven to be a very capable anode material for Li-ion batteries, especially when mixed with graphene to overcome the volume expansion and pulverization that would normally occur. It has a theoretical energy storage capacity more than twice the standard graphite anode, as well as superior cyclability.

CHAPTER 3: SYNTHESIS AND CHARACTERIZATION OF MoO_2 NANOPARTICLES AND THEIR ABILITY TO DECONTAMINATE WATER

3.1 Introduction

The decontamination of wastewater containing pollutants, such as organic dyes, specifically from the textile industry, has become a huge research area. Worldwide, the textile industry is responsible for up to 20% of the dyes used, followed by paper printing, leather production, photography, coating, and photochemical industries [122, 123]. Not only are these dyes toxic, carcinogenic and mutagenic, but the presence of these dyes in water can cause a depletion of dissolved oxygen, causing even more issues. Some estimates show that 10-15% of the dye used in the textile processing industry are lost into the effluent [124, 125].

As more research is conducted in this area, new materials are constantly being discovered to decontaminate the dyes from water. While there have been numerous reports of the use of Molybdenum oxide (MoO_3) to decontaminate water [79, 82, 86, 90, 92, 95, 103, 126], there have only been a couple reports of the use of MoO_2 to decontaminate water, however the results have been promising [23, 24]. In this paper, we have synthesized nanostructured MoO_3 and MoO_2 and tested their abilities to decontaminate methylene blue (MB) from an aqueous solution.

3.2 Experimental

3.2.1 Synthesis

MoO_3, ammonium molybdate (AM), and ethylene glycol (EG) were purchased from Sigma Aldrich and used without any modification unless otherwise noted.

3.2.1.1 Synthesis of Nanostructured Molybdenum Trioxide (AM-MoO_3)

Ammonium molybdate was heated in an oven at 350 °C for 12 hours to form nanostructured MoO_3, which was labeled AM-MoO_3 to distinguish it from the commercially produced MoO_3 from Sigma Aldrich.

3.2.1.2 Synthesis of Molybdenum Dioxide (MoO_2)

Two sets of experiments were conducted to synthesize MoO_2; one set of experiments using MoO_3, and the other set of experiments using the nanostructured AM-MoO_3.

Initially 75 mg of either MoO_3 or AM-MoO_3 was continuously stirred into 7.5 mL of deionized water and 2.5 mL of ethylene glycol. The mixture was added to a teflon lined stainless steel pressure, sealed, and heated at 180 °C for 12 hours. The resulting reaction produced a black powder that was subsequently separated via centrifugation and cleaned with ethanol and deionized water. The powder was then dried overnight in an oven at 80 °C. Figure 3.1 shows a schematic of the MoO_3 reduction to MoO_2 nanoparticles using ethylene glycol as the reducing agent.

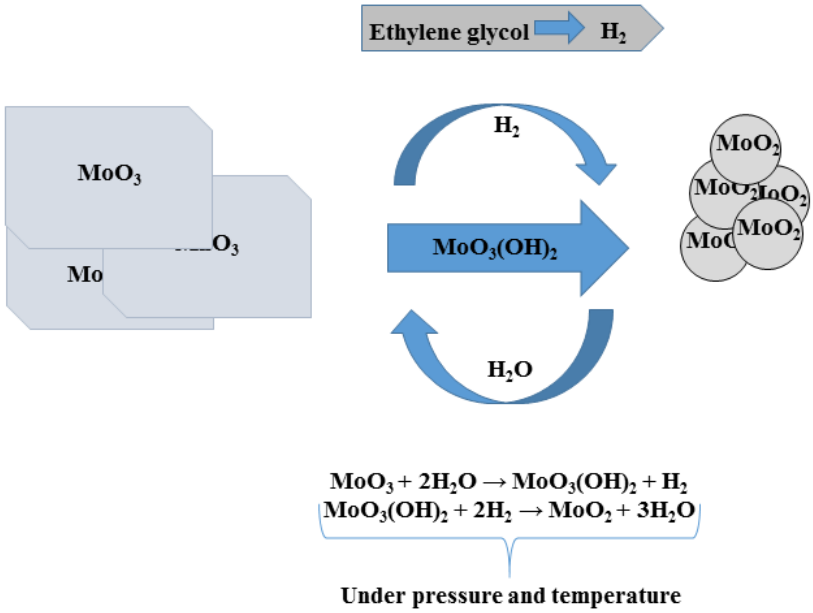

Figure 3.1 Schematic of the reduction of MoO_3 to MoO_2.

A summary of the various experiments conducted is shown in Table 3.1.

Table 3.1 Summary of MoO_2 synthesis experiments.

Sample	Amount of MoO_3 or AM-MoO_3 (mg)	Amount of H_2O (mL)	Amount of EG (mL)	Time (hours)
MoO_2	75	7.5	2.5	12
AM-MoO_2	75	7.5	2.5	12
MoO_2-2h	75	7.5	2.5	2
MoO_2-4h	75	7.5	2.5	4
MoO_2-6h	75	7.5	2.5	6
MoO_2-8h	75	7.5	2.5	8

3.2.2 Characterization

X-ray diffraction (XRD) patterns were collected from the samples using a PANalytical X'Pert PRO diffractometer with CuKα radiation (λ=1.5406 Å). Scanning electron microscope (SEM) images were acquired with a Hitachi SU-70 ultra-high resolution SEM at various operating voltages. High resolution transmission electron microscope (HR-TEM) images were acquired with a FEI TECNAI F20 TEM at 200kV.

3.2.3 Water Decontamination Setup

The degradation of an aqueous solution of methylene blue (MB) was used to determine the ability of the samples to decontaminate organic pollutants from water with and without exposure to visible light. Visible light was provided by a 30 watt light bulb with an intensity of 800 W/m^2. To prepare the aqueous MB solution, 10mg of MB was continuously stirred in to 1 L of water, yielding a concentration of 10 mg L^{-1}, which is a commonly used concentration for degradation experiments [24, 95, 103]. In a typical decontamination experiment, 5mg of sample material were continuously stirred in to 10 mL of MB solution. Samples were collected at 1 minute intervals for 5 minutes, and a final sample was collected at 10 minutes. The samples were immediately placed into the centrifuge upon collection to minimize any extra time the particles were exposed to the contaminant. Once the sample material had been separated from the MB solution, the MB solution was analyzed using a Jasco J-530 UV-Vis Spectrophotometer to determine the concentration of

MB remaining in the solution, using the characteristic absorption peak of MB around 661 nm. A step-by-step schematic of this process is shown in Figure 3.2.

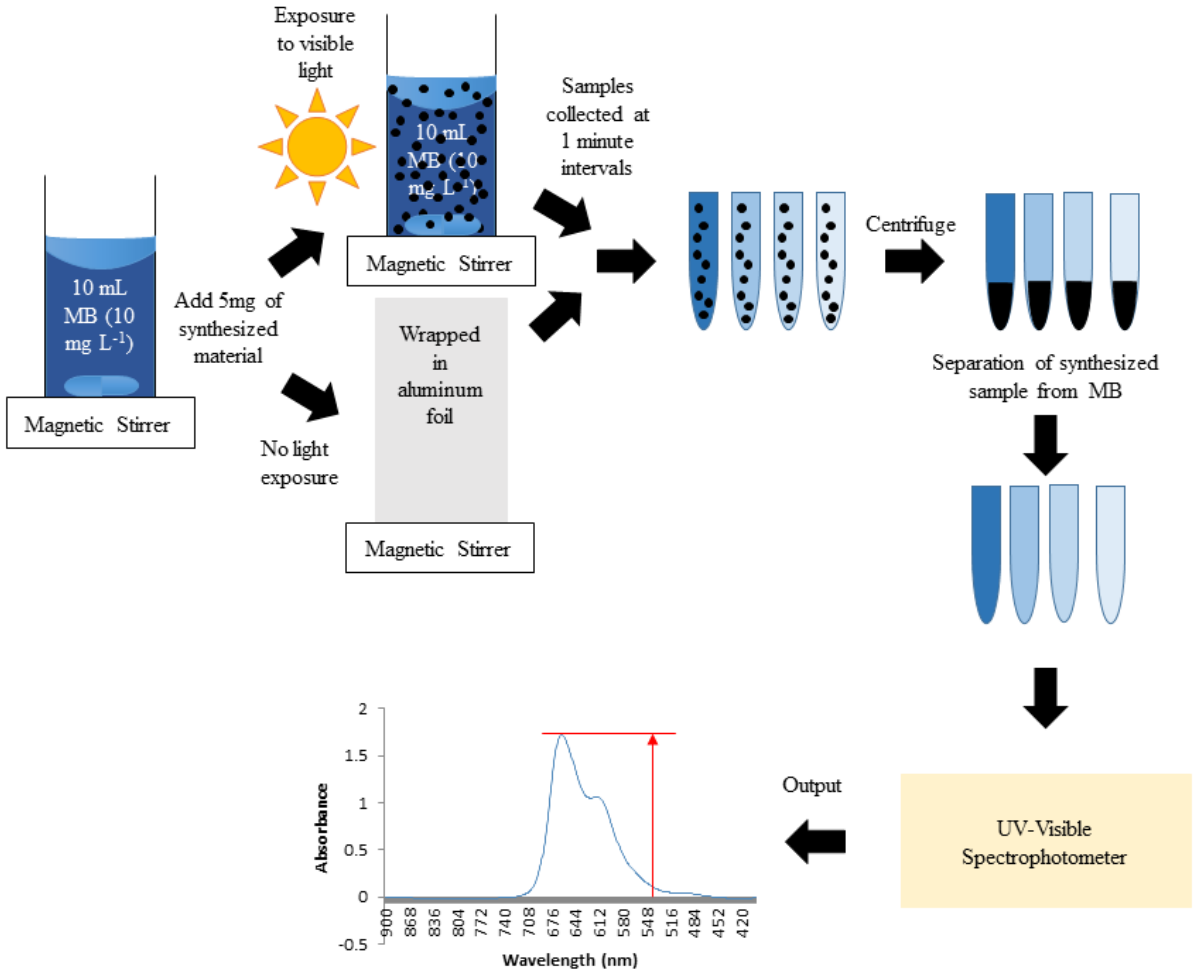

Figure 3.2 Step-by-step schematic of the typical MB degradation experiment, sample collection and analysis process.

3.3 Results and Discussion

3.3.1 Electron Microscopy

An SEM image of the commercial MoO_3 is shown in Figure 3.3a. The image reveals the material has a platelet like structure, with large particles up to 20 µm long. Meanwhile, an SEM image of the AM-MoO_3 is shown in Figure 3.3b, where it is clear that the AM-MoO_3 still has the same platelet-like structure as the commercial MoO_3, except the platelets are now nano-sized. The

nanostructured AM-MoO_3 platelets are a few hundred nanometers wide, with the largest particles around 1µm long. It is also clear from the SEM images that the AM-MoO_3 seems to be much more uniform in size and shape compared to the commercial MoO_3. Figure 3.3c shows an SEM image of the hydrothermally synthesized MoO_2 nanoparticles. It is clear that the MoO_2 nanoparticles are relatively uniform in shape and size, with most particles ranging from 30 to 50 nm. Figure 3.3d shows an SEM image of the AM-MoO_2 nanoparticles ranging from 30 to 50 nm. It is clear that there are no longer any AM-MoO_3 platelets present, indicating all of the AM-MoO_3 has been reduced to MoO_2, as also confirmed by XRD.

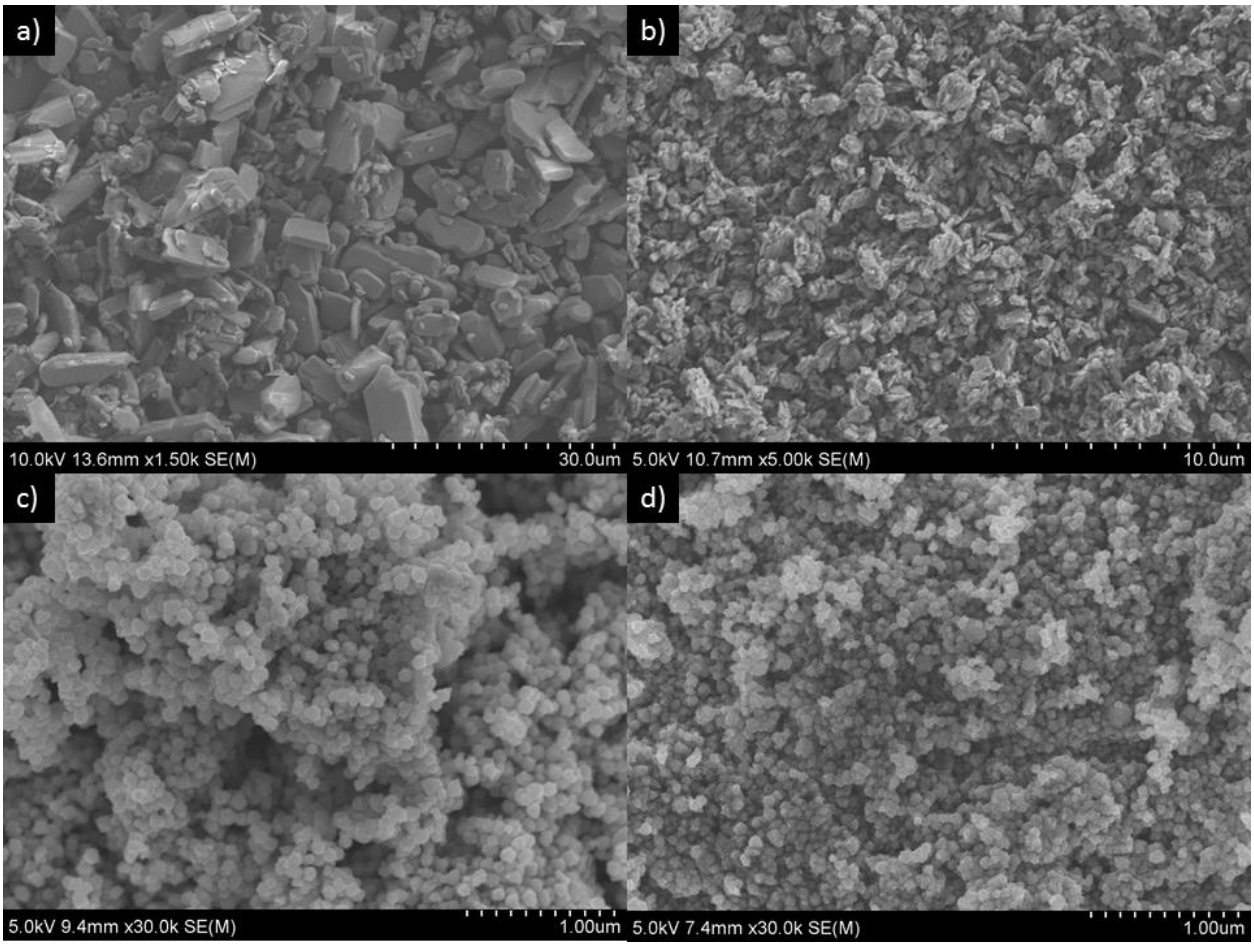

Figure 3.3 SEM images of a) MoO_3, b) AM-MoO_3, c) MoO_2, and d) AM-MoO_2.

A TEM image of the hydrothermally synthesized MoO_2 is shown in Figure 3.4. Both the TEM image and the inset diffraction pattern show an atomic d-spacing of approximately 1.7, 2.4

and 3.4 Å, which correspond to the (-111), (111) and (022) planes of monoclinic MoO_2, respectively. The d-spacing values obtained from the TEM match the d-spacing results obtained from XRD, further confirming the formation of monoclinic MoO_2.

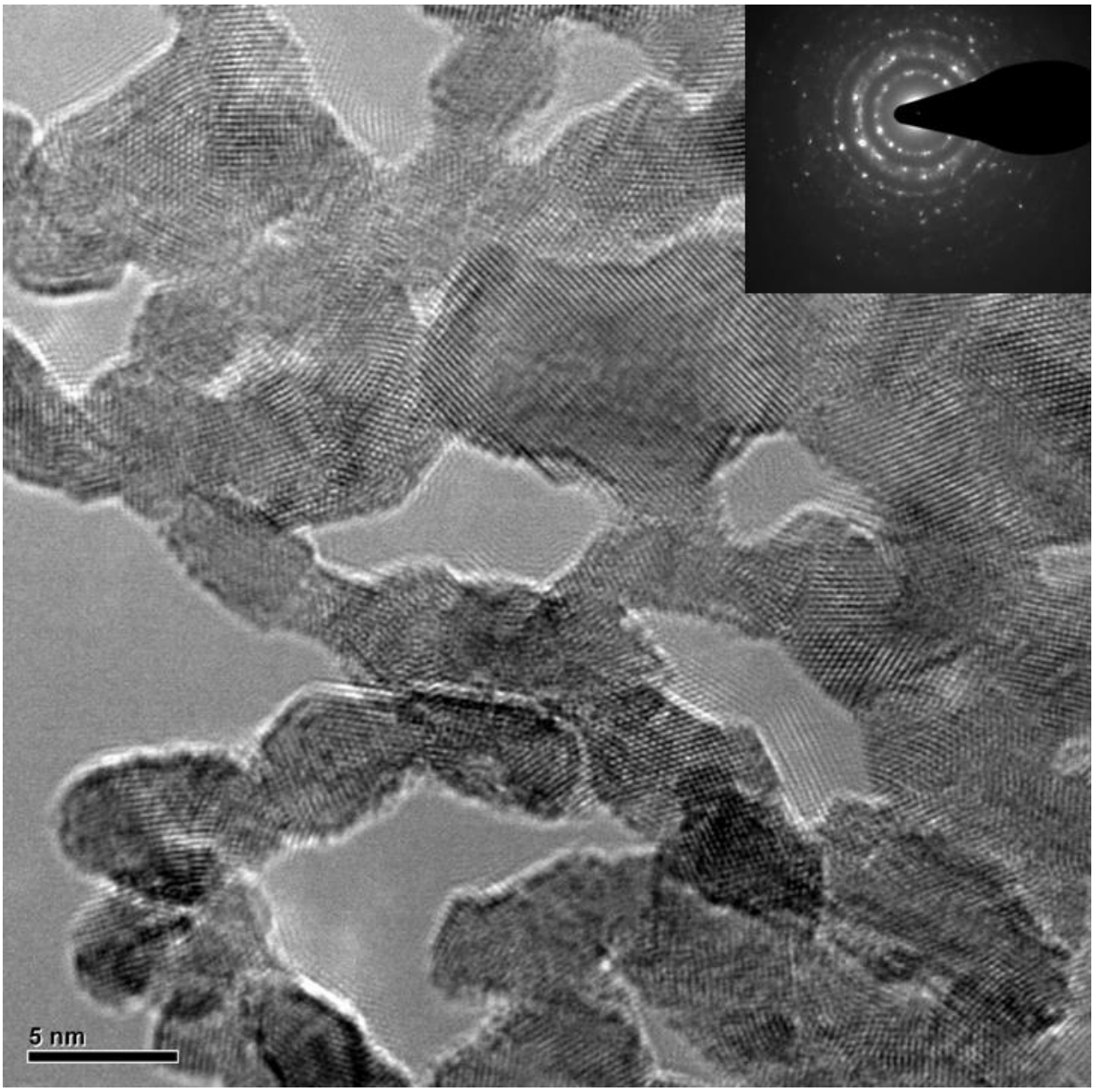

Figure 3.4 HR-TEM image of MoO_2, with the selected area diffraction pattern inset.

The results from the time dependent experiment are shown in Figure 3.5. The 2 hour sample shown in Figure 3.5a clearly shows that the MoO_3 platelets had already been reduced to form MoO_2 nanoparticles, however a few larger pieces are still present. As the reaction time progresses

to 4 hours or more, it is clear that the MoO_3 platelets have been completely reduced, leaving only uniform MoO_2 nanoparticles, as confirmed by XRD.

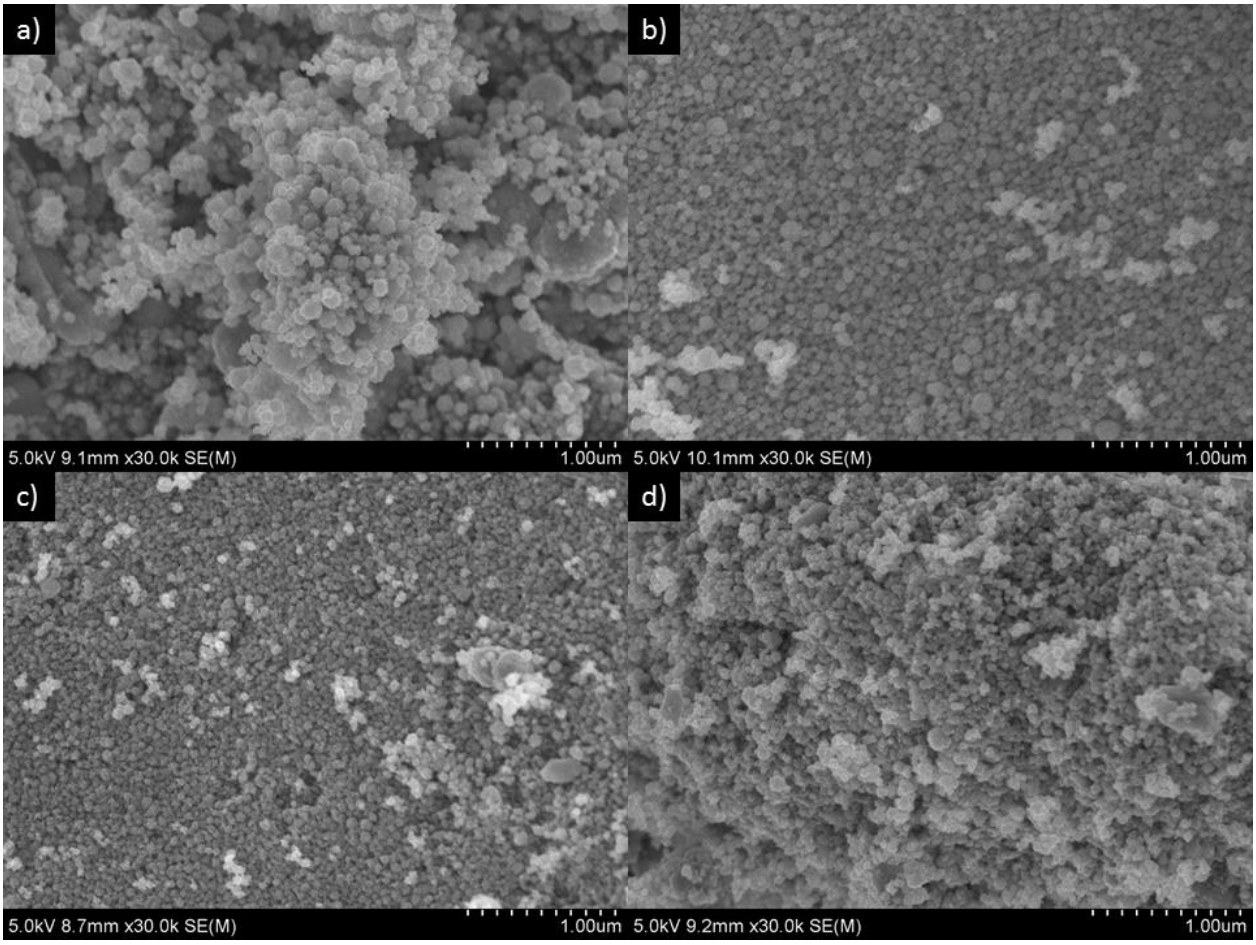

Figure 3.5 SEM images of MoO_2 after a reaction time of a) 2 hours, b) 4 hours, c) 6 hours and d) 8 hours.

3.3.2 X-ray Diffraction (XRD)

XRD patterns for MoO_3, AM-MoO_3, MoO_2, and AM-MoO_2 are shown in Figure 3.6. Both the MoO_3 and AM-MoO_3 powders can be indexed to the orthorhombic phase of MoO_3; with major characteristic diffraction peaks at 12.77°, 23.33°, 25.70°, 27.32°, and 38.97°, which correspond to the (020), (110), (040), (021), and (060) planes, respectively. The diffraction peaks for AM-MoO_3 are less intense and slightly broader that the diffraction peaks for MoO_3, indicating the AM-MoO_3 has a smaller crystallite/particle size, as later confirmed by SEM. The diffraction patterns for both

MoO_2 and AM-MoO_2 can be indexed to the monoclinic phase of MoO_2, with major characteristic peaks at 26.11°, 36.75°, 53.69°, which correspond to the (-111), (200),and (022) planes, respectively. Again it is clear that the diffraction peaks for both MoO_2 and AM-MoO_2 have an even lower intensity and are even broader than the diffraction peaks for AM-MoO_3, indicating even smaller crystallite/particle size, as later confirmed by SEM.

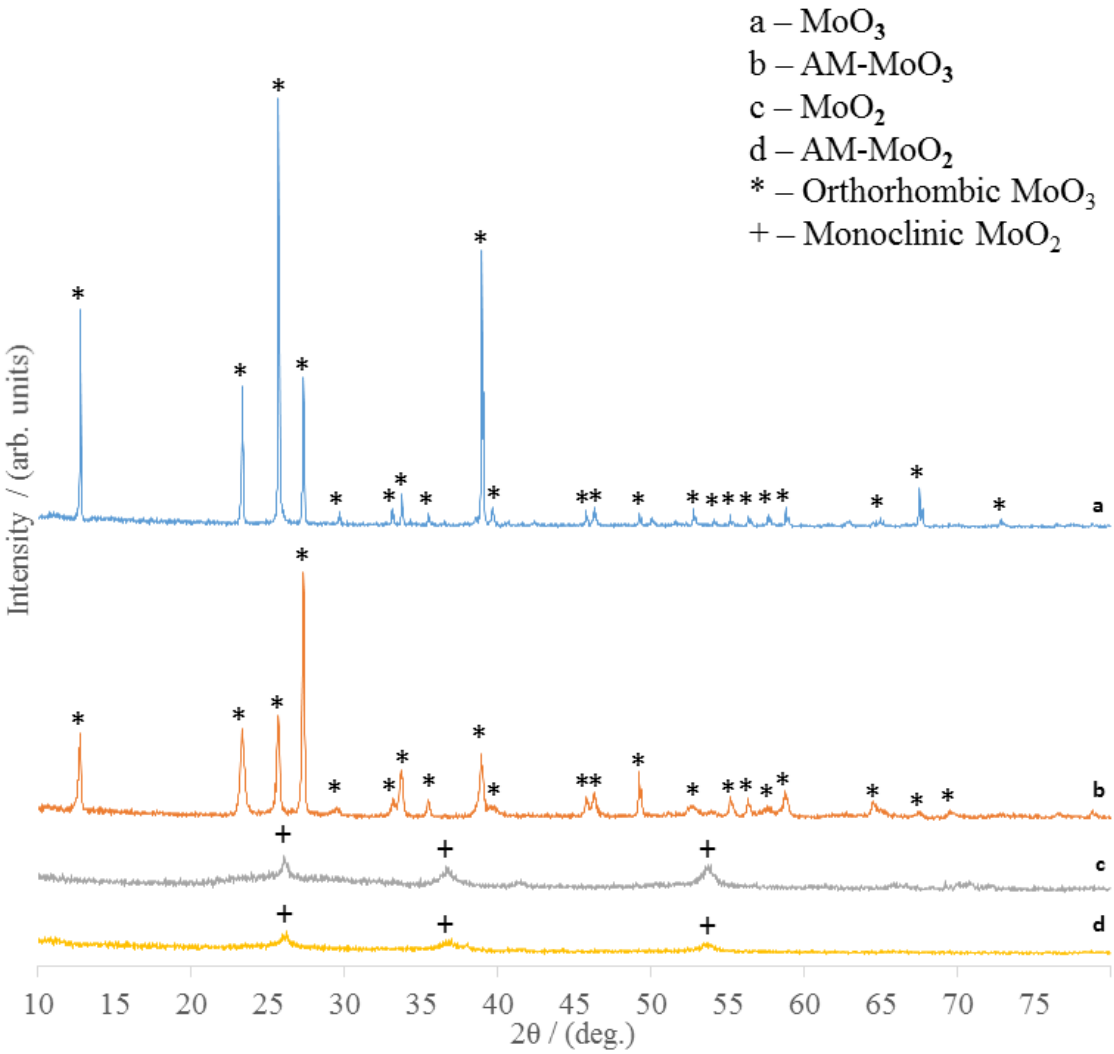

Figure 3.6 XRD patterns for the various samples.

XRD patterns for the time dependent experiments are shown in Figure 3.7. It is clear that within 2 hours all of the MoO_3 has been completely reduced to MoO_2, as there are no longer any characteristic diffraction peaks related to MoO_3.

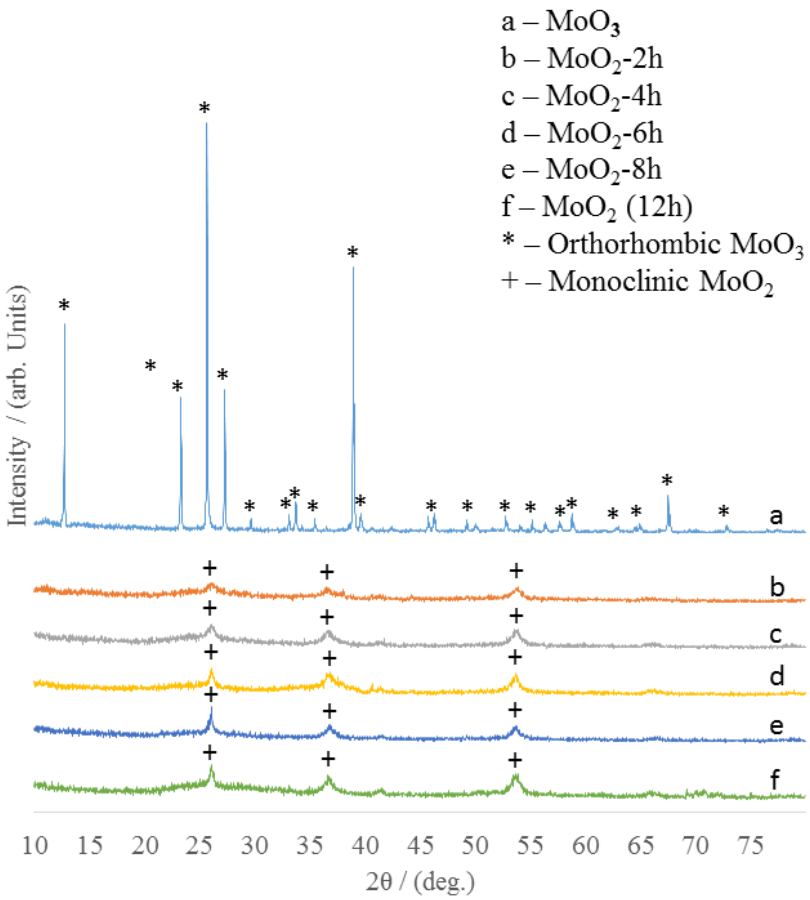

Figure 3.7 XRD patterns for the time dependent experiments.

3.3.3 Decontamination

To determine the ability of the samples to decontaminate organic pollutants from water, experiments were conducted to measure the degradation of MB. Until now, all previous reports of MoO_2 and MoO_3 for the decontamination of water have been photocatalytic, requiring the sample be exposed to ultraviolet (UV) or visible light radiation. In these previous decontamination experiments the sample was mixed in to the MB solution with no exposure to light, and allowed to mix for at least 30 minutes to come to an adsorption/desorption equilibrium. At that point, the samples were then exposed to either UV or visible light radiation for a determined period of time [24, 79, 82, 86, 90, 92, 95, 103]. When this same experiment was attempted with the hydrothermally synthesized MoO_2 and AM-MoO_2 detailed above, the MB had been completely

decontaminated by the end of the 30 minute adsorption/desorption equilibrium. At that point, it became clear that the MoO_2 and AM-MoO_2 materials were highly adsorbent; so the experiment was modified to see how quickly the samples could adsorb the MB, and if the exposure of visible light affected the rate at which the MB was decontaminated.

For this decontamination experiment, 2 sets of experiments were conducted; one set with exposure to visible light radiation and one set with no exposure to light. Typically, 5 mg of sample was added to 10 mL of MB (10 mg L^{-1}) under continuous stirring. The concentration of MB was monitored using UV-visible spectrophotometry, and measuring the maximum absorbance at the characteristic wavelength of MB, near 661 nm, as shown in Figure 3.8. The initial concentration, C_0, of MB was measured before any material was added, and then the concentration was measured from the samples collected in 1 minute intervals.

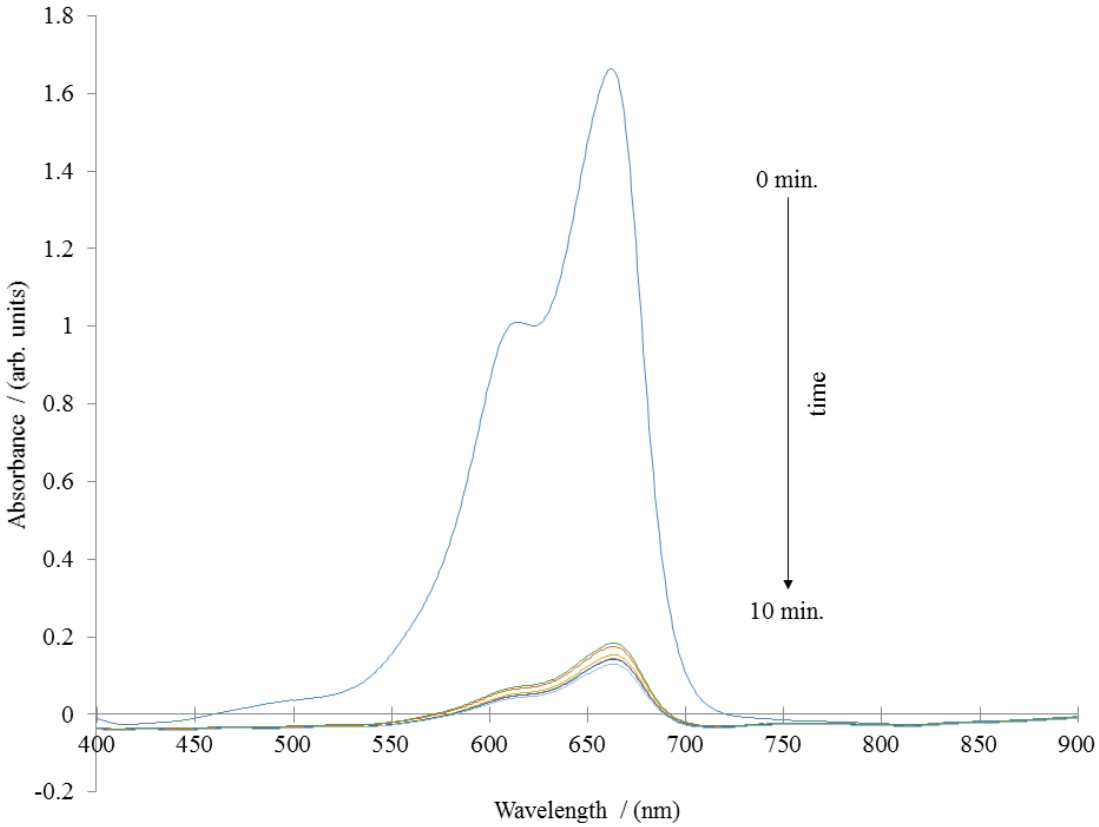

Figure 3.8 UV-visible absorption spectra for AM-MoO_3 with no light exposure.

Figure 3.9 shows a plot of the concentration, C, over time that has been normalized to the initial MB concentration (C/C_0).

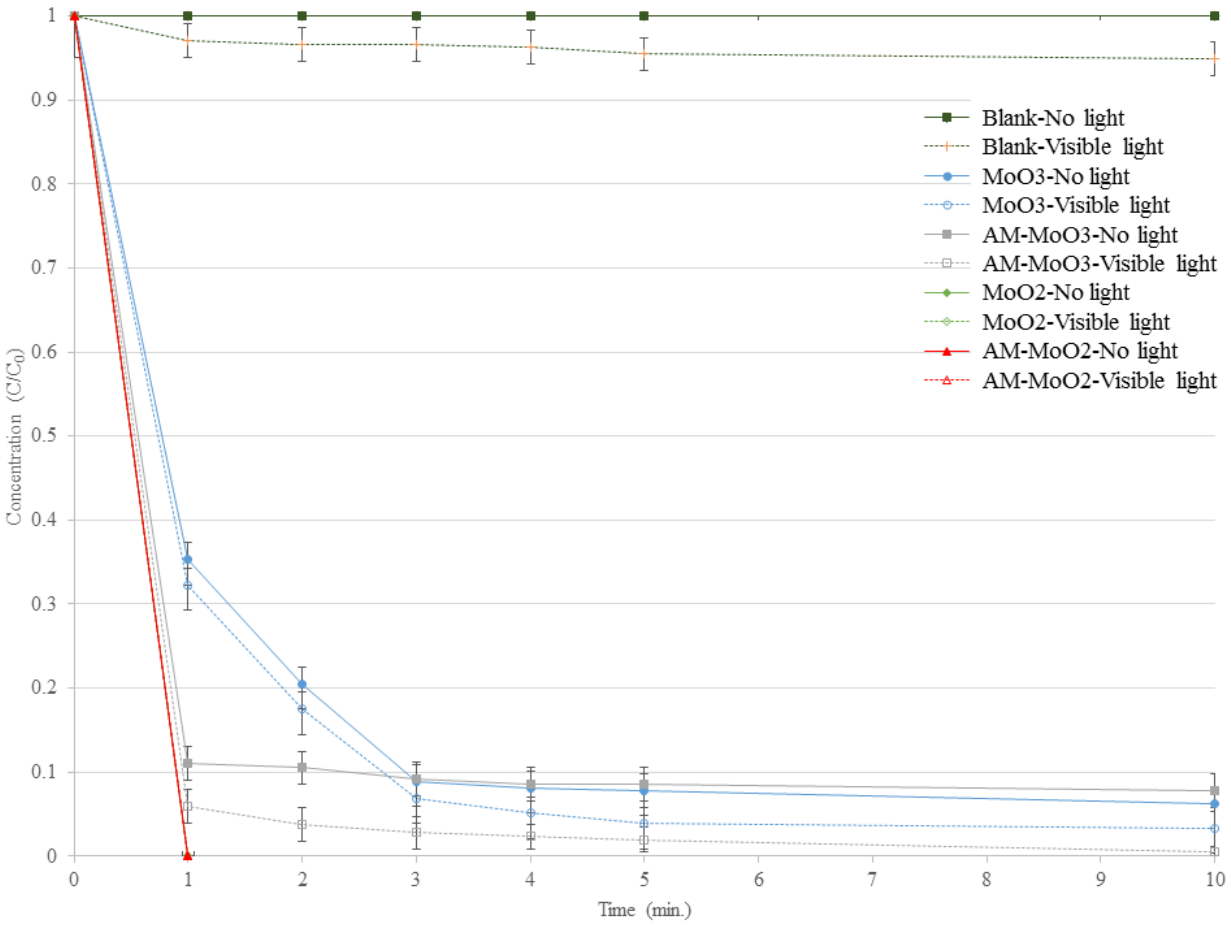

Figure 3.9 Concentration (C/C_0) vs. time (min) for the decontamination of 10 mL MB by 5 mg of sample.

With no exposure to light, the MB is degraded less than 0.5% during the 10 minute period. If exposed to light, the MB degraded about 5% during that same 10 minute period, leaving 95% of the MB remaining. When MoO_3 was added to a MB solution, with no visible light exposure, over 90% of the MB was adsorbed within the first 3 minutes, and 93.7% adsorbed by the end of 10 minutes. When MoO_3 was added to a MB solution, with visible light exposure, over 93% of the MB was removed within the first 3 minutes, and 96.7% removed by the end of 10 minutes. When AM-MoO_3 was added to a MB solution, with no visible light exposure, 89% of the MB was

adsorbed within the first minute, and 92.3% adsorbed by the end of 10 minutes. When AM-MoO_3 was added to a MB solution, with visible light exposure, over 94% of the MB was removed within the first minute, and over 99.4% removed by the end of 10 minutes. When MoO_2 was added to a MB solution, with or without visible light exposure, 100% of the MB was removed within 1 minute. The same thing happened when AM-MoO_2 was added to a MB solution; regardless of light exposure, 100% of the MB was removed within 1 minute. A summary of these results is shown in Table 3.2.

Table 3.2 Decontamination results for 5 mg of sample in 10 mL MB (10 mg L^{-1})

Sample	Amount of MB decontaminated	Time
Blank - No light exposure	0.05%	10 min
Blank - Visible light exposure	5.1%	10 min
MoO_3 - No light exposure	93.7%	10 min
MoO_3 - Visible light exposure	96.7%	10 min
AM-MoO_3 - No light exposure	92.3%	10 min
AM-MoO_3 - Visible light exposure	99.4%	10 min
MoO_2 - No light exposure	100%	1 min
MoO_2 - Visible light exposure	100%	1 min
AM-MoO_2 - No light exposure	99.95	1 min
AM-MoO_2 - Visible light exposure	100%	1 min

Since both the MoO_2 and AM-MoO_2 performed the exact same for the previous experiment, the experiment was modified again to test 5 mg of sample in 50 mL of MB with exposure to: visible light radiation, UV light radiation, and no light exposure. It is clear from Figure 3.10 that both the MoO_2 and AM-MoO_2 performed incredibly well, and that the MoO_2 was able to absorb 99.6% of the MB within one minute, and 100% within two minutes, with no exposure to visible light. When the MoO_2 was exposed to visible light, it was able to remove 100% of the MB within the first minute. The AM-MoO_2 was able to absorb 99.95% of the MB within one minute, and 100% within two minutes, with no exposure to visible light. When the AM-MoO_2 was exposed to visible light, it was able to remove 100% of the MB within the first minute.

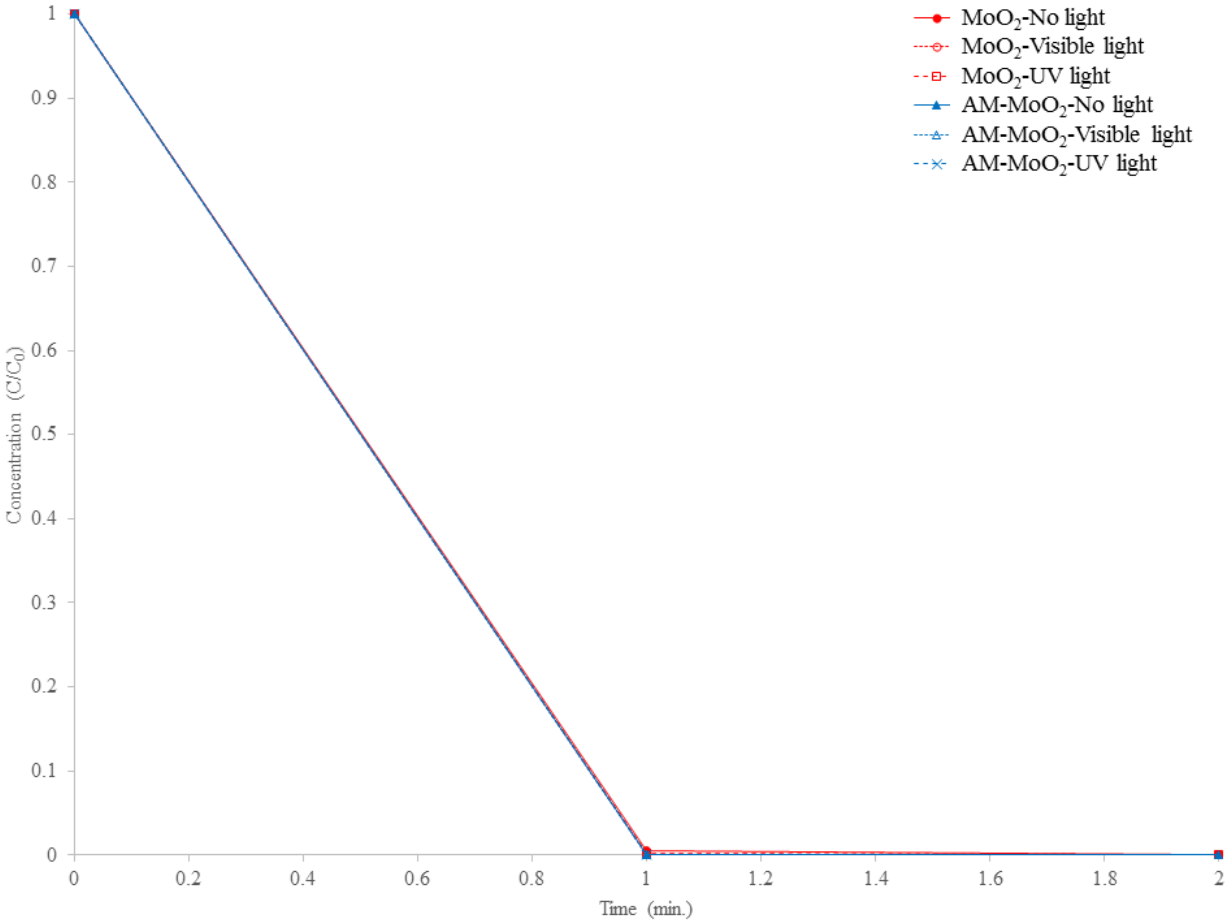

Figure 3.10 Concentration (C/C_0) vs. time (min) for the decontamination of 50 mL MB by 5 mg of sample.

A summary of these results is shown in Table 3.3.

Table 3.3 Decontamination results for 5 mg of sample in 50 mL of MB (10 mg L^{-1}).

Sample	Amount of MB decontaminated in 1 min	Amount of MB decontaminated in 2 min
MoO_2 - No light exposure	99.56%	100%
MoO_2 - Visible light exposure	100%	N/A
MoO_2 - UV light exposure	99.82	100%
AM-MoO_2 - No light exposure	99.95%	100%
AM-MoO_2 - Visible light exposure	100%	N/A
AM-MoO_2 - UV light exposure	100%	N/A

To determine how the MB and MoO_2 were bonding with each other, FTIR measurements were taken and are shown in Figure 3.11. It is clear that the ethylene glycol has functionalized the MoO_2, as indicated by the peaks around 2900, 1600, and 800 cm^{-1}.

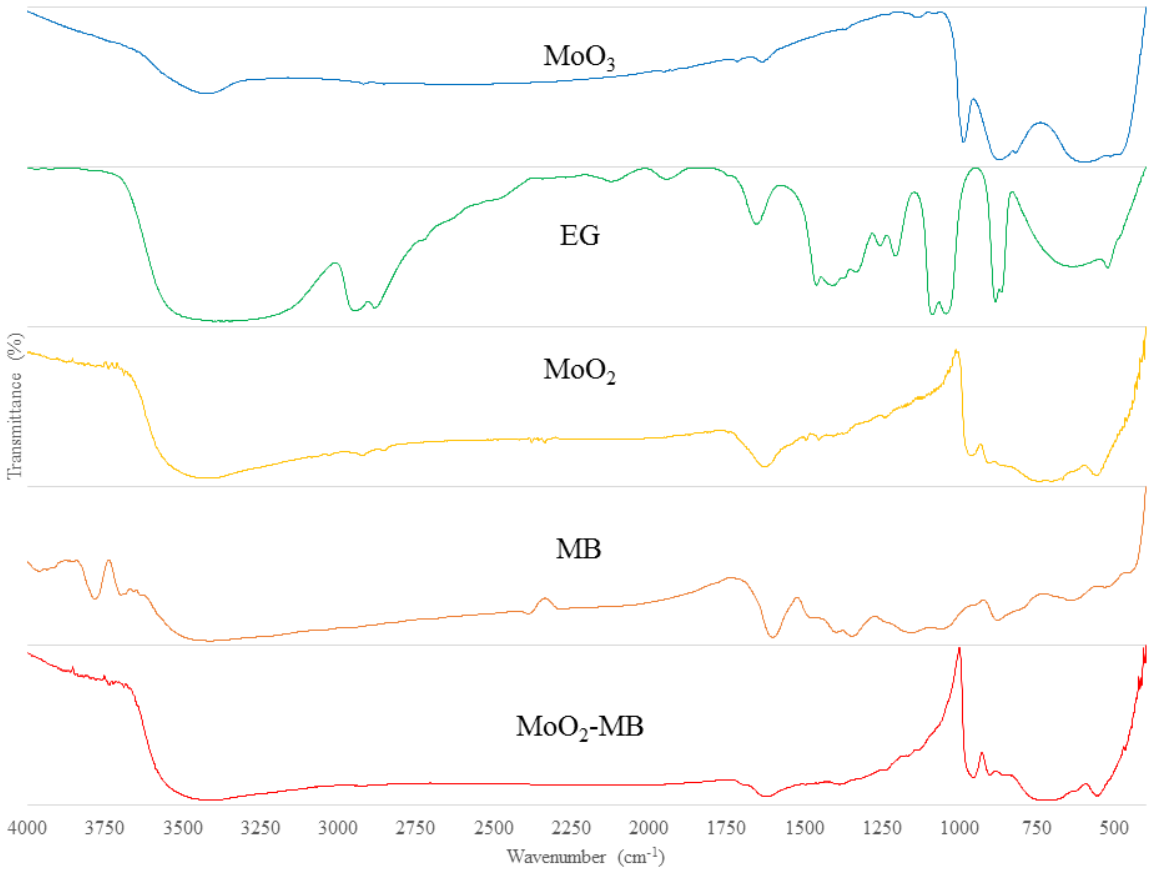

Figure 3.11 FTIR data showing the functionalization of MoO_2.

Figure 3.12 shows a possible mechanism for the adsorption of MB onto the MoO_2 due to the functionalization from ethylene glycol, where oxygen from the MoO_2 and sulfur from the MB are attracted due to having the opposite charge. In the presence of visible light, the oxygen transfers an electron to the sulfur, generating an electron hole pair. This electron hole pair can than react with available oxidants and reductants to form radials, which cause the MB to be broken down into CO_2, H_2O, and other byproducts.

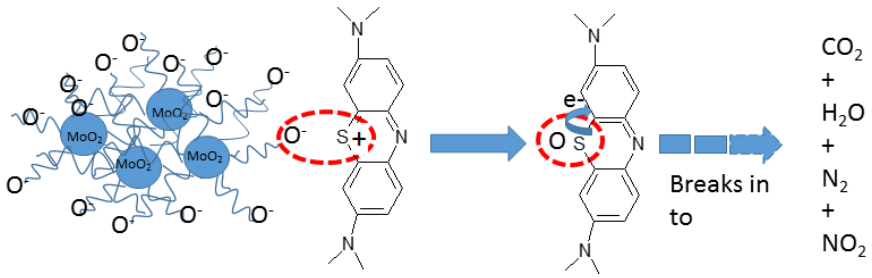

Figure 3.12 Possible mechanism for the adsorption and photocatalytic remediation of MB.

Table 3.4 shows a comparison of the results obtained in this report versus the previously reported data for the decontamination of water using MoO_2. It is clear that the results from the MoO_2 nanoparticles from this report are significantly better than previous reports.

Table 3.4 Comparison of decontamination results with previously published data.

Sample	Sample Weight	Pollutant (volume)	Pollutant Concentration	Source of irradiation	Decontamination	Time	Ref.
MoO_2	500 mg	Methylene Blue (50 mL)	10 mg L^{-1}	UV light	30%	140 min	[24]
MoO_2	500 mg	Rhodamine B (50 mL)	10 mg L^{-1}	UV light	70%	140 min	[24]
MoO_2	25 mg	Rhodamine B (50 mL)	10 mg L^{-1}	UV and visible light	15.8%	90 min	[23]
MoO_2	5 mg	Methylene Blue (50 mL)	10 mg L^{-1}	No light exposure	100%	2 min	This work
MoO_2	5 mg	Methylene Blue (50 mL)	10 mg L^{-1}	Visible light	100%	1 min	This work
MoO_2	5 mg	Methylene Blue (50 mL)	10 mg L^{-1}	UV light	100%	2 min	This work
AM-MoO_2	5 mg	Methylene Blue (50 mL)	10 mg L^{-1}	No light exposure	100%	2 min	This work
AM-MoO_2	5 mg	Methylene Blue (50 mL)	10 mg L^{-1}	Visible light	100%	1 min	This work
AM-MoO_2	5 mg	Methylene Blue (50 mL)	10 mg L^{-1}	UV light	100%	1 min	This work

3.4 Conclusion

MoO_2 nanoparticles were hydrothermally synthesized using MoO_3 or nanostructured AM-MoO_3 as the molybdenum precursor. SEM and TEM were used to determine the size and morphology of the particles, while XRD was used to confirm composition and crystallinity of the samples. During the decontamination experiments, it became obvious that the synthesized MoO_2 and AM-MoO_2 samples appear to have both adsorbent properties and photocatalytic properties;

something that has not been previously reported. In every single experiment conducted, the same sample always decontaminated the MB faster when exposed to light. Even with only 5 mg of sample in 50 mL of MB (10 mg L^{-1}), both materials were able to adsorb 100% of the MB within 2 minutes when not exposed to light, and in only one minute when the samples were exposed to visible light. The best results were able to remove 100% of the MB using up to 100 times less sample (500 mg vs. 5 mg), and up to 140 times less time (140 min vs. 1 min) than previously reported.

CHAPTER 4: MORPHOLOGY CONTROLLED SYNTHESIS OF MoO_2 NANOSTRUCTURES AND THEIR ABILITY TO DECONTAMINATE WATER

4.1 Introduction

The controlled morphology of a material during the synthesis process is one of the biggest challenges in nanoscience and nanotechnology, since the size and shape of the synthesized material can greatly change the properties of a material [7, 22, 35, 127-135]. Cetyltrimethylammonium bromide (CTAB) is a commonly used cationic surfactant employed to modify the morphology of materials [134-146]. There have been several detailed reports of using CTAB to modify MoO_3 [134, 140], but there appears to be very few reports for using CTAB to modify MoO_2 [147], and none of the reports for MoO_2 have shown how concentration of CTAB will affect the morphology of the material.

Herein, we present a simple, one-step hydrothermal synthesis method for various MoO_2 morphologies, including nanoparticles, nanospheres, and microspheres (solid and hollow). We have proposed a possible formation mechanism, as well as tested the materials ability to decontaminate methylene blue (MB) from water, with and without exposure to visible light.

4.2 Experimental

All chemicals were purchased from Sigma Aldrich and used without any modification unless otherwise noted.

4.2.1 Synthesis of Molybdenum Dioxide (MoO_2)

Initially 75 mg of MoO_3 was added to 7.5 mL of various concentrations of cetyltrimethylammonium bromide (CTAB) under magnetic stirring. The concentrations of CTAB ranged from 0.1, 0.5, 1, 2.5, 5, 10, and 15 millimolar (mM). Then 2.5 mL of ethylene glycol was added to the mixture under continued stirring. The mixture was poured into a teflon lined stainless steel pressure vessel and heated at 180 °C for 12 hours. The resulting reaction produced a black precipitate, which was then separated and cleaned via centrifugation with ethanol and DI water. The resulting powder was dried overnight in an oven at 80 °C. The samples were labeled 0.1 mm MoO_2, 0.5 mm MoO_2, 1 mm MoO_2, etc.

4.2.2 Characterization

A PANalytical X'Pert PRO diffractometer with Cu Kα radiation (λ=1.5406 Å) was used to collect x-ray diffraction (XRD) patterns from the samples. A Hitachi SU-70 ultra-high resolution scanning electron microscope (SEM) was used to acquire SEM images of the samples. And an FEI TECNAI F20 transmission electron microscope (TEM) was used to acquire TEM images.

4.2.3 Water Decontamination Setup

To measure the ability of the samples to decontaminate organic pollutants from water, the degradation of an aqueous methylene blue (MB) solution was measured with and without exposure to visible light. A 30 watt lightbulb with an intensity of 800 W/m^2 was used as the visible light source. In a typical setup, 5mg of the synthesized sample was continuously stirred in to 10 mL of MB (10 mg L^{-1}). Samples were collected once per minute for the first 5 minutes, and a final sample was collected at 10 minutes. An initial sample of MB was collected before the addition of any particles. The samples were than analyzed using a Jasco J-530 UV-Vis Spectrophotometer to determine the concentration of MB remaining in the water.

4.3 Results and Discussion

4.3.1 Electron Microscopy

Figures 4.1a and 4.1b show SEM images of the MoO_3 precursor. It is clear from the image that the MoO_3 consists of relatively large platelets that are up to 20 µm in length, with smaller platelets mixed in. Figure 4.1c and 4.1d show SEM images of the hydrothermally synthesized 0.1 mM CTAB MoO_2. It is clear from the image that there is no hierarchy to the 0.1 mM CTAB MoO_2 nanoparticles, which ranged in size from approximately 30-50 nm. It is also clear from the SEM images that there are no MoO_3 platelets visible in the synthesized material, indicating a complete conversion from MoO_3, as later confirmed by XRD.

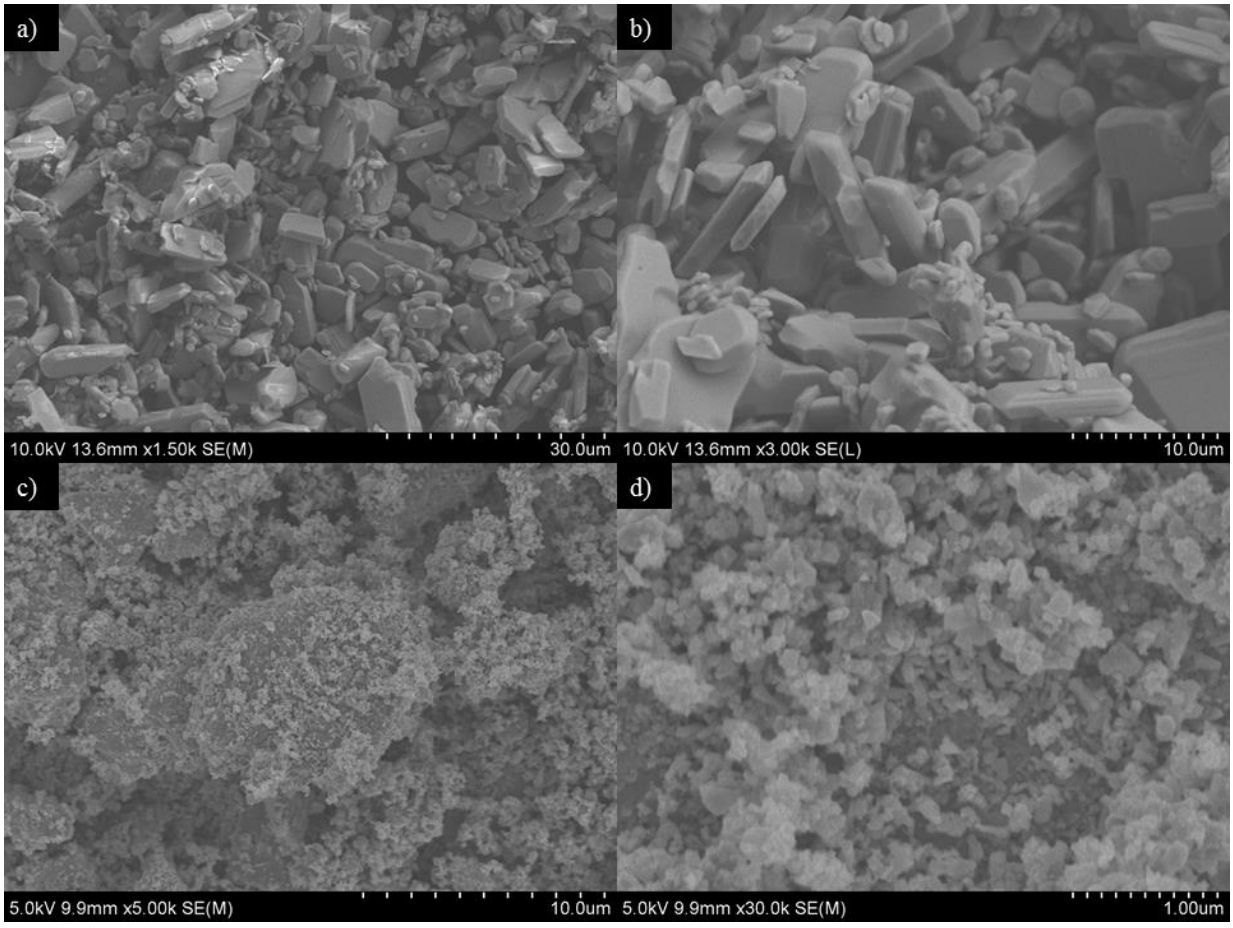

Figure 4.1 SEM images of MoO_3 (a & b) and 0.1 mM CTAB MoO_2 (c & d).

Figures 4.2a and 4.2b show SEM images of 0.5 mM CTAB MoO_2, while Figures 4.2c and 4.2d show SEM images of 1 mM CTAB MoO_2. The 0.5 mM CTAB MoO_2 sample clearly formed nanoparticles that ranged from approximately 40-70 nm, which appear to have no hierarchy. While the 1 mM CTAB MoO_2 samples formed nanospheres that ranged from 150-250 nm. The nanospheres were made of nanoparticles that ranged from 20-30 nm. Just like with the previous experiments, none of the MoO_3 platelet structure are present, indicating a complete conversion from MoO_3.

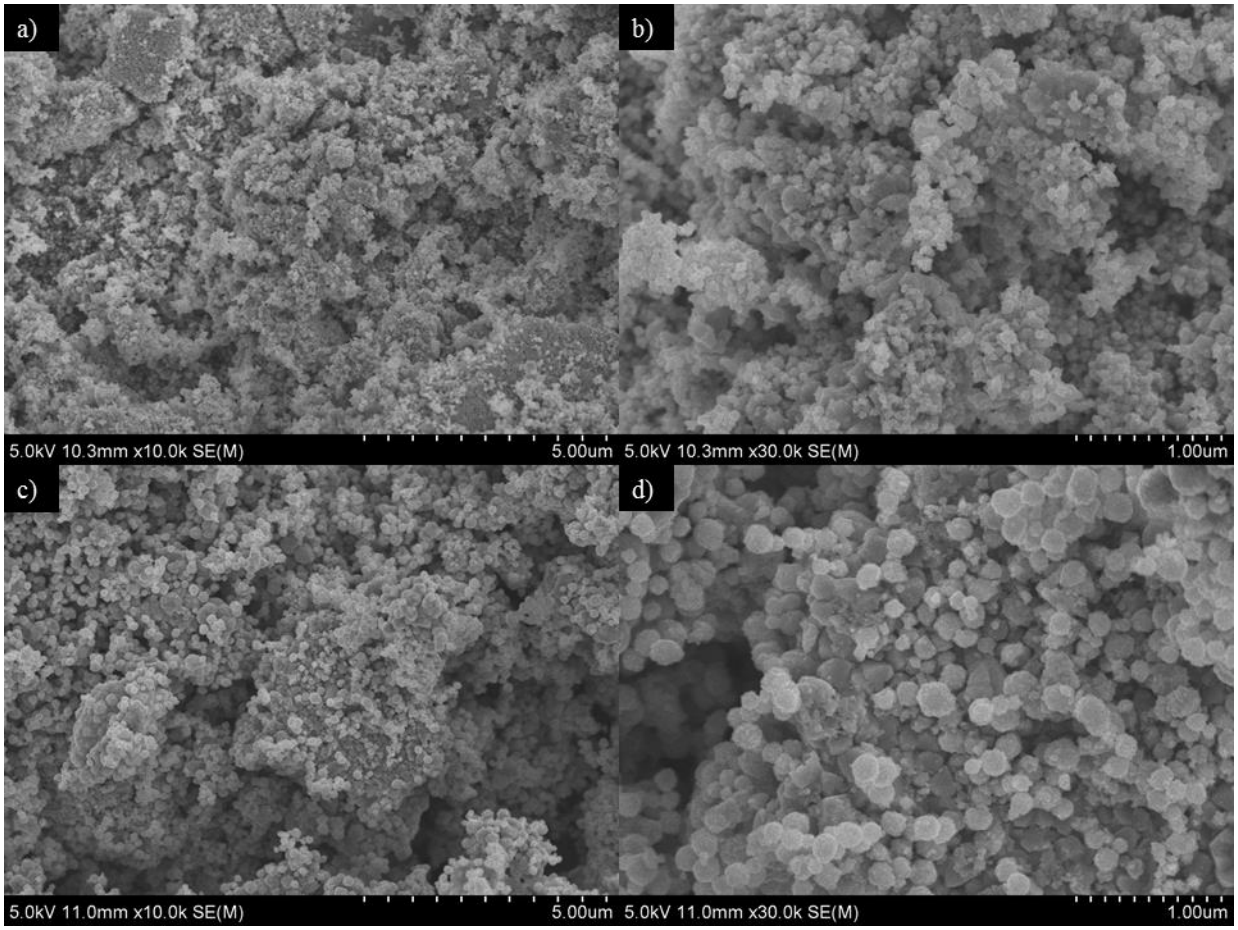

Figure 4.2 SEM images of 0.5 mM CTAB MoO_2 (a & b), and 1 mM CTAB MoO_2 (c & d).

Figures 4.3a and 4.3b show SEM images of 2.5 mM CTAB MoO_2. It is immediately clear that this sample has a completely different morphology compared to the previous experiments. It consisted of nanospheres approximately 180-250 nm in diameter. Those nanospheres are actually

composed of 10-30 nm nanoparticles. Figure 4.3c and 4.3d show SEM images of 5 mM CTAB MoO_2. In this case the morphology is completely different yet again; microspheres are clearly visible, with diameters ranging from approximately 2-7 µm. Upon closer inspection the microspheres are actually made of nanoparticles that range in size from 20-40 nm.

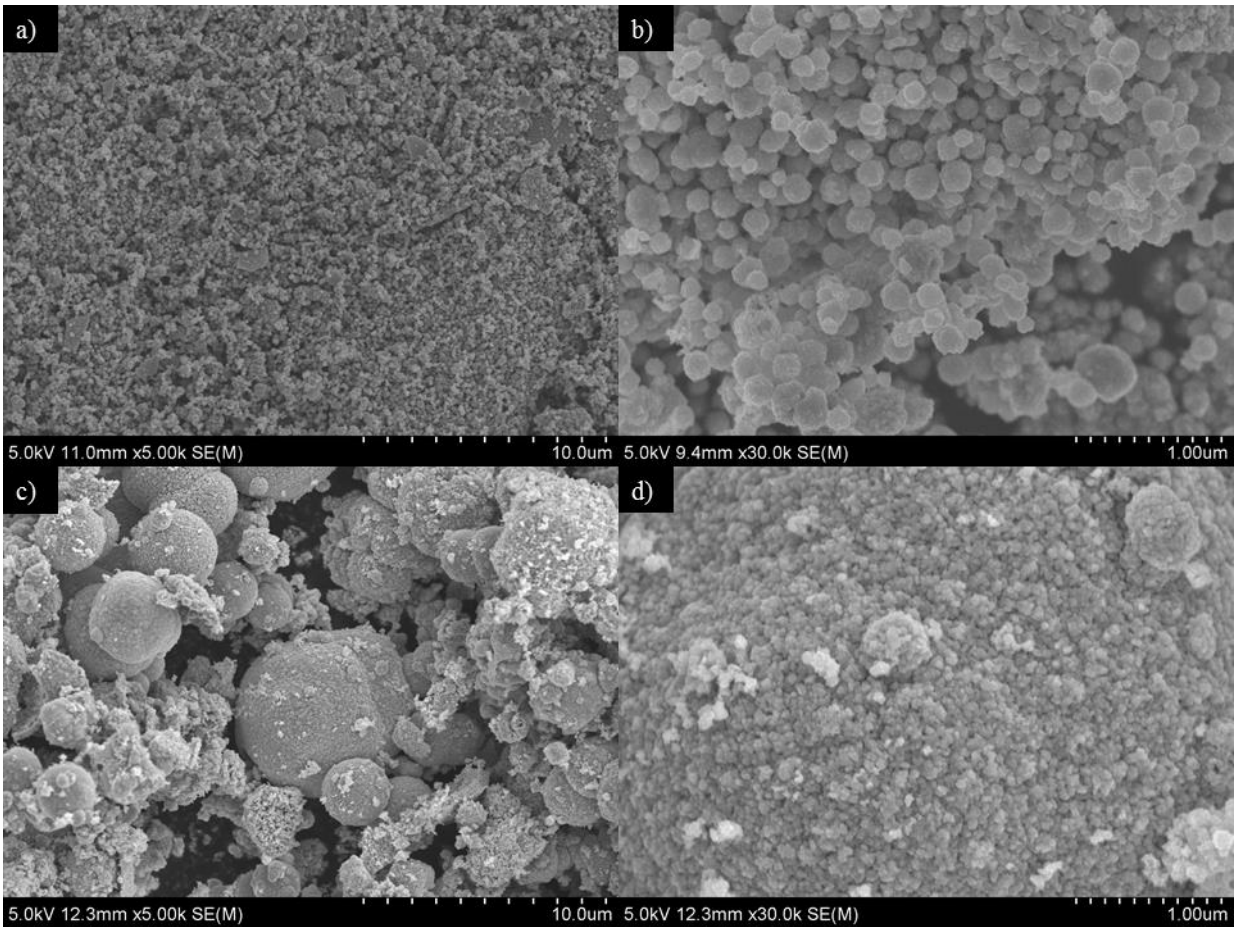

Figure 4.3 SEM images of 2.5 mM CTAB MoO_2 (a & b), and 5 mM CTAB MoO_2 (c & d).

Figures 4.4a and 4.4b show SEM images of 10 mM CTAB MoO_2, which reveals hollow microspheres with diameters ranging from 1-3 µm, and a thickness of approximately 100-150 nm. Figure 4.4b reveals the microspheres are made of nanoparticles ranging in size from 40-50 nm. Figures 4.4c and 4.4d show SEM images of 15 mM CTAB MoO_2, where the morphology has changed yet again. In this case there are 2-5 µm microspheres visible, but they are entangled in a heavily agglomerated mass of 10-20 nm nanoparticles.

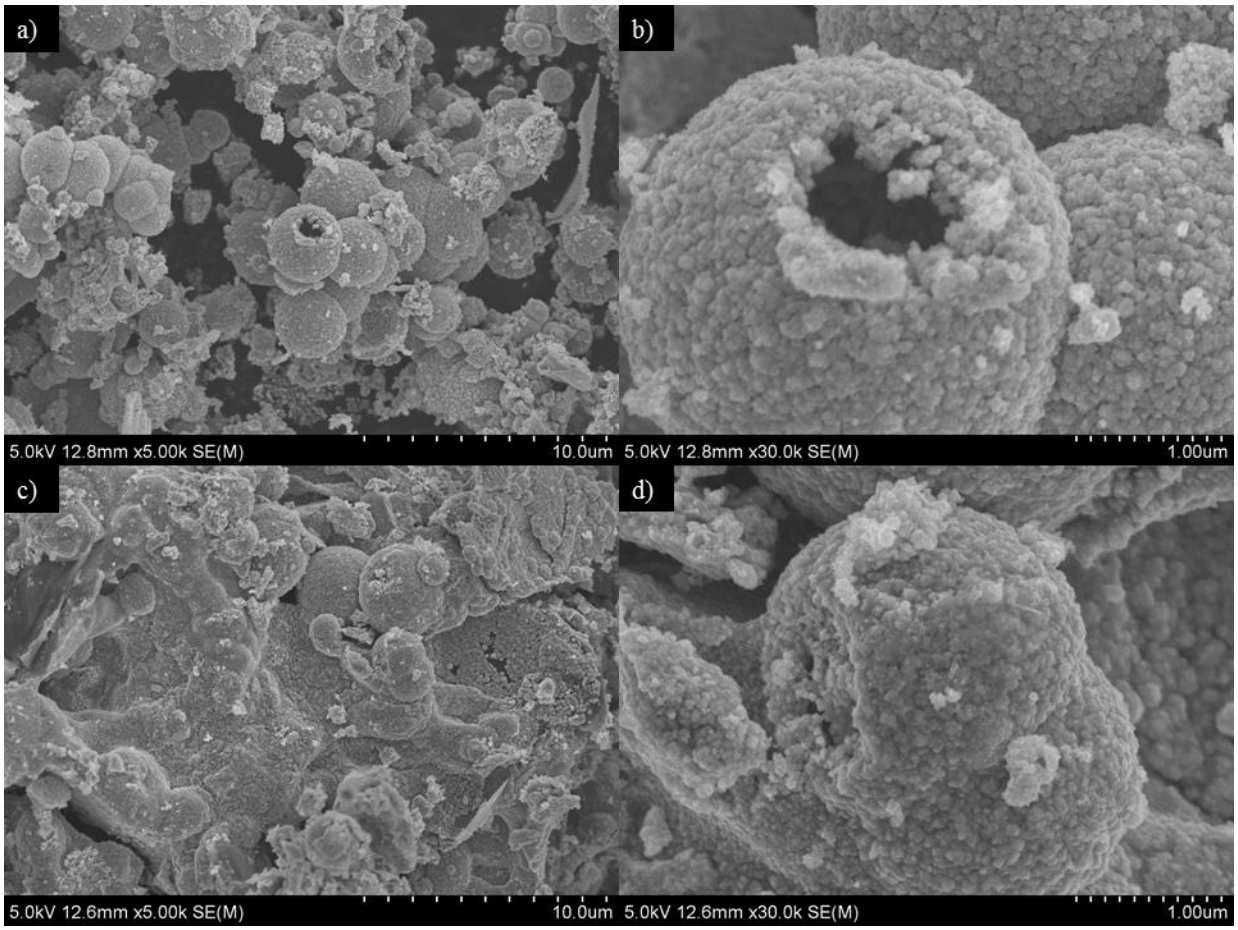

Figure 4.4 SEM images of 10 mM CTAB MoO_2 (a & b), and 15 mM CTAB MoO_2 (c & d).

A summary of the various morphologies of the synthesized CTAB MoO_2 is shown in Table 4.1.

Table 4.1 Summary of the morphology of the synthesized CTAB MoO_2 nanomaterials

Sample	Morphology	Size
0.1 mM MoO_2	Nanoparticles	30-50 nm
0.5 mM MoO_2	Nanoparticles	40-70 nm
1 mM MoO_2	Nanospheres (made of nanoparticles)	120-260 nm (20-50 nm)
2.5 mM MoO_2	Nanospheres (made of nanoparticles)	180-250 nm (10-20 nm)
5 mM MoO_2	Microspheres (made of nanoparticles)	1-6 µm (20-30 nm)
10 mM MoO_2	Hollow microspheres (made of nanoparticles)	1-3 µm (40-50 nm)
15 mM MoO_2	Microspheres (highly agglomerated)	2-5 µm (10-20nm)

To further investigate the formation mechanism of the microspheres, time dependent experiments were conducted to analyze the various morphologies throughout the synthesis

process. Samples were prepared for 4, 6, and 8 hours using 5 mM CTAB. SEM images of the time dependent experiments using 5 mM CTAB are shown in Figure 4.5.

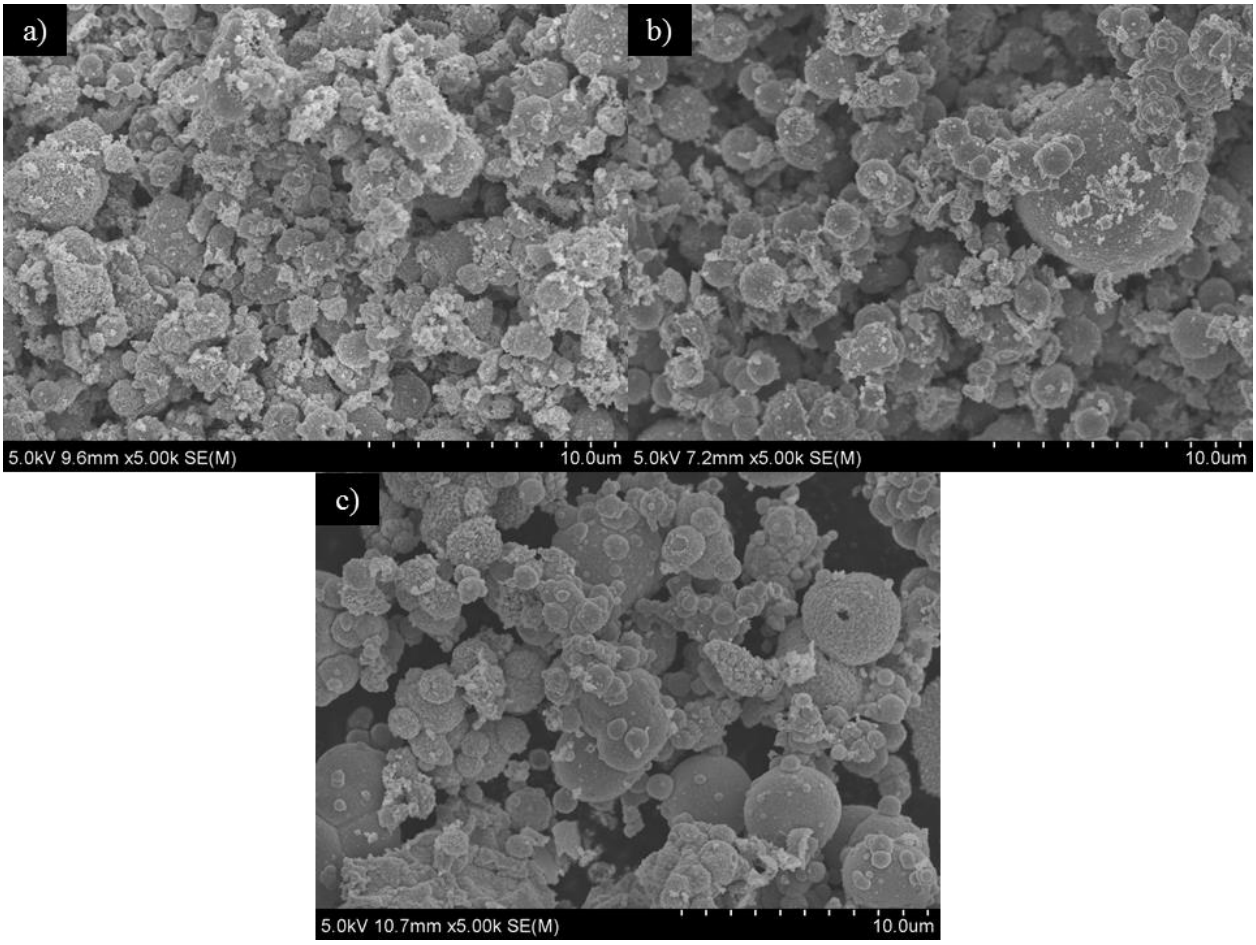

Figure 4.5 SEM images of 5 mM CTAB MoO_2 synthesized for a) 4 hours, b) 6 hours and c) 8 hours.

The growth and formation of the spheres appear to be a combination of aggregation and the very well-known Ostwald ripening process [22, 35, 41, 61, 148], as shown in Figure 4.6.

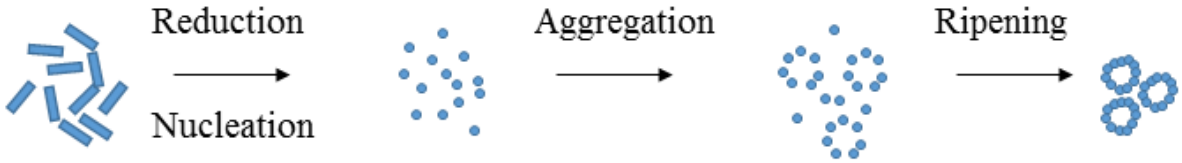

Figure 4.6 Schematic representation of the formation mechanism of the MoO_2 nano- and microspheres.

4.3.2 X-ray Diffraction (XRD)

To collect the XRD patterns, the various synthesized powders were coated on to a zero background diffraction holder using isopropyl alcohol as a solvent. The samples were then scanned from 5-80° in 2θ axis, with a step size of 0.02 ° and a scan step time of 1 second, for a total time of approximately 62 minutes. Figure 4.7 shows the XRD patterns collected from the MoO_3 precursor, the CTAB surfactant, and the various MoO_2 materials synthesized.

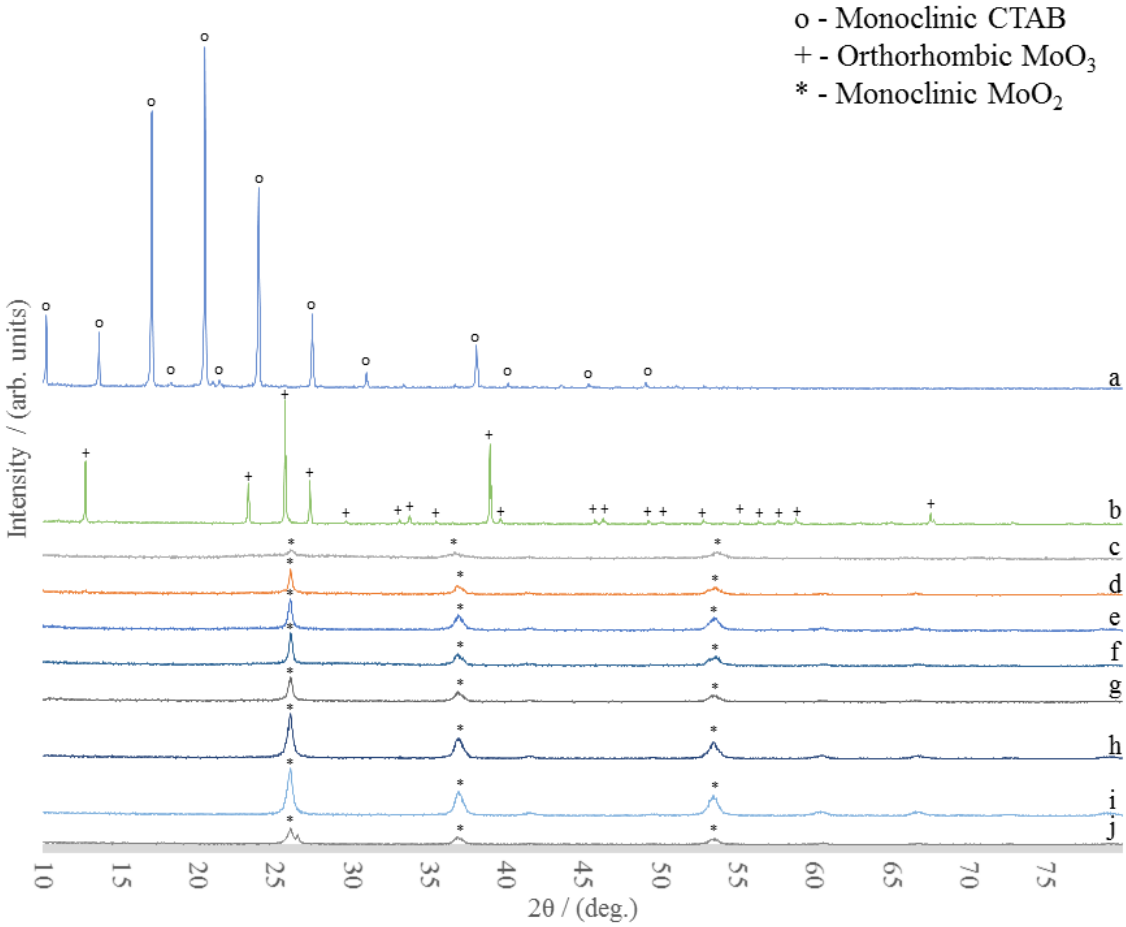

Figure 4.7 XRD patterns for the various MoO_2 materials using CTAB. a) CTAB, b) MoO_3, c) MoO_2, d) 0.1 mM CTAB MoO_2, e) 0.5 mM CTAB MoO_2, f) 1 mM CTAB MoO_2, g) 2.5 mM CTAB MoO_2, h) 5 mM CTAB MoO_2, i) 10 mM CTAB MoO_2, j) 15 mM CTAB MoO_2

The XRD pattern for CTAB can be indexed to a monoclinic phase of CTAB, with the major diffraction peaks at 10.21°, 13.63° 17.06°, 20.51°, 23.97° correspond to the (300), (400), (500), (600), and (700) planes, respectively. The XRD patterns obtained for MoO_3 can be indexed to an

orthorhombic phase of MoO_3, with characteristic diffraction peaks at 12.77°, 23.33°, 25.70°, 27.32°, and 38.97°, that correspond to the (020), (110), (040), (021), and (060) planes, respectively. The pattern for the pristine MoO_2 can be indexed to a monoclinic phase of MoO_2, with the characteristic diffraction peaks at 26.11°, 36.75°, 41.50°, 53.69°, and 70.04°, which correspond to the (-111), (200), (-210), (022), and (-232) planes, respectively. It is clear that the synthesized MoO_2 materials have no diffraction peaks related to the precursors, indicating a complete reduction of MoO_3 to MoO_2 in all cases. In general, as the concentration of CTAB increased, the diffraction peaks for the MoO_2 samples with CTAB became less broad compared to pristine MoO_2 indicating a larger crystallite size, as confirmed by the SEM images.

Figure 4.8 shows XRD patterns for 5 mM CTAB MoO_2 samples synthesized for 4, 6, 8 and 12 hours to see the reduction of MoO_3 over time. It is clear that the MoO_3 has been completely reduced to MoO_2 within 4 hours. As the reaction time increased, the diffraction peaks became slightly less broad and more intense, as the nanoparticles came together to form the larger microspheres, as confirmed by the SEM images.

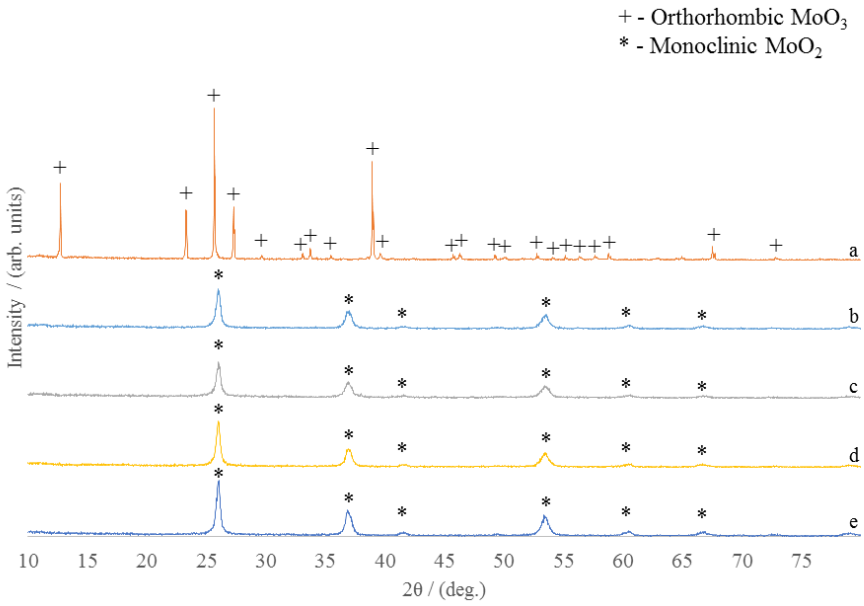

Figure 4.8 XRD patterns for the time dependent experiment with 5 mM CTAB MoO_2. a) MoO_3, b) 5 mM MoO_2-4 hours, c) 5 mM MoO_2-6 hours, d) 5 mM MoO_2-8 hours, e) 5 mM MoO_2-4 hours.

4.3.3 Decontamination

While conducting the decontamination experiments, it became obvious some of the materials were hydrophobic. As some of the samples were added to the continuously stirred MB solution, they simply formed a layer on top of the surface, preventing most of the material from coming into contact with pollutant, preventing decontamination. Figure 4.9 shows the results of 5 mg of the various CTAB MoO_2 samples in 10 mL MB (10 mg L^{-1}) with and without exposure to visible light.

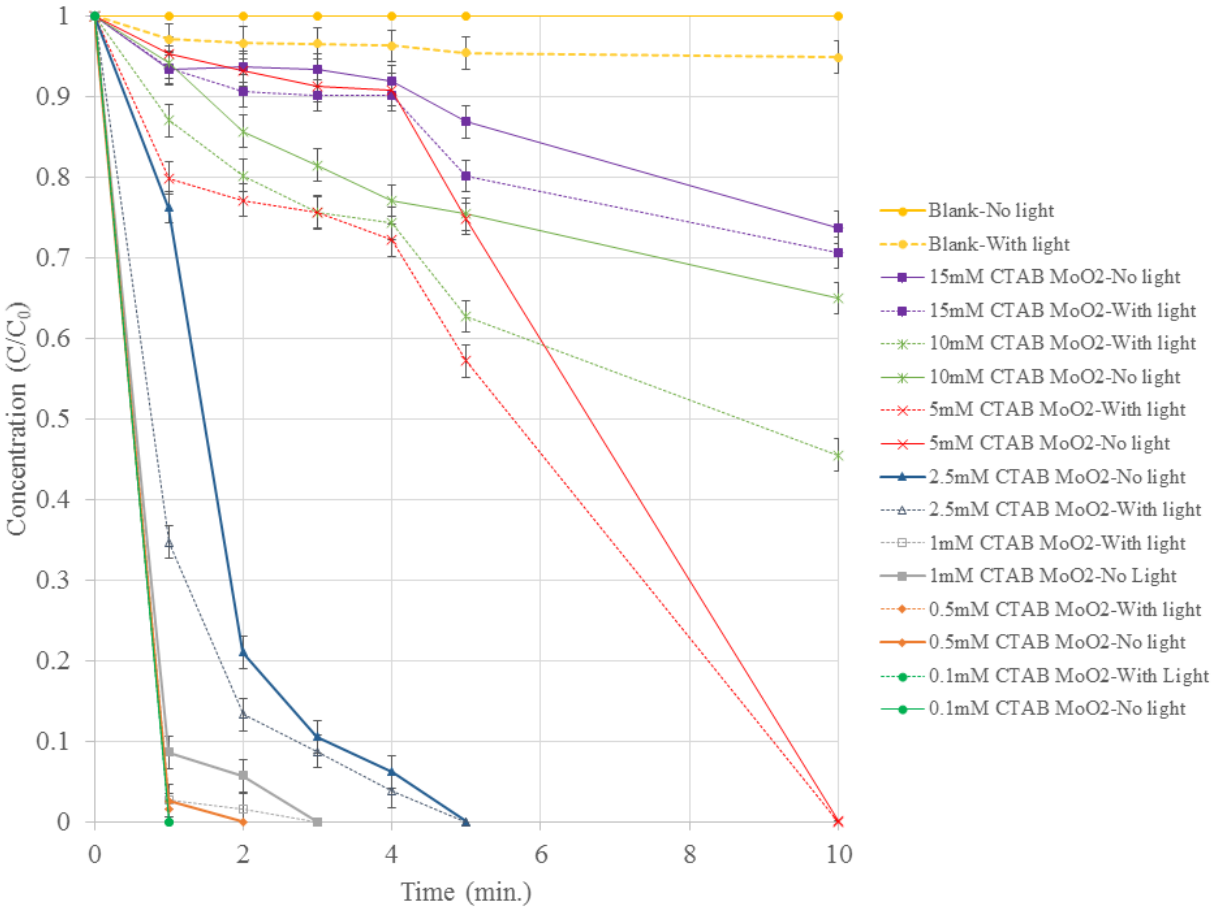

Figure 4.9 Concentration (C/C_0) vs. time (min.) for the decontamination of 10 mL MB by 5 mg of CTAB MoO_2 sample.

It is clear from the image that all of the samples are able to absorb MB without exposure to any visible light, and when the same sample was tested with exposure to visible light, the

performance increased in every case. It is also clear that as the concentration of CTAB increased, the decontamination ability of the material decreased. This is not believed to be related to material composition, as XRD confirmed they are all the same, but could be surface morphology induced hydrophobicity, as shown by the surface roughness seen in the TEM images in Figure 4.10 [149, 150].

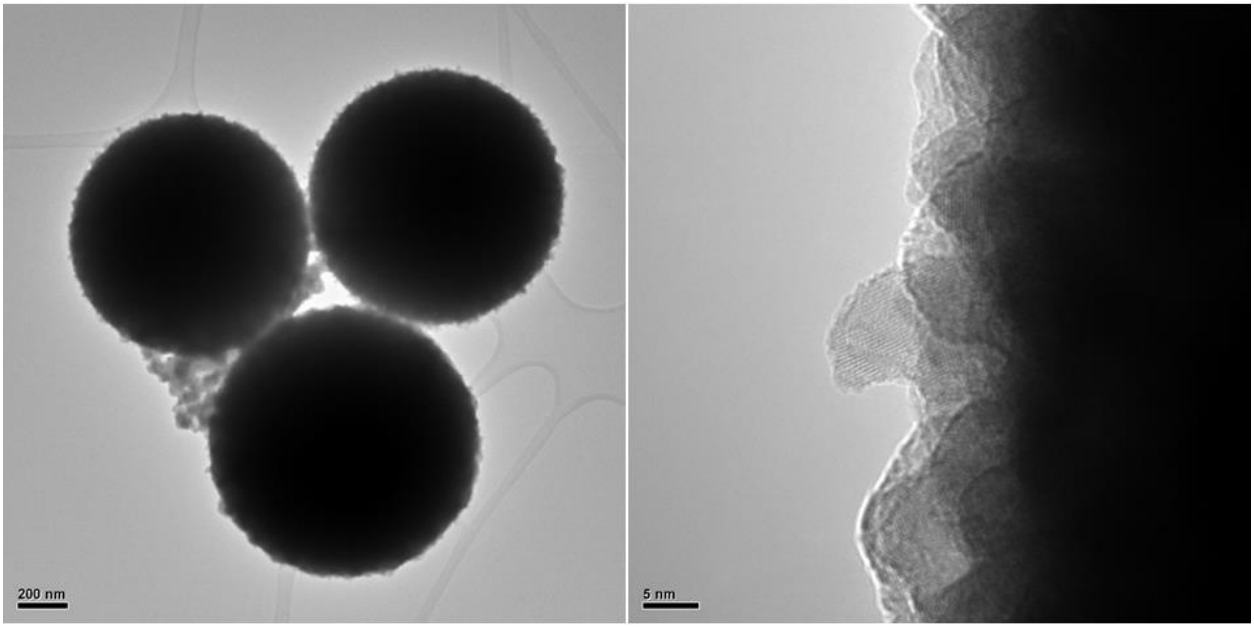

Figure 4.10 TEM images of the 5mM CTAB MoO_2 microspheres.

While the samples synthesized with a higher concentration were hydrophobic, they were still able to decontaminate some of the MB. This can be explained in two ways; first is that even if the particles are hydrophobic, there still some in direct contact with the surface of the MB, which allow for a small amount of decontamination close to the surface. The second way it can be explained is due to the set-up of this particular experiment. When the sample is first added, it forms a layer on top of the surface of the MB. As samples are collected from the beaker, the level in the beaker drops, causing the sample to eventually be physically forced to mix into the MB by coming into direct contact with the magnetic stirrer, as shown in Figure 4.11.

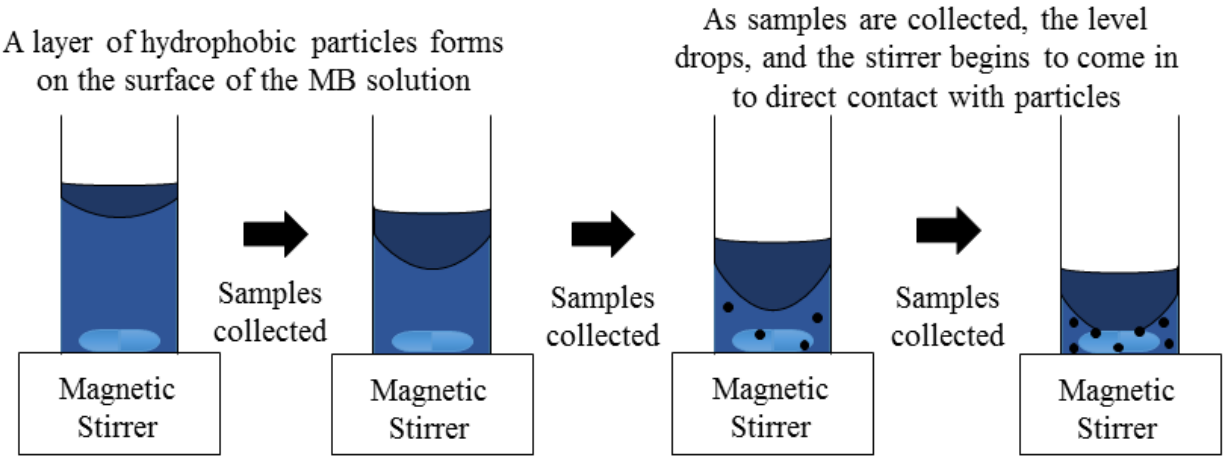

Figure 4.11 Schematic representation of how the hydrophobic particles are mixed into the MB solution.

A summary of the decontamination results is shown in Table 4.2. It is clear from the table that while nano- and microspheres are capable of decontaminating MB from water, the most effective samples are plain nanoparticles with no hierarchy.

Table 4.2 Decontamination results for 5mg of the various CTAB MoO_2 samples in 10 mL MB (10 mg L^{-1})

Sample	Amount of MB decontaminated	Time
Blank - No light exposure	0.04%	10 min.
Blank - Visible light exposure	5.20%	10 min.
0.1 mM MoO_2 - No light exposure	100%	1 min.
0.1 mM MoO_2 - Visible light exposure	100%	1 min.
0.5 mM MoO_2 - No light exposure	100%	2 min.
0.5 mM MoO_2 - Visible light exposure	100%	2 min.
1 mM MoO_2 - No light exposure	100%	3 min.
1 mM MoO_2 - Visible light exposure	100%	3 min.
2.5 mM MoO_2 - No light exposure	100%	5 min.
2.5 mM MoO_2 - Visible light exposure	100%	5 min.
5 mM MoO_2 - No light exposure	99.81%	10 min.
5 mM MoO_2 - Visible light exposure	100%	10 min.
10 mM MoO_2 - No light exposure	35.00%	10 min.
10 mM MoO_2 - Visible light exposure	54.44%	10 min.
15 mM MoO_2 - No light exposure	26.25%	10 min.
15 mM MoO_2 - Visible light exposure	29.38%	10 min.

4.4 Conclusion

A variety of MoO_2 were successfully synthesized using a hydrothermal method, with CTAB as a surfactant. The various samples were all proven to be made of the same material composition using XRD, however they possessed different morphologies, including nanoparticles, nanospheres, microspheres (hollow and solid), as shown by the SEM images. A formation mechanism was proposed for the formation of the nano- and microspheres, as well as an explanation for the apparent decrease in decontamination, which was cause by the particles becoming hydrophobic. All of the samples were able to decontaminate MB to some degree, and in every case the addition of the exposure to light sped up the rate at which MB was decontaminated. This phenomenon can only be explained by a combination of adsorption and photocatalysis. The most effective material was found to be the 0.1 mM CTAB MoO_2 nanoparticles, which were able to decontaminate 100% of the MB within one minute, with or without exposure to light.

CHAPTER 5: HYDROTHERMAL SYNTHESIS OF MoO_2 NANOPARTICLES DIRECTLY ONTO A COPPER SUBSTRATE AND THEIR ABILITY TO DECONTAMINATE WATER[1]

5.1 Introduction

Most decontamination of water by a photocatalyst is done in what is called a slurry. In these cases, the active material used to decontaminate the solution is mixed directly into the solution to allow the reaction to occur. Since the mixture in continually mixing, the active material is almost always in constant with the pollutant, allowing for maximum effectiveness. The downside to this process is that once the active material has decontaminated the original pollutant in the water, the active material is now a pollutant of its own that must be removed from the water by filtration, centrifugation, etc.

Herein, we describe a process to synthesize MoO_2 directly onto a copper substrate, with no binder material. This could be a huge breakthrough in the world of Li-ion batteries, as currently anode materials are synthesized alone, and must then be coated onto a current collector in a spate step. The coating usually involves mixing the active material into a slurry, with a solvent, and a binder material, then coating the slurry onto a current collector (usually copper for anode materials) and then heated in an oven to drive out the solvent. Not only that, but the MoO_2 coated copper

[1] Michael McCrory, Ashok Kumar, Manoj K. Ram, "Hydrothermal Synthesis of MoO_2 Nanoparticles Directly onto a Copper Substrate", MRS Advances, 1, 1051-1054, reproduced with permission.
Appendix A for copyright permission

substrate was able to decontaminate over 50% of the Mb within 10 minutes, with no exposure to light, and over 71% with exposure to light.

5.2 Experimental

All materials were purchased from Sigma Aldrich and used without any modification unless otherwise noted.

5.2.1 Synthesis of Molybdenum Dioxide (MoO_2) onto a Copper Substrate

To begin the experiment, a 1 x 1 cm (.25 mm thick) 99.9% pure copper substrate was treated in hydrochloric acid for 15 min, followed by an ultrasonic bath in ethanol for 5 min. Next, 7.5 mL of deionized water and 2.5 mL of ethylene glycol were magnetically stirred, while 75 mg of MoO_3 powder was added. After 10 minutes of mixing, the solution was placed into a teflon-lined stainless steel pressure vessel along with the clean copper substrate. The pressure vessel was then sealed and placed into an oven at 180 °C 12 hours. After allowing the pressure vessel to naturally cool overnight and reach room temperature, the resulting solution was emptied into a beaker to retrieve the copper substrate. The copper substrate was then rinsed 3 times with DI water and ethanol before being placed in an oven to dry overnight. The weight of the copper before coating was approximately 250.5 mg, and after coating was approximately 252.5 mg.

5.2.2 Characterization

The samples were characterized by X-ray diffraction (XRD), scanning electron microscopy (SEM) and UV-visible spectrophotometry. For XRD measurements, a PANalytical X'Pert PRO diffractometer with Cu Kα radiation (λ=1.5406 Å) was used. For SEM measurements, a Hitachi SU-70 ultra-high resolution scanning electron microscope was used. And for UV-visible spectrophotometry, a Jasco J-530 UV-Vis Spectrophotometer was used.

5.2.3 Water Decontamination Setup

To determine the ability of the MoO_2 coated copper samples to decontaminate water, the samples were suspended in 10 mL of a methylene blue solution that was continuously stirred, with a concentration of 10 mg L^{-1}. One set of experiments were conducted with exposure to visible light in the form of a 30 watt light with an intensity of 800W/m^2, and another set were conducted without exposure to visible light, as shown in Figure 5.1.

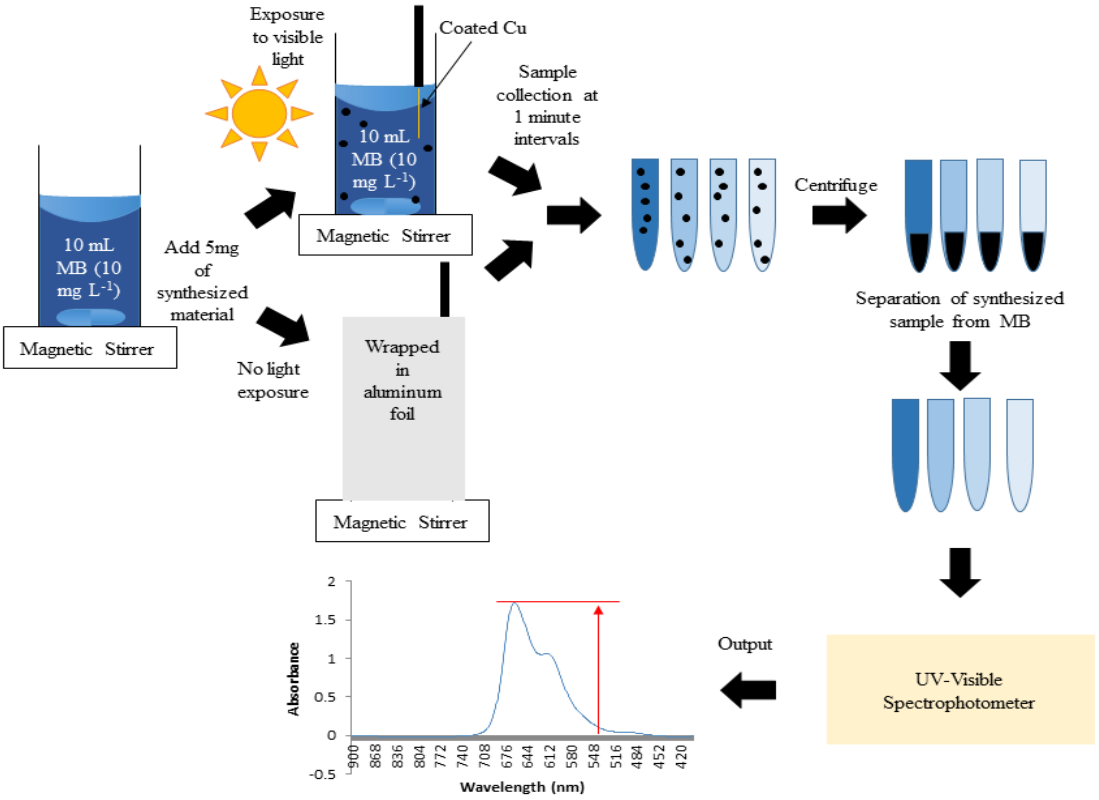

Figure 5.1 Step-by-step schematic of the typical MB degradation experiment, sample collection and analysis process for the MoO_2 coated copper samples.

5.3 Results and Discussion

A schematic of the formation mechanism of MoO_2 nanoparticles directly onto a copper substrate is shown in Figure 5.2. MoO_3, ethylene glycol, and water react under temperature and pressure to produce $MoO_3(OH)_2$, which is a volatile vapor phase that condensed onto the copper substrate, and subsequently dehydrated to form MoO_2 [151-153].

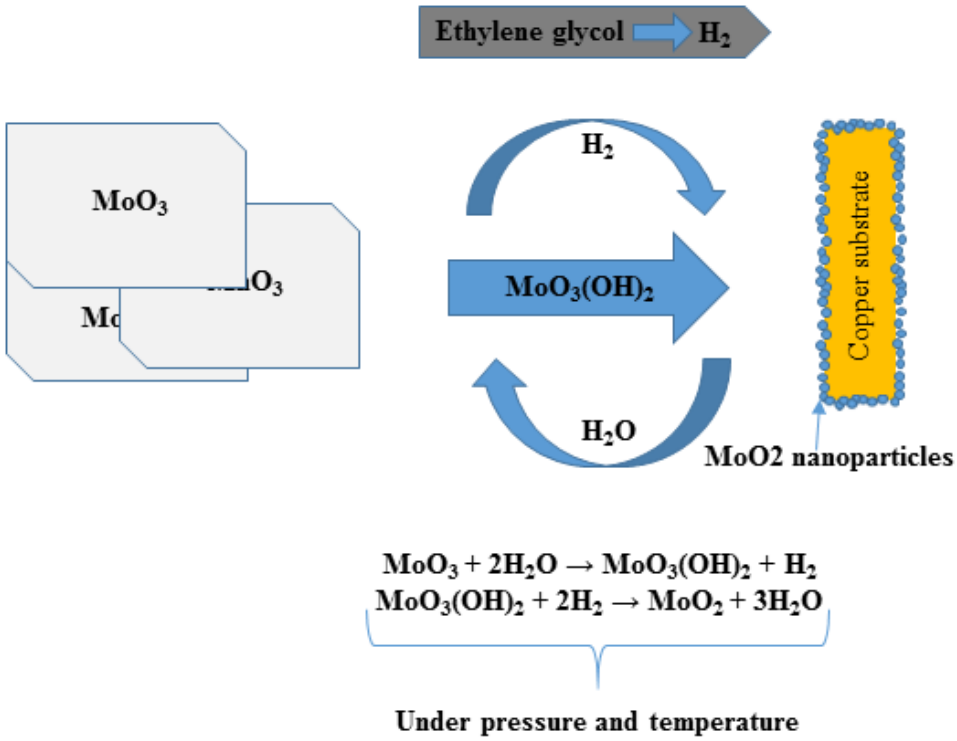

Figure 5.2 Formation mechanism of MoO_2 nanoparticles onto a copper substrate.

5.3.1 Scanning Electron Microscopy

Figure 5.3 shows SEM images of the MoO_3 precursor powder with its platelet type structure. It is clear from Figure 5.3 that the MoO_3 consists of large (>2µm) platelet shaped particles.

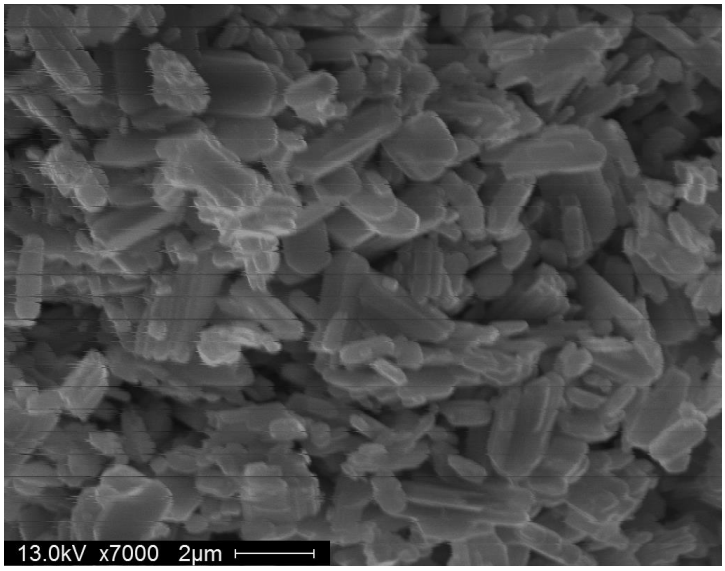

Figure 5.3 SEM image of the MoO_3 precursor.

Figure 5.4 shows the resulting MoO_2 nanoparticle coated on a copper substrate. It is clear that the synthesized MoO_2 coating consists of nanoparticles approximately 30-50 nm in diameter. There are clearly no larger MoO_3 pieces could be found anywhere on the samples, indicating all of the MoO_3 platelets had converted to MoO_2 nanoparticles, as later confirmed by the XRD analysis.

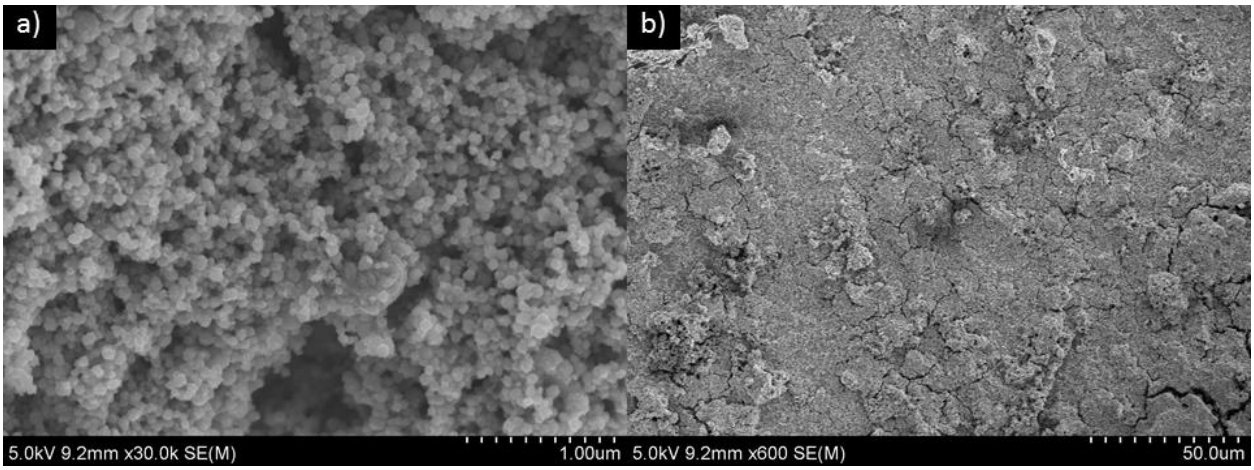

Figure 5.4 SEM images of the MoO_2 coated copper.

5.3.2 X-ray Diffraction (XRD)

The MoO_2 coated copper substrate was analyzed using grazing incident angle X-ray diffraction (GIXRD). The coated samples were scanned with a fixed incident angle of 1°, while the pure Cu and MoO_3 were scanned using regular powder diffraction mode. Figure 5.5 shows the XRD patterns for the materials used in this experiment. It should be noted that the patterns are not displayed at the same scale for clarity. It is clear from Figure 5.5 that the synthesized films show a completely different XRD pattern when compared to the MoO_3 precursor. The coated samples show no indication of MoO_3 peaks, indicating a full conversion of MoO_3 to MoO_2. The MoO_2 coated sample had diffraction peaks at 26.1°, 36.8°, 43.4°, 50.5°, 53.3° and 74.1°. The diffraction peaks at 26.1°, 36.8°, and 53.3° correspond to the (-111), (200) and (022) planes of monoclinic

MoO_2, respectively. The diffraction peaks seen at 43.4°, 50.5° and 74.1° are from the Cu substrate, and correspond to the (111), (200), and (220) planes of cubic copper, respectively.

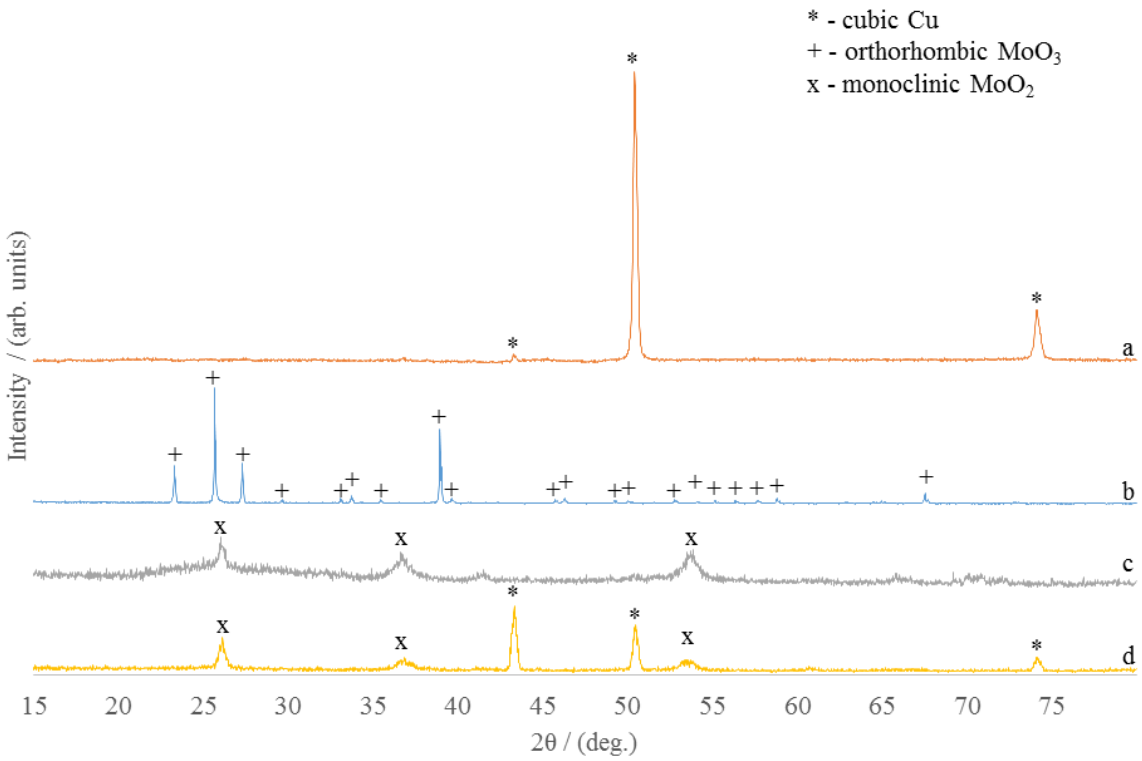

Figure 5.5 XRD patterns for a) copper substrate, b) MoO_3, c) MoO_2, and d) MoO_2 coated copper.

5.3.3 Decontamination

The results of the decontamination experiments are shown in Figure 5.6. It is clear from the image that the MoO_2 coated copper substrate is very effective at decontaminating MB from water. The MB degraded less than 0.05% during 10 minutes with no light exposure, and degraded 5.1% with exposure to light for 10 minutes. The coated samples were able to adsorb 57.5% of the MB with no exposure to light, while it was able to decontaminate 71.7% of the MB with light exposure.

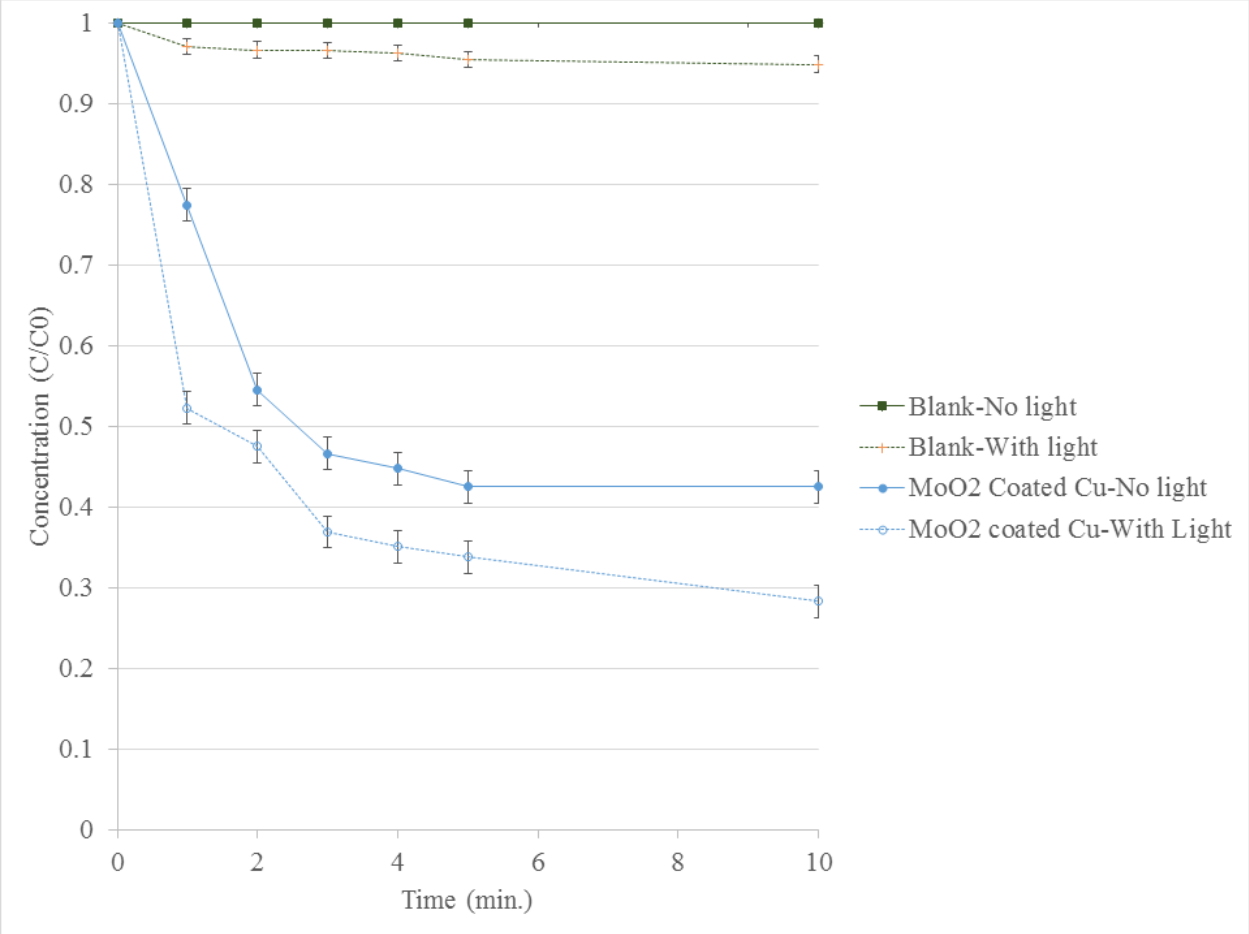

Figure 5.6 Concentration (C/C_0) vs. time (min.) for the decontamination of 10 mL MB by the MoO_2 coated copper substrate.

5.4 Conclusion

MoO_2 nanoparticles were successfully synthesized onto a copper substrate for the first time, as proven by XRD and SEM. The MoO_2 coated copper substrates were then tested for their ability to decontaminate MB from water. The MoO_2 coated copper substrates were not able to remove 100% of the MB, however it still was able to decontaminate over 50% of the MB from the water in 10 minutes with no light exposure, and over 70% removed in 10 minutes with light exposure.

CHAPTER 6: CONCLUSION

Nanostructured AM-MoO_3 was synthesized and used as a precursor in a comparative study, along with MoO_3, to synthesize AM-MoO_2 and MoO_2, respectively. XRD confirmed a full reduction from orthorhombic MoO_3 to monoclinic MoO_2 in all cases. Time dependent experiments showed the MoO_3 is fully reduced within 2 hours. During the decontamination experiments, all of the materials were proven to be excellent absorbent materials, as well as photocatalysts. Both MoO_2 and AM-MoO_2 performed almost exactly the same, with both samples being able to remove 100% of the MB in one minute with light, and in two minutes without light.

The morphology of MoO_2 was controlled in a comparative study by varying the concentration of CTAB present during the hydrothermal reaction. Samples synthesized with 0.1-0.5 mM CTAB formed nanoparticles, sample with 1-2.5 mM CTAB formed nanospheres, samples with 5mM formed solid microspheres, samples with 10 mM CTAB formed hollow microspheres, and samples with 15 mM CTAB formed microspheres that were highly agglomerated. A formation mechanism for the formation of the nano- and microspheres was proposed with a combination of aggregation and Ostwald ripening. XRD confirmed a full reduction from orthorhombic MoO_3 to monoclinic MoO_2, along with no residual peaks from the CTAB that was present during the reaction. During the decontamination experiments, some of the materials were found to be hydrophobic. The apparent decrease in decontamination performance was proposed to be caused by surface morphology induced hydrophobicity. The decontamination results once again showed that the synthesized MoO_2 materials were not only photocatalysts, but adsorbents as well. Samples

synthesized with 0.1-5 mM CTAB were able to remove 100% of the MB in 10 minutes or less. Samples synthesized with 10 mM CTAB were able to remove 54.4% and 35% of the MB in 10 minutes, with and without light, respectively. Samples synthesized with 15 mM CTAB were able to remove 29.4% and 26.3% of the MB in 10 minutes, with and without light, respectively. A mechanism to describe why the hydrophobic particles were still able to decontaminate the water was proposed to be caused by coming into direct contact with the magnetic stirrer as the water level dropped due to sample collection.

MoO_2 nanoparticles were successfully synthesized onto a copper substrate, in a single step. We believe this is the first report of such a synthesis method, and that it can be extended to other materials and other substrates. XRD confirmed a full reduction of orthorhombic MoO_3 to monoclinic MoO_2, as well as confirmed there were no other by products that formed on the surface of the copper during the synthesis process. SEM images of the MoO_2 coated copper substrate showed uniform nanoparticles ranging from 30-50 nm. The MoO_2 coated copper substrate was able to decontaminate 57.5% and 71.7% of the MB from water in 10 minutes, with and without exposure to light, respectively.

6.1 Future Work

MoO_2 is a relatively new material in the world of water decontamination, there needs to be research done into the effects of MoO_2 on the environment to determine its toxicity and viability to safely decontaminate water. Work also needs to be done to look at the recyclability of the MoO_2 materials, as well as its ability to decontaminate other dyes and organic pollutants. The coating process for MoO_2 should be optimized to prevent as much of the material from detaching from the substrate as possible. This would decrease the amount of material that must be removed from the water before it is useable. Tests should also be conducted to see if the coated copper substrate still

has any of the antimicrobial properties associated with copper, as this would help to further decontaminate the water.

REFERENCES

1. Bhaskar, A., M. Deepa, and T. Narasinga Rao, *MoO_2/multiwalled carbon nanotubes (MWCNT) hybrid for use as a Li-ion battery anode.* ACS Appl Mater Interfaces, 2013. **5**(7): p. 2555-66.

2. Chen, Y., X. Di, C. Ma, C. Zhu, P. Gao, J. Li, C. Sun, and Q. Ouyang, *Graphene–MoO_2 hierarchical nanoarchitectures: in situ reduction synthesis and high rate cycling performance as lithium-ion battery anodes.* RSC Advances, 2013. **3**(39): p. 17659.

3. Cho, W., J.H. Song, J.-H. Kim, G. Jeong, E.Y. Lee, and Y.-J. Kim, *Electrochemical characteristics of nano-sized MoO_2/C composite anode materials for lithium-ion batteries.* Journal of Applied Electrochemistry, 2012. **42**(11): p. 909-915.

4. Choi, S.H. and Y.C. Kang, *Crumpled graphene-molybdenum oxide composite powders: preparation and application in lithium-ion batteries.* ChemSusChem, 2014. **7**(2): p. 523-8.

5. He, J., H. Wang, C. Gu, and S. Liu, *Characterization and electrochemical performances of MoO_2 modified LiFePO4/C cathode materials synthesized by in situ synthesis method.* Journal of Alloys and Compounds, 2014. **604**: p. 239-244.

6. Guo, B., X. Fang, B. Li, Y. Shi, C. Ouyang, Y.-S. Hu, Z. Wang, G.D. Stucky, and L. Chen, *Synthesis and Lithium Storage Mechanism of Ultrafine MoO_2Nanorods.* Chemistry of Materials, 2012. **24**(3): p. 457-463.

7. Lei, Y., J. Hu, H. Liu, and J. Li, *Template-free synthesis of hollow core–shell MoO_2 microspheres with high lithium-ion storage capacity.* Materials Letters, 2012. **68**: p. 82-85.

8. Liang, Y., S. Yang, Z. Yi, X. Lei, J. Sun, and Y. Zhou, *Low temperature synthesis of a stable MoO_2 as suitable anode materials for lithium batteries.* Materials Science and Engineering: B, 2005. **121**(1-2): p. 152-155.

9. Liang, Y., S. Yang, Z. Yi, J. Sun, and Y. Zhou, *Preparation, characterization and lithium-intercalation performance of different morphological molybdenum dioxide*. Materials Chemistry and Physics, 2005. **93**(2-3): p. 395-398.

10. Liang, Y., Z. Yi, S. Yang, L. Zhou, J. Sun, and Y. Zhou, *Hydrothermal synthesis and lithium-intercalation properties of MoO_2 nano-particles with different morphologies.* Solid State Ionics, 2006. **177**(5-6): p. 501-505.

11. Liu, J., S. Tang, Y. Lu, G. Cai, S. Liang, W. Wang, and X. Chen, *Synthesis of Mo2N nanolayer coated MoO_2 hollow nanostructures as high-performance anode materials for lithium-ion batteries.* Energy & Environmental Science, 2013. **6**(9): p. 2691.

12. Liu, S., H. Yin, H. Wang, J. He, and H. Wang, *Synthesis, characterization and electrochemical performances of MoO_2 and carbon co-coated LiFePO4 cathode materials.* Ceramics International, 2014. **40**(2): p. 3325-3331.

13. Liu, X., D. Wu, W. Ji, and W. Hou, *Uniform MoO_2@carbon hollow nanospheres with superior lithium-ion storage properties.* J. Mater. Chem. A, 2015. **3**(3): p. 968-972.

14. Liu, Y., H. Zhang, P. Ouyang, W. Chen, and Z. Li, *Microstructure evolution of Li uptake/removal in MoO_2@C nanoparticles with high lithium storage performance.* Materials Research Bulletin, 2014. **50**: p. 95-102.

15. Liu, Y., H. Zhang, P. Ouyang, W. Chen, Y. Wang, and Z. Li, *High electrochemical performance and phase evolution of magnetron sputtered MoO_2 thin films with hierarchical structure for Li-ion battery electrodes.* Journal of Materials Chemistry A, 2014. **2**(13): p. 4714.

16. Liu, Y., H. Zhang, P. Ouyang, and Z. Li, *One-pot hydrothermal synthesized MoO_2 with high reversible capacity for anode application in lithium ion battery.* Electrochimica Acta, 2013. **102**: p. 429-435.

17. Palanisamy, K., Y. Kim, H. Kim, J.M. Kim, and W.-S. Yoon, *Self-assembled porous MoO_2/graphene microspheres towards high performance anodes for lithium ion batteries.* Journal of Power Sources, 2015. **275**: p. 351-361.

18. Park, J., I. Choi, M.J. Lee, M.H. Kim, T. Lim, K.H. Park, J. Jang, S.M. Oh, S.K. Cho, and J.J. Kim, *Effect of fluoroethylene carbonate on electrochemical battery performance and the surface chemistry of amorphous MoO_2 lithium-ion secondary battery negative electrodes.* Electrochimica Acta, 2014. **132**: p. 338-346.

19. Shi, Y., B. Guo, S.A. Corr, Q. Shi, Y.-S. Hu, K.R. Heier, L. Chen, R. Seshadri, and G.D. Stucky, *Ordered Mesoporous Metallic MoO_2 Materials with Highly Reversible Lithium Storage Capacity.* Nano Letters, 2009. **9**(12): p. 4215-4220.

20. Tang, Q., Z. Shan, L. Wang, and X. Qin, *MoO_2–graphene nanocomposite as anode material for lithium-ion batteries.* Electrochimica Acta, 2012. **79**: p. 148-153.

21. Xu, Y., R. Yi, B. Yuan, X. Wu, M. Dunwell, Q. Lin, L. Fei, S. Deng, P. Andersen, D. Wang, and H. Luo, *High Capacity MoO_2/Graphite Oxide Composite Anode for Lithium-Ion Batteries.* J Phys Chem Lett, 2012. **3**(3): p. 309-14.

22. Hu, H., J. Xu, C. Deng, and X. Ge, *Hierarchical mesoporous MoO_2 hollow microspheres: Synthesis, mechanism and application in removing Cr (VI) from wastewater*. Materials Research Bulletin, 2014. **51**: p. 402-410.

23. Hu, H.-M., J.-C. Xu, X.-Q. Ge, M. Sun, H. Xuan, and K.-H. Zhang, *Heirarchical MoO_2 Microshperes: Hydrothermal Synthesis and Photocatalytic Performance for Degradation of Rhodamine B.* Chinese J. Inorg. Chem., 2014. **30**.

24. Zhou, E., C. Wang, Q. Zhao, Z. Li, M. Shao, X. Deng, X. Liu, and X. Xu, *Facile synthesis of MoO_2 nanoparticles as high performance supercapacitor electrodes and photocatalysts.* Ceramics International, 2016. **42**(2): p. 2198-2203.

25. Rajeswari, J., P.S. Kishore, B. Viswanathan, and T.K. Varadarajan, *One-dimensional MoO_2 nanorods for supercapacitor applications.* Electrochemistry Communications, 2009. **11**(3): p. 572-575.

26. Li, X., J. Shao, J. Li, L. Zhang, Q. Qu, and H. Zheng, *Ordered mesoporous MoO_2 as a high-performance anode material for aqueous supercapacitors.* Journal of Power Sources, 2013. **237**: p. 80-83.

27. Hercule, K.M., Q. Wei, A.M. Khan, Y. Zhao, X. Tian, and L. Mai, *Synergistic effect of hierarchical nanostructured MoO_2/$Co(OH)_2$ with largely enhanced pseudocapacitor cyclability.* Nano Lett, 2013. **13**(11): p. 5685-91.

28. Ellefson, C.A., O. Marin-Flores, S. Ha, and M.G. Norton, *Synthesis and applications of molybdenum (IV) oxide.* Journal of Materials Science, 2011. **47**(5): p. 2057-2071.

29. Avendano, C., A. Briceno, F.J. Mendez, J.L. Brito, G. Gonzalez, E. Canizales, R. Atencio, and P. Dieudonne, *Novel MoO_2/carbon hierarchical nano/microcomposites: synthesis, characterization, solid state transformations and thiophene HDS activity.* Dalton Trans, 2013. **42**(8): p. 2822-30.

30. Liang, Y., Z. Yi, X. Lei, X. Ma, S. Yang, J. Sun, L. Yuan, and Y. Zhou, *A novel route to prepare nano-sized MoO_2 powders in various dimensions.* Journal of Alloys and Compounds, 2006. **421**(1-2): p. 133-135.

31. Nagaraju, G., K.V. Thipperudraiah, and G.T. Chandrappa, *Organic assisted hydrothermal route to MoO_2/HDA composite microspheres and their characterization.* Materials Research Bulletin, 2008. **43**(12): p. 3297-3304.

32. Yang, Q., Q. Liang, J. Liu, S. Liang, S. Tang, P. Lu, and Y. Lu, *Ultrafine MoO_2 nanoparticles grown on graphene sheets as anode materials for lithium-ion batteries.* Materials Letters, 2014. **127**: p. 32-35.

33. Yoon, S., K.-N. Jung, C.S. Jin, and K.-H. Shin, *Synthesis of nitrided MoO_2 and its application as anode materials for lithium-ion batteries.* Journal of Alloys and Compounds, 2012. **536**: p. 179-183.

34. Yunusi, T., C. Yang, W. Cai, F. Xiao, J. Wang, and X. Su, *Synthesis of MoO_3 submicron belts and MoO_2 submicron spheres via polyethylene glycol-assisted hydrothermal method and their gas sensing properties.* Ceramics International, 2013. **39**(3): p. 3435-3439.

35. Zhang, H., Y. Li, Z. Hong, and M. Wei, *Fabrication of hierarchical hollow MoO_2 microspheres constructed from small spheres.* Materials Letters, 2012. **79**: p. 148-151.

36. Zhu, Y., X. Xu, G. Chen, Y. Zhong, R. Cai, L. Li, and Z. Shao, *Surfactant-free self-assembly of reduced graphite oxide-MoO_2 nanobelt composites used as electrode for lithium-ion batteries.* Electrochimica Acta, 2016. **211**: p. 972-981.

37. Bhaskar, A., M. Deepa, T.N. Rao, and U.V. Varadaraju, *Enhanced nanoscale conduction capability of a MoO_2/Graphene composite for high performance anodes in lithium ion batteries.* Journal of Power Sources, 2012. **216**: p. 169-178.

38. Chen, X., Z. Zhang, X. Li, C. Shi, and X. Li, *Selective synthesis of metastable MoO_2 nanocrystallites through a solution-phase approach.* Chemical Physics Letters, 2006. **418**(1-3): p. 105-108.

39. Sun, Y., X. Hu, W. Luo, and Y. Huang, *Self-Assembled Hierarchical MoO_2/Graphene Nanoarchitectures and Their Application as a High-Performance Anode Material for Lithium-Ion Batteries.* ACS Nano, 2011. **5**(9): p. 7100-7107.

40. Zhang, H., L. Zeng, X. Wu, L. Lian, and M. Wei, *Synthesis of MoO_2 nanosheets by an ionic liquid route and its electrochemical properties.* Journal of Alloys and Compounds, 2013. **580**: p. 358-362.

41. Zhang, X., X. Song, S. Gao, Y. Xu, X. Cheng, H. Zhao, and L. Huo, *Facile synthesis of yolk–shell MoO_2 microspheres with excellent electrochemical performance as a Li-ion battery anode.* Journal of Materials Chemistry A, 2013. **1**(23): p. 6858.

42. Liu, X., Y. He, S. Wang, and Q. Zhang, *Preparation of MoO_2 sub-micro scale sheets and their optical properties.* Journal of Alloys and Compounds, 2011. **509**: p. S408-S411.

43. Zhang, X., X. Huang, L. Xia, B. Zhong, X. Zhang, T. Zhang, and G. Wen, *Facile synthesis of flexible and free-standing cotton covered by graphene/MoO_2 for lithium-ions batteries.* Ceramics International, 2017. **43**(6): p. 4753-4760.

44. Gao, H., C.-L. Liu, Y. Liu, Z.-H. Liu, and W.-S. Dong, *MoO_2-loaded porous carbon hollow spheres as anode materials for lithium-ion batteries.* Materials Chemistry and Physics, 2014. **147**(1-2): p. 218-224.

45. Gao, Q., L. Yang, X. Lu, J. Mao, Y. Zhang, Y. Wu, and Y. Tang, *Synthesis, characterization and lithium-storage performance of MoO_2/carbon hybrid nanowires.* Journal of Materials Chemistry, 2010. **20**(14): p. 2807.

46. Agency, U.S.E.P. *Municipal solid waste*. 2016; Available from: http://www3.epa.gov/epawaste/nonhaz/municipal/.

47. Pearce, C., *The removal of colour from textile wastewater using whole bacterial cells: a review*. Dyes and Pigments, 2003. **58**(3): p. 179-196.

48. Shannon, M.A., P.W. Bohn, M. Elimelech, J.G. Georgiadis, B.J. Marinas, and A.M. Mayes, *Science and technology for water purification in the coming decades.* Nature, 2008. **452**(7185): p. 301-10.

49. Ghoreishi, S.M. and R. Haghighi, *Chemical catalytic reaction and biological oxidation for treatment of non-biodegradable textile effluent.* Chemical Engineering Journal, 2003. **95**(1-3): p. 163-169.

50. Robinson, T., G. McMullan, R. Marchant, and P. Nigam, *Remediation of dyes in textile e,uent: a critical review on current treatment technologies with a proposed alternative.* Bioresource Technology, 2001. **77**: p. 247-255.

51. Gunti, S., A. Kumar, and M.K. Ram, *Nanostructured photocatalysis in the visible spectrum for the decontamination of air and water.* International Materials Reviews, 2017: p. 1-26.

52. Kampa, M. and E. Castanas, *Human health effects of air pollution.* Environ Pollut, 2008. **151**(2): p. 362-7.

53. Becker, S., S. Mundandhara, R.B. Devlin, and M. Madden, *Regulation of cytokine production in human alveolar macrophages and airway epithelial cells in response to ambient air pollution particles: further mechanistic studies.* Toxicol Appl Pharmacol, 2005. **207**(2 Suppl): p. 269-75.

54. Lisk, D.J., *Environmental implications of incineration of municipal solid waste and ash disposal.* The Science of the Total Environment, 1988. **74**: p. 39-66.

55. Giusti, L., *A review of waste management practices and their impact on human health.* Waste Manag, 2009. **29**(8): p. 2227-39.

56. Stoner, G.D., F.B. Daniel, and K.M. Schenck, *Metabolism and DNA binding of benzo [a] pyrene in cultured human bladder and bronchus.* Carcinogenesis, 1989. **3**(2): p. 195-201.

57. Reid, W.D., K.F. Ilett, J.M. Glick, and G. Krishna, *Metabolism and binding of aromatic hydrocarbons in the lung: relationship to experimental bronchiolar necrosis 1.* American Review of Respiratory Disease, 1973. **107**(4): p. 539-551.

58. Greenlee, L.F., D.F. Lawler, B.D. Freeman, B. Marrot, and P. Moulin, *Reverse osmosis desalination: water sources, technology, and today's challenges.* Water Research, 2009. **43**(9): p. 2317-2348.

59. Pérez-González, A., A. Urtiaga, R. Ibáñez, and I. Ortiz, *State of the art and review on the treatment technologies of water reverse osmosis concentrates.* Water Research, 2012. **46**(2): p. 267-283.

60. Fakhru'l-Razi, A., A. Pendashteh, L.C. Abdullah, D.R. Biak, S.S. Madaeni, and Z.Z. Abidin, *Review of technologies for oil and gas produced water treatment.* J Hazard Mater, 2009. **170**(2-3): p. 530-51.

61. Pradeep, T. and Anshup, *Noble metal nanoparticles for water purification: A critical review*. Thin Solid Films, 2009. **517**(24): p. 6441-6478.

62. Dadd, R.C., *Ozone/ultraviolet water purification*, in *Google Patents*. 1980.

63. Leek Jr, K.F., *Domestic grey water purifier using diverter and UV filter treater with preheater*, in *Google Patents*. 1992.

64. Papic, S., *Removal of some reactive dyes from synthetic wastewater by combined Al(III) coagulation/carbon adsorption process.* Dyes and Pigments, 2004. **62**(3): p. 291-298.

65. Shukla, A., Y.-H. Zhang, P. Dubey, J.L. Margrave, and S.S. Shukla, *The role of sawdust in the removal of unwanted materials from water.* Journal of Hazardous Materials, 2002. **95**: p. 137-152.

66. Kurniawan, T.A., G.Y. Chan, W.-H. Lo, and S. Babel, *Physico–chemical treatment techniques for wastewater laden with heavy metals.* Chemical Engineering Journal, 2006. **118**: p. 83-98.

67. Am Water Works Res, F., B. Langlais, D.A. Reckhow, and D.R. Brink, *Ozone in water treatment: application and engineering*. 1991: CRC press.

68. Kang, J.-W., W.H. Glaze, and D.H. Chapin, *The Chemistry of Water Treatment Processes Involving Ozone, Hydrogen Peroxide and Ultraviolet Radiation.* Ozone Science and Engineering, 1987. **9**(4): p. 335-352.

69. Gupta, V.K., I. Ali, T.A. Saleh, A. Nayak, and S. Agarwal, *Chemical treatment technologies for waste-water recycling—an overview*. RSC Advances, 2012. **2**(16): p. 6380.

70. Zularisam, A.W., A.F. Ismail, and R. Salim, *Behaviours of natural organic matter in membrane filtration for surface water treatment — a review*. Desalination, 2006. **194**(1-3): p. 211-231.

71. Hagen, K., *Removal of particles, bacteria and parasites with ultrafiltration for drinking water treatment.* Desalination, 1998. **119**: p. 85-91.

72. Simpson, D.R., *Biofilm processes in biologically active carbon water purification.* Water Res, 2008. **42**(12): p. 2839-48.

73. Wiszniowski, J., D. Robert, J. Surmacz-Gorska, K. Miksch, and J. Weber, *Landfill leachate treatment methods: A review.* Environmental Chemistry Letters, 2006. **2006**(4).

74. Sarria, V., S. Parra, N. Adler, P. Péringer, N. Benitez, and C. Pulgarin, *Recent developments in the coupling of photoassisted and aerobic biological processes for the treatment of biorecalcitrant compounds.* Catalysis Today, 2002. **75**(2): p. 301-315.

75. Fujishima, A., K.-i. Honda, and S.-i. Kikuchi, *Photosensitized Electrolytic Oxidation on Semiconducting n-Type TiO2 Electrode.* The Journal of the Society of Chemical Industry, 1969. **72**: p. 108-113.

76. Gunti, S., A. Kumar, and M.K. Ram, *Comparative Organics Remediation Properties of Nanostructured Graphene Doped Titanium Oxide and Graphene Doped Zinc Oxide Photocatalysts.* American Journal of Analytical Chemistry, 2015. **06**(08): p. 708-717.

77. Gunti, S., M. McCrory, A. Kumar, and M.K. Ram, *Enhanced Photocatalytic Remediation Using Graphene (G)-Titanium Oxide (TiO₂) Nanocomposite Material in Visible Light Radiation.* American Journal of Analytical Chemistry, 2016. **07**(07): p. 576-587.

78. Affam, A.C. and M. Chaudhuri, *Degradation of pesticides chlorpyrifos, cypermethrin and chlorothalonil in aqueous solution by TiO2 photocatalysis.* J Environ Manage, 2013. **130**: p. 160-5.

79. Ghaffar, I., M.F. Warsi, M. Shahid, and I. Shakir, *Unprecedented photocatalytic activity of carbon coated/MoO_3 core–shell nanoheterostructurs under visible light irradiation.* Physica E: Low-dimensional Systems and Nanostructures, 2016. **79**: p. 1-7.

80. Gupta, V.K., T. Eren, N. Atar, M.L. Yola, C. Parlak, and H. Karimi-Maleh, *CoFe2O4@TiO2 decorated reduced graphene oxide nanocomposite for photocatalytic degradation of chlorpyrifos.* Journal of Molecular Liquids, 2015. **208**: p. 122-129.

81. Hossain, E. and C.C. Jarrold, *Electronic structure of coordinatively unsaturated molybdenum and molybdenum oxide carbonyls.* J Chem Phys, 2009. **130**(6): p. 064301.

82. Kumar, V.V., K. Gayathri, and S.P. Anthony, *Synthesis of α-MoO_3 nanoplates using organic aliphatic acids and investigation of sunlight enhanced photodegradation of organic dyes.* Materials Research Bulletin, 2016. **76**: p. 147-154.

83. Li, J., K. Yu, Y. Tan, H. Fu, Q. Zhang, W. Cong, C. Song, H. Yin, and Z. Zhu, *Facile synthesis of novel MoS(2)@SnO(2) hetero-nanoflowers and enhanced photocatalysis and field-emission properties.* Dalton Trans, 2014. **43**(34): p. 13136-44.

84. Li, N., G. Liu, C. Zhen, F. Li, L. Zhang, and H.-M. Cheng, *Battery Performance and Photocatalytic Activity of Mesoporous Anatase TiO2 Nanospheres/Graphene Composites by Template-Free Self-Assembly.* Advanced Functional Materials, 2011. **21**(9): p. 1717-1722.

85. Li, W., D. Li, Y. Lin, P. Wang, W. Chen, X. Fu, and Y. Shao, *Evidence for the Active Species Involved in the Photodegradation Process of Methyl Orange on TiO2.* The Journal of Physical Chemistry C, 2012. **116**(5): p. 3552-3560.

86. Mahalingam, S., J. Ramasamy, and Y.-H. Ahn, *Synthesis and application of graphene-αMoO 3 nanocomposite for improving visible light irradiated photocatalytic decolorization of methylene blue dye.* Journal of the Taiwan Institute of Chemical Engineers, 2017.

87. Mkhalid, I.A., *Photocatalytic remediation of atrazine under visible light radiation using Pd-Gd2O3 nanospheres.* Journal of Alloys and Compounds, 2016. **682**: p. 766-772.

88. Qiu, J., P. Zhang, M. Ling, S. Li, P. Liu, H. Zhao, and S. Zhang, *Photocatalytic synthesis of TiO(2) and reduced graphene oxide nanocomposite for lithium ion battery.* ACS Appl Mater Interfaces, 2012. **4**(7): p. 3636-42.

89. Santacruz-Chávez, J.A., S. Oros-Ruiz, B. Prado, and R. Zanella, *Photocatalytic degradation of atrazine using TiO 2 superficially modified with metallic nanoparticles.* Journal of Environmental Chemical Engineering, 2015. **3**(4): p. 3055-3061.

90. Szkoda, M., K. Trzciński, K. Siuzdak, and A. Lisowska-Oleksiak, *Photocatalytical properties of maze-like MoO_3 microstructures prepared by anodization of Mo plate.* Electrochimica Acta, 2017. **228**: p. 139-145.

91. Wang, C., A.-W. Wang, J. Feng, Z. Li, B. Chen, Q.-H. Wu, J. Jiang, J. Lu, and Y.Y. Li, *Hydrothermal preparation of hierarchical MoS2-reduced graphene oxide nanocomposites towards remarkable enhanced visible-light photocatalytic activity.* Ceramics International, 2017. **43**(2): p. 2384-2388.

92. Yang, H., X. Li, A. Wang, Y. Wang, and Y. Chen, *Photocatalytic degradation of methylene blue by MoO_3 modified TiO2 under visible light.* Chinese Journal of Catalysis, 2014. **35**(1): p. 140-147.

93. Yola, M.L., T. Eren, and N. Atar, *A novel efficient photocatalyst based on TiO2 nanoparticles involved boron enrichment waste for photocatalytic degradation of atrazine.* Chemical Engineering Journal, 2014. **250**: p. 288-294.

94. Zhai, H., J. Qi, X. Zhang, H. Li, L. Yang, C. Hu, H. Liu, and J. Yang, *Preparation and Photocatalytic Performance of Hollow Structure LiNb3O8 Photocatalysts.* Nanoscale Res Lett, 2017. **12**(1): p. 519.

95. Zhang, L., Y. Tu, J.H. Cui, W.C. Shi, and Q. Li, *Synthesis and Photo-Catalytic Properties of M_OO₃Nanosheets.* Key Engineering Materials, 2014. **602-603**: p. 42-45.

96. Cabir, B., M. Yurderi, N. Caner, M.S. Agirtas, M. Zahmakiran, and M. Kaya, *Methylene blue photocatalytic degradation under visible light irradiation on copper phthalocyanine-sensitized TiO 2 nanopowders.* Materials Science and Engineering: B, 2017. **224**: p. 9-17.

97. Fisli, A., R. Ridwan, Y. K. Krisnandi, and J. Gunlazuardi, *Preparation and Characterization of Fe3O4/SiO2/TiO2 Composite for Methylene Blue Removal in Water.* International Journal of Technology, 2017. **8**(1): p. 76.

98. Khaki, M.R.D., M.S. Shafeeyan, A.A.A. Raman, and W. Daud, *Application of doped photocatalysts for organic pollutant degradation - A review.* J Environ Manage, 2017. **198**(Pt 2): p. 78-94.

99. Liu, D., R. Tian, J. Wang, E. Nie, X. Piao, X. Li, and Z. Sun, *Photoelectrocatalytic degradation of methylene blue using F doped TiO2 photoelectrode under visible light irradiation.* Chemosphere, 2017. **185**: p. 574-581.

100. Liu, Y., Y. Shi, X. Liu, and H. Li, *A facile solvothermal approach of novel Bi2S3/TiO2/RGO composites with excellent visible light degradation activity for methylene blue.* Applied Surface Science, 2017. **396**: p. 58-66.

101. Nawawi, W., R. Zaharudin, A. Zuliahani, D. Shukri, T. Azis, and Z. Razali, *Immobilized TiO2-Polyethylene Glycol: Effects of Aeration and pH of Methylene Blue Dye.* Applied Sciences, 2017. **7**(5): p. 508.

102. Wan, G., X. Peng, M. Zeng, L. Yu, K. Wang, X. Li, and G. Wang, *The Preparation of Au@TiO2 Yolk-Shell Nanostructure and its Applications for Degradation and Detection of Methylene Blue.* Nanoscale Res Lett, 2017. **12**(1): p. 535.

103. Li, Z., J. Ma, B. Zhang, C. Song, and D. Wang, *Crystal phase- and morphology-controlled synthesis of MoO_3materials.* CrystEngComm, 2017. **19**(11): p. 1479-1485.

104. Tarascon, J.M. and M. Armand, *Issues and challenges facing rechargeable lithium batteries.* Nature, 2001. **414**: p. 359-367.

105. Scrosati, B. and J. Garche, *Lithium batteries: Status, prospects and future.* Journal of Power Sources, 2010. **195**(9): p. 2419-2430.

106. Schalkwijk, W.v. and B. Scrosati, *Advances in Lithium-Ion Batteries*. 2004, Boston: Kluwer Acedemic/Plenum.

107. Etacheri, V., R. Marom, R. Elazari, G. Salitra, and D. Aurbach, *Challenges in the development of advanced Li-ion batteries: a review.* Energy & Environmental Science, 2011. **4**(9): p. 3243.

108. Auborn, J.J., Y.L. Barberio, K.J. Hanson, D.M. Schleich, and M.J. Martin, *Amorphous Molybdenum Sulfide Electrodes for Nonaqueous Electrochemical Cells.* Journal of The Electrochemical Society, 1987. **134**(3): p. 580-586.

109. Zeng, L., C. Zheng, C. Deng, X. Ding, and M. Wei, *MoO_2-ordered mesoporous carbon nanocomposite as an anode material for lithium-ion batteries.* ACS Appl Mater Interfaces, 2013. **5**(6): p. 2182-7.

110. Wang, Z., J.S. Chen, T. Zhu, S. Madhavi, and X.W. Lou, *One-pot synthesis of uniform carbon-coated MoO(2) nanospheres for high-rate reversible lithium storage.* Chem Commun (Camb), 2010. **46**(37): p. 6906-8.

111. Hwang, M.-J., K.M. Kim, and K.-S. Ryu, *Effects of graphene on MoO_2-MoS_2 composite as anode material for lithium-ion batteries.* Journal of Electroceramics, 2014. **33**(3-4): p. 239-245.

112. Koziej, D., M.D. Rossell, B. Ludi, A. Hintennach, P. Novak, J.D. Grunwaldt, and M. Niederberger, *Interplay between size and crystal structure of molybdenum dioxide nanoparticles--synthesis, growth mechanism, and electrochemical performance.* Small, 2011. **7**(3): p. 377-87.

113. Ku, J.H., Y.S. Jung, K.T. Lee, C.H. Kim, and S.M. Oh, *Thermoelectrochemically Activated MoO[sub 2] Powder Electrode for Lithium Secondary Batteries.* Journal of The Electrochemical Society, 2009. **156**(8): p. A688.

114. Dahn, J.R. and W.R. McKinnon, *Structure and Electrochemistry of Li_xMoO_2.* Solid State Ionics, 1987. **23**: p. 1-7.

115. Wu, Z.-S., W. Ren, L. Wen, L. Gao, Z. Jinping, Z. Chen, G. Zhou, F. Li, and H.-M. Cheng, *Graphene Anchored with Co_3O_4 Nanoparticles as Anode of Lithium Ion Batteries with Enhanced Reversible Capacity and Cyclic Performance.* ACS Nano, 2010. **4**(6): p. 3187-3194.

116. Wang, X., X. Zhou, K. Yao, J. Zhang, and Z. Liu, *A SnO_2/graphene composite as a high stability electrode for lithium ion batteries.* Carbon, 2011. **49**(1): p. 133-139.

117. Zhou, G., D.-W. Wang, F. Li, L. Zhang, N. Li, Z.-S. Wu, L. Wen, G.Q. Lu, and H.-M. Cheng, *Graphene-Wrapped Fe_3O_4Anode Material with Improved Reversible Capacity and Cyclic Stability for Lithium Ion Batteries.* Chemistry of Materials, 2010. **22**(18): p. 5306-5313.

118. Wang, H., L.-F. Cui, Y. Yang, H.S. Casalongue, J.T. Robinson, Y. Liang, L. Cui, and H. Dai, *Mn_3O_4−Graphene Hybrid as a High-Capacity Anode Material for Lithium Ion Batteries.* Journal of the American Chemical Society, 2010. **132**(40): p. 13978-13980.

119. Wang, D., D. Choi, J. Li, Z. Yang, Z. Nie, R. Kou, D. Hu, C. Wang, L.V. Saraf, J. Zhang, I. Aksay, and J. Liu, *Self-Assembled TiO_2–Graphene Hybrid Nanostructures for Enhanced Li-Ion Insertion.* ACS Nano, 2009. **3**(4): p. 907-914.

120. Ferrari, A.C., J.C. Meyer, V. Scardaci, C. Casiraghi, M. Lazzeri, F. Mauri, S. Piscanec, D. Jiang, K.S. Novoselov, S. Roth, and A.K. Geim, *Raman spectrum of graphene and graphene layers.* Phys Rev Lett, 2006. **97**(18): p. 187401.

121. Itagaki, M., S. Yotsuda, N. Kobari, K. Watanabe, S. Kinoshita, and M. Ue, *Electrochemical impedance of electrolyte/electrode interfaces of lithium-ion rechargeable batteries.* Electrochimica Acta, 2006. **51**(8-9): p. 1629-1635.

122. Mahmoodi, N.M., S. Keshavarzi, and M. Ghezelbash, *Synthesis of nanoparticle and modelling of its photocatalytic dye degradation ability from colored wastewater.* Journal of Environmental Chemical Engineering, 2017. **5**(4): p. 3684-3689.

123. Mageshwari, K., R. Sathyamoorthy, and J. Park, *Photocatalytic activity of hierarchical CuO microspheres synthesized by facile reflux condensation method.* Powder Technology, 2015. **278**: p. 150-156.

124. Mahmoud, M.S., M.K. Mostafa, S.A. Mohamed, N.A. Sobhy, and M. Nasr, *Bioremediation of red azo dye from aqueous solutions by Aspergillus niger strain isolated from textile wastewater.* Journal of Environmental Chemical Engineering, 2017. **5**(1): p. 547-554.

125. El-Kassas, H.Y. and L.A. Mohamed, *Bioremediation of the textile waste effluent by Chlorella vulgaris.* The Egyptian Journal of Aquatic Research, 2014. **40**(3): p. 301-308.

126. Ma, Y., Y. Jia, Z. Jiao, L. Wang, M. Yang, Y. Bi, and Y. Qi, *Facile synthesize α-MoO_3 nanobelts with high adsorption property.* Materials Letters, 2015. **157**: p. 53-56.

127. Zhao, X., M. Cao, and C. Hu, *Thermal oxidation synthesis hollow MoO_3 microspheres and their applications in lithium storage and gas-sensing.* Materials Research Bulletin, 2013. **48**(6): p. 2289-2295.

128. Zong, L., P. Cui, F. Qin, K. Zhao, Z. Wang, and R. Yu, *Heterostructured bismuth vanadate multi-shell hollow spheres with high visible-light-driven photocatalytic activity.* Materials Research Bulletin, 2017. **86**: p. 44-50.

129. Tang, S., C. Shen, W. Ji, J. Liu, and D. Fichou, *Template-free synthesis of hierarchical MoO_2 multi-shell architectures with improved lithium storage capability.* Materials Research Bulletin, 2017. **91**: p. 85-90.

130. Tiwari, J.N., R.N. Tiwari, and K.S. Kim, *Zero-dimensional, one-dimensional, two-dimensional and three-dimensional nanostructured materials for advanced electrochemical energy devices.* Progress in Materials Science, 2012. **57**(4): p. 724-803.

131. Li, Y., L. Yu, N. Li, W. Yan, and X. Li, *Heterostructures of Ag(3)PO(4)/TiO(2) mesoporous spheres with highly efficient visible light photocatalytic activity.* J Colloid Interface Sci, 2015. **450**: p. 246-53.

132. Cui, Y., J. He, F. Yuan, J. Xue, X. Li, and J. Wang, *Preparation of MoS_2 microspheres through surfactants-assisted hydrothermal synthesis using thioacetamide as reducing agent.* Hydrometallurgy, 2016. **164**: p. 184-188.

133. Zhai, W., Y. Xu, X. Cheng, S. Gao, X. Zhang, H. Zhao, and L. Huo, *Facile synthesis of monodisperse hierarchical MoO_2 porous spheres for high-performance Li-ion battery.* Materials Letters, 2015. **145**: p. 287-290.

134. Li, Y., T. Liu, T. Li, and X. Peng, *Hydrothermal fabrication of controlled morphologies of MoO_3 with CTAB: Structure and growth.* Materials Letters, 2015. **140**: p. 48-50.

135. Tang, G., J. Sun, C. Wei, K. Wu, X. Ji, S. Liu, H. Tang, and C. Li, *Synthesis and characterization of flowerlike MoS_2 nanostructures through CTAB-assisted hydrothermal process.* Materials Letters, 2012. **86**: p. 9-12.

136. Calheiros, L.F., B.G. Soares, and G.M.O. Barra, *DBSA-CTAB mixture as the surfactant system for the one step inverse emulsion polymerization of aniline: Characterization and blend with epoxy resin.* Synthetic Metals, 2017. **226**: p. 139-147.

137. Cao, J., B. Yang, Y. Wang, C. Wei, H. Wang, and S. Li, *Polymer brush hexadecyltrimethylammonium bromide (CTAB) modified poly (propylene-g-styrene sulphonic acid) fiber (ZB-1): CTAB/ZB-1 as a promising strategy for improving the dissolution and physical stability of poorly water-soluble drugs.* Mater Sci Eng C Mater Biol Appl, 2017. **80**: p. 282-295.

138. Elfeky, S.A., S.E. Mahmoud, and A.F. Youssef, *Applications of CTAB modified magnetic nanoparticles for removal of chromium (VI) from contaminated water.* J Adv Res, 2017. **8**(4): p. 435-443.

139. Guo, Z., Q. Ma, Z. Xuan, F. Du, and Y. Zhong, *Facile surfactant-assisted synthesis of CTAB-incorporated MoS_2 ultrathin nanosheets for efficient hydrogen evolution.* RSC Adv., 2016. **6**(20): p. 16730-16735.

140. Li, Y., H. Yu, X. Huang, Z. Wu, and H. Xu, *Improved performance for polymer solar cells using CTAB-modified MoO_3 as an anode buffer layer.* Solar Energy Materials and Solar Cells, 2017. **171**: p. 72-84.

141. Lin, Y.F. and S.H. Hsu, *Solvent-resistant CTAB-modified polymethylsilsesquioxane aerogels for organic solvent and oil adsorption.* J Colloid Interface Sci, 2017. **485**: p. 152-158.

142. Liu, X., S. Liu, M. Fan, and L. Zhang, *Decrease of hydrophilicity of lignite using CTAB: Effects of adsorption differences of surfactant onto mineral composition and functional groups.* Fuel, 2017. **197**: p. 474-481.

143. Wang, F., D. Liu, P. Zheng, and X. Ma, *Synthesis of rectorite/Fe 3 O 4 -CTAB composite for the removal of nitrate and phosphate from water.* Journal of Industrial and Engineering Chemistry, 2016. **41**: p. 165-174.

144. Wang, T., W. Li, D. Xu, X. Wu, L. Cao, and J. Meng, *A novel and facile synthesis of black TiO_2 with improved visible-light photocatalytic H 2 generation: Impact of surface modification with CTAB on morphology, structure and property.* Applied Surface Science, 2017. **426**: p. 325-332.

145. Wang, Z., T. Chen, W. Chen, K. Chang, L. Ma, G. Huang, D. Chen, and J.Y. Lee, *CTAB-assisted synthesis of single-layer MoS_2–graphene composites as anode materials of Li-ion batteries.* J. Mater. Chem. A, 2013. **1**(6): p. 2202-2210.

146. Yusuf, M., M.A. Khan, M. Otero, E.C. Abdullah, M. Hosomi, A. Terada, and S. Riya, *Synthesis of CTAB intercalated graphene and its application for the adsorption of AR265 and AO7 dyes from water.* J Colloid Interface Sci, 2017. **493**: p. 51-61.

147. Chen, A., C. Li, R. Tang, L. Yin, and Y. Qi, *MoO_2-ordered mesoporous carbon hybrids as anode materials with highly improved rate capability and reversible capacity for lithium-ion battery.* Phys Chem Chem Phys, 2013. **15**(32): p. 13601-10.

148. Chen, M., C. Du, B. Song, K. Xiong, G. Yin, P. Zuo, and X. Cheng, *High-performance $LiFePO_4$ cathode material from FePO4 microspheres with carbon nanotube networks embedded for lithium ion batteries.* Journal of Power Sources, 2013. **223**: p. 100-106.

149. Fang, J.S., C.S. Lin, Y.Y. Huang, and T.S. Chin, *Surface-Morphology-Induced Hydrophobicity of Fluorocarbon Films Grown by a Simultaneous Etching and Deposition Process.* Journal of Electronic Materials, 2015. **44**(8): p. 2908-2914.

150. Zong, J., K. Feng, Z. Li, A.M. Qasim, and P.K. Chu, *Studies on the surface morphology and hydrophobic property of NiTi thin films under in situ and post annealing various temperatures.* Materials Letters, 2016. **183**: p. 244-247.

151. Lee, Y.J., C.W. Park, D.-G. Kim, W.T. Nichols, S.-T. Oh, and Y.D. Kim, *MoO_3 thin film synthesis by chemical vapor transport of volatile $MoO_3(OH)_2$.* Journal of Ceramic Processing Research, 2010. **11**(1): p. 52-55.

152. Lee, Y.J., Y.I. Seo, S.H. Kim, D.-G. Kim, and Y.D. Kim, *Deposition of Mo Oxide and Metallic Mo Films by Chemical Vapor Transport of $MoO_3(OH)_2$.* Chemical Vapor Deposition, 2009. **15**(7-9): p. 199-203.

153. Lee, Y.J., Y.I. Seo, S.-H. Kim, D.-G. Kim, and Y.D. Kim, *Optical properties of molybdenum oxide thin films deposited by chemical vapor transport of $MoO_3(OH)_2$.* Applied Physics A, 2009. **97**(1): p. 237-241.

APPENDIX A: COPYRIGHT PERMISSIONS FOR MATERIAL USED IN CHAPTER 5

Below is permission for the use of material in Chapter 5.

CAMBRIDGE UNIVERSITY PRESS LICENSE TERMS AND CONDITIONS

Oct 14, 2017

This Agreement between Michael S McCrory ("You") and Cambridge University Press ("Cambridge University Press") consists of your license details and the terms and conditions provided by Cambridge University Press and Copyright Clearance Center.

License Number	4207871146144
License date	Oct 14, 2017
Licensed Content Publisher	Cambridge University Press
Licensed Content Publication	MRS Advances
Licensed Content Title	Hydrothermal Synthesis of MoO2 Nanoparticles Directly onto a Copper Substrate
Licensed Content Author	Michael McCrory, Ashok Kumar, Manoj K. Ram
Licensed Content Date	Apr 5, 2016
Licensed Content Volume	1
Licensed Content Issue	15
Start page	1051
End page	1054
Type of Use	Dissertation/Thesis
Requestor type	Author
Portion	Text extract
Number of pages requested	2
Author of this Cambridge University Press article	Yes
Author / editor of the new work	Yes
Order reference number	
Territory for reuse	World
Title of your thesis / dissertation	Synthesis, Characterization, and Application of Molybdenum Oxide Nanomaterials
Expected completion date	Dec 2017
Estimated size(pages)	80
Requestor Location	Michael S McCrory
	[redacted]
Publisher Tax ID	
Billing Type	
Billing Address	

APPENDIX B: COPYRIGHT PERMISSION FOR FIGURES

Below is copyright permission for Figure 2.1.

ELSEVIER LICENSE
TERMS AND CONDITIONS

Oct 18, 2017

This Agreement between Michael S McCrory ("You") and Elsevier ("Elsevier") consists of your license details and the terms and conditions provided by Elsevier and Copyright Clearance Center.

License Number	4212100142255
License date	Oct 18, 2017
Licensed Content Publisher	Elsevier
Licensed Content Publication	Journal of Environmental Management
Licensed Content Title	Application of doped photocatalysts for organic pollutant degradation - A review
Licensed Content Author	Mohammad Reza Delsouz Khaki,Mohammad Saleh Shafeeyan,Abdul Aziz Abdul Raman,Wan Mohd Ashri Wan Daud
Licensed Content Date	Aug 1, 2017
Licensed Content Volume	198
Licensed Content Issue	n/a
Licensed Content Pages	17
Start Page	78
End Page	94
Type of Use	reuse in a thesis/dissertation
Portion	figures/tables/illustrations
Number of figures/tables/illustrations	1
Format	both print and electronic
Are you the author of this Elsevier article?	No
Will you be translating?	No
Original figure numbers	Figure 2
Title of your thesis/dissertation	Synthesis, Characterization, and Application of Molybdenum Oxide Nanomaterials
Expected completion date	Dec 2017
Estimated size (number of pages)	80
Requestor Location	Michael S McCrory [redacted]
Publisher Tax ID	
Total	
Terms and Conditions	

Below is copyright permission for Figures 2.2 and 2.3

ELSEVIER LICENSE
TERMS AND CONDITIONS

Oct 14, 2017

This Agreement between Michael S McCrory ("You") and Elsevier ("Elsevier") consists of your license details and the terms and conditions provided by Elsevier and Copyright Clearance Center.

License Number	4207870454897
License date	Oct 14, 2017
Licensed Content Publisher	Elsevier
Licensed Content Publication	Ceramics International
Licensed Content Title	Facile synthesis of MoO2 nanoparticles as high performance supercapacitor electrodes and photocatalysts
Licensed Content Author	E. Zhou,Chenggang Wang,Qinqin Zhao,Zhipeng Li,Minghui Shao,Xiaolong Deng,Xiaojing Liu,Xijin Xu
Licensed Content Date	Feb 1, 2016
Licensed Content Volume	42
Licensed Content Issue	2
Licensed Content Pages	6
Start Page	2198
End Page	2203
Type of Use	reuse in a thesis/dissertation
Intended publisher of new work	other
Portion	figures/tables/illustrations
Number of figures/tables/illustrations	2
Format	both print and electronic
Are you the author of this Elsevier article?	No
Will you be translating?	No
Original figure numbers	Figures 1 (a&b), and 5
Title of your thesis/dissertation	Synthesis, Characterization, and Application of Molybdenum Oxide Nanomaterials
Expected completion date	Dec 2017
Estimated size (number of pages)	80
Requestor Location	Michael S McCrory [redacted]
Publisher Tax ID	

Below is copyright permission for Figure 2.4.

NATURE PUBLISHING GROUP LICENSE TERMS AND CONDITIONS

Oct 14, 2017

This Agreement between Michael S McCrory ("You") and Nature Publishing Group ("Nature Publishing Group") consists of your license details and the terms and conditions provided by Nature Publishing Group and Copyright Clearance Center.

License Number	4207851377868
License date	Oct 14, 2017
Licensed Content Publisher	Nature Publishing Group
Licensed Content Publication	Nature
Licensed Content Title	Issues and challenges facing rechargeable lithium batteries
Licensed Content Author	J.-M. Tarascon and M. Armand
Licensed Content Date	Nov 15, 2001
Licensed Content Volume	414
Licensed Content Issue	6861
Type of Use	reuse in a dissertation / thesis
Requestor type	academic/educational
Format	print and electronic
Portion	figures/tables/illustrations
Number of figures/tables/illustrations	1
Figures	Figure 1 Comparison of the different battery technologies in terms of volumetric and gravimetric energy density.
Author of this NPG article	no
Your reference number	
Title of your thesis / dissertation	Synthesis, Characterization, and Application of Molybdenum Oxide Nanomaterials
Expected completion date	Dec 2017
Estimated size (number of pages)	80
Requestor Location	Michael S McCrory [redacted]
Billing Type	
Billing Address	

Below is copyright permission for Figure 2.5

ROYAL SOCIETY OF CHEMISTRY LICENSE TERMS AND CONDITIONS

Oct 14, 2017

This Agreement between Michael S McCrory ("You") and Royal Society of Chemistry ("Royal Society of Chemistry") consists of your license details and the terms and conditions provided by Royal Society of Chemistry and Copyright Clearance Center.

License Number	4207860480498
License date	Oct 14, 2017
Licensed Content Publisher	Royal Society of Chemistry
Licensed Content Publication	Energy & Environmental Science
Licensed Content Title	Challenges in the development of advanced Li-ion batteries: a review
Licensed Content Author	Vinodkumar Etacheri,Rotem Marom,Ran Elazari,Gregory Salitra,Doron Aurbach
Licensed Content Date	Jul 26, 2011
Licensed Content Volume	4
Licensed Content Issue	9
Type of Use	Thesis/Dissertation
Requestor type	academic/educational
Portion	figures/tables/images
Number of figures/tables/images	1
Format	print and electronic
Distribution quantity	100
Will you be translating?	no
Order reference number	
Title of the thesis/dissertation	Synthesis, Characterization, and Application of Molybdenum Oxide Nanomaterials
Expected completion date	Dec 2017
Estimated size	80
Requestor Location	Michael S McCrory [redacted]
Billing Type	
Billing Address	

Below is copyright permission for Figures 2.6 - 2.8.

PERMISSION/LICENSE IS GRANTED FOR YOUR ORDER AT NO CHARGE

This type of permission/license, instead of the standard Terms & Conditions, is sent to you because no fee is being charged for your order. Please note the following:

- Permission is granted for your request in both print and electronic formats, and translations.
- If figures and/or tables were requested, they may be adapted or used in part.
- Please print this page for your records and send a copy of it to your publisher/graduate school.
- Appropriate credit for the requested material should be given as follows: "Reprinted (adapted) with permission from (COMPLETE REFERENCE CITATION). Copyright (YEAR) American Chemical Society." Insert appropriate information in place of the capitalized words.
- One-time permission is granted only for the use specified in your request. No additional uses are granted (such as derivative works or other editions). For any other uses, please submit a new request.

If credit is given to another source for the material you requested, permission must be obtained from that source.

BACK CLOSE WINDOW

Below is copyright permission for Figures 2.9 -2.11

ELSEVIER LICENSE
TERMS AND CONDITIONS

Oct 14, 2017

This Agreement between Michael S McCrory ("You") and Elsevier ("Elsevier") consists of your license details and the terms and conditions provided by Elsevier and Copyright Clearance Center.

License Number	4207861133525
License date	Oct 14, 2017
Licensed Content Publisher	Elsevier
Licensed Content Publication	Electrochimica Acta
Licensed Content Title	MoO2–graphene nanocomposite as anode material for lithium-ion batteries
Licensed Content Author	Qiwei Tang,Zhongqiang Shan,Li Wang,Xue Qin
Licensed Content Date	Sep 30, 2012
Licensed Content Volume	79
Licensed Content Issue	n/a
Licensed Content Pages	6
Start Page	148
End Page	153
Type of Use	reuse in a thesis/dissertation
Intended publisher of new work	other
Portion	figures/tables/illustrations
Number of figures/tables/illustrations	3
Format	both print and electronic
Are you the author of this Elsevier article?	No
Will you be translating?	No
Original figure numbers	Figures 5, 7 and 8
Title of your thesis/dissertation	Synthesis, Characterization, and Application of Molybdenum Oxide Nanomaterials
Expected completion date	Dec 2017
Estimated size (number of pages)	80
Requestor Location	Michael S McCrory [redacted]
Publisher Tax ID	
Total	

Below is copyright permission for Figures 2.12 -2.14

ELSEVIER LICENSE
TERMS AND CONDITIONS

Oct 14, 2017

This Agreement between Michael S McCrory ("You") and Elsevier ("Elsevier") consists of your license details and the terms and conditions provided by Elsevier and Copyright Clearance Center.

License Number	4207870079101
License date	Oct 14, 2017
Licensed Content Publisher	Elsevier
Licensed Content Publication	Journal of Power Sources
Licensed Content Title	Enhanced nanoscale conduction capability of a MoO2/Graphene composite for high performance anodes in lithium ion batteries
Licensed Content Author	Akkisetty Bhaskar,Melepurath Deepa,T.N. Rao,U.V. Varadaraju
Licensed Content Date	Oct 15, 2012
Licensed Content Volume	216
Licensed Content Issue	n/a
Licensed Content Pages	10
Start Page	169
End Page	178
Type of Use	reuse in a thesis/dissertation
Intended publisher of new work	other
Portion	figures/tables/illustrations
Number of figures/tables/illustrations	3
Format	both print and electronic
Are you the author of this Elsevier article?	No
Will you be translating?	No
Original figure numbers	Figures 3, 7b, and 8b
Title of your thesis/dissertation	Synthesis, Characterization, and Application of Molybdenum Oxide Nanomaterials
Expected completion date	Dec 2017
Estimated size (number of pages)	80
Requestor Location	Michael S McCrory [redacted]
Publisher Tax ID	
Total	